Abstract

Determining the Function and ATPase/RNA Remodeling Cycle of Dbp5

Shawn Dean Gray

2022

Dbp5 from *Saccharomyces cerevisiae* is an essential DEAD-box protein required for many aspects of mRNA metabolism including nuclear mRNA export. The ATPase cycle of Dbp5 is required for its *in vivo* function in mRNA export. The Dbp5 ATPase cycling kinetics dictate how the energy from ATP binding and hydrolysis is coupled to RNA remodeling. Several factors are known to regulate Dbp5 ATPase and mRNA export activity including the small molecule inositol hexaphosphate ($InsP_6$), RNA, and the nucleoporins Gle1 and Nup159. In order to quantify how these regulatory factors, influence the ATPase activity and functionality of Dbp5, we measured the rate and equilibrium constants of the Dbp5 ATPase alone and in conjunction with these regulatory factors using various steady-state and transient kinetic techniques. Knowledge of how Nup159, Gle1, and RNA modulate the Dbp5 ATPase kinetics allows us to identify the mechanism of Dbp5 mediated mRNA export and regulation.

Determining the Function and ATPase/RNA Remodeling Cycle of Dbp5

A Dissertation

Presented to the Faculty of the Graduate School

of

Yale University

In Candidacy for the Degree of

Doctor of Philosophy

By

Shawn Dean Gray

Dissertation Director: Enrique M. De La Cruz

December 2022

TABLE OF CONTENTS

For Hailey

CHAPTER 1: Introduction

Significance

Considering most eukaryotic protein-encoding genes are housed in the nucleus (1), export of mRNA through the nuclear pore complex (NPC) to the site of protein synthesis in the cytoplasm is paramount for cell viability. Like many steps of gene expression, messenger ribonucleoprotein complex (mRNP) export is regulated in response to external stimuli and cellular stress (2-4). Although it is clear that ATPase competent Dbp5 is requisite for mRNA nuclear export (5), little is known about the mechanistic details of mRNA export or its regulation.

Dbp5 (DDX19 in humans) is a conserved, essential DEAD-box protein (DBP) with a pivotal role in mRNP export (5-7). Moreover, the mechanistic details and regulation of transcription (8), mRNP maturation (9-11), and translation (12) have largely been established, while those of mRNP export, specifically concerning Dbp5 mediated mRNP remodeling, remain unknown (10). Clearly, there is a gap in our collective knowledge concerning eukaryotic gene expression. The studies presented herein are therefore significant as I endeavor to determine the mechanism of Dbp5 mediated mRNA nuclear export.

Although Dbp5 has been localized to both the nucleus (13-15) and cytoplasm (5-7,16), a clear concentration around the nuclear rim exists (5-7,16). Dbp5 localizes to the NPC cytoplasmic fibril via a conserved interaction with Nup159 (5,14,17) and associates with Nup42 bound Gle1 (14,16,18). Together, Nup159 and Gle1 regulate Dbp5 at the cytoplasmic face of the NPC to achieve

mRNP remodeling and export (19). Multiple studies have investigated the influence of Nup159 and Gle1 on Dbp5 steady-state ATPase activity (17,18,20-24). However, only a few labs have assayed the transient kinetics of specific steps in Dbp5's ATPase cycle (25-27). Consequently, the molecular details of how Nup159 and Gle1 influence Dbp5 ATPase cycling are unknown. The studies outlined herein will delineate the mechanism of Nup159 and Gle1 regulation of Dbp5 ATPase/RNA remodeling to form a predictive model of nucleocytoplasmic export.

Many human diseases (certain cancers, viral replications pathways, etc.) are driven by misfunction or misregulation of factors involved in mRNP export including Dbp5, Nup159, and Gle1 (28,29). Additionally, many viruses target NPC or mRNA export components in one or more stages of infection (30,31). Conservation between yeast and human mRNP export factors, specifically Dbp5 and its regulators is substantial (5,22,32,33). Consequently, this study will prove applicable to the human homolog of Dbp5 and its regulators and may lead to treatment advances for diseases and viral infections targeting mRNP export.

DBPs are found in all domains of life and participate in nearly every aspect of RNA metabolism, from transcription to RNA degradation (34). The structure and sequence motifs that make up DBPs are conserved across all DBPs, regardless of cellular function (34). Moreover, all DBPs employ energy from cycles of ATP binding, hydrolysis and/or product release to catalyze RNA unwinding or remodeling (34). Thus, studies on Dbp5 activity and regulation will

likely provide mechanistic information for general DBP function and control. This research is significant for human health and all facets of RNA metabolism.

Nuclear mRNA Export in *Saccharomyces cerevisiae*

Nuclear-cytoplasmic mRNA export represents a vital step in eukaryotic gene expression. Compartmental separation of transcription and translation allows for complex mRNA post processing that is unavailable in prokaryotes. In order for efficient mRNA processing to occur, it is critical ribosomes and other translational machinery are confined to the cytoplasm (10). However, this requires that mRNA in the nucleus must be exported to the cytoplasm for translation to occur. Tightly regulated control over nuclear import/export is maintained through a physical barrier formed by the nuclear envelope and selective “gates” of nuclear membrane embedded NPCs. The NPC is a massive multi-protein complex (~ 52 MDa in yeast) that provides a nuclear barrier to passive diffusion of macromolecules greater than ~ 40 kDa, helping maintain the specialized microenvironment within the nucleus. Thusly, import and export of most biological macromolecules requires specialized carrier proteins that are able to transverse NPC central channels.

NPCs are comprised of ~30 proteins, referred to collectively as “Nups”, organized into 8-fold radially repeated substructures (Figure 1.1) (35). The internal “nups” that comprise the central channel of functional NPCs form a diffusive barrier using specialized sequences of hydrophobic amino acids rich in phenylalanine and glycine (FG repeats). Transport factors are able to overcome

NPC diffusive barriers by transiently interacting with FG repeats, and in so doing, facilitate vectorial movement of bound cargo. One such transport factor required for mRNA export in all eukaryotes is Mex67-Mtr2 (TAP-p15 in humans). mRNP is carried through the NPC central channel by Mex67-Mtr2 and other carrier molecules. Although vectoral movement of mRNA from the nucleus to cytoplasm is a diffusive process, it differs from simple passive diffusion in that vectoral movement is likely driven by concentration gradients of mature mRNP in the nucleus and Dbp5-remodeled mRNP on the cytoplasmic face.

The nuclear and cytoplasmic face of the NPC is characterized by protruding structures termed the “nuclear basket” and “cytoplasmic fibrils”, respectively. Both the nuclear basket and cytoplasmic fibrils constitute sites of mRNA processing and a myriad of other cellular activities including serving as docking sites for distinct stages of mRNP nuclear export. The majority of Dbp5 is found attached to the cytoplasmic fibrils “nups” Nup159 and Gle1, although a significant population of diffuse Dbp5 exists in the nucleus and cytoplasm (5).

mRNA is exported as a large complex of RNA and accessory proteins collectively referred to as an mRNP. Transcript export only occurs once a complex, coordinated series of mRNP “maturation” steps involving mRNA nucleotide modification, loading and unloading of various protein complexes, etc. have been completed. Mature mRNP export consists of 3 distinct stages: a “nuclear docking” step, movement through the NPC central channel (translocation), and a “dwell” step at the NPC cytoplasmic fibrils (36). Active (ATPase competent) Dbp5 is requisite for efficient mRNA export (5), although it

is unclear which step(s) is directly mediated by Dbp5. Average mRNP export times range from ~ 50 – 200 milliseconds, although transport times of up to a few seconds have been observed with exceptionally long RNA (36). Dbp5 is thought to bind and remodel mRNP transcripts following export, likely during the cytoplasmic fibril “dwell” step. Dbp5 mediated remodeling displaces certain mRNP components required for NPC translocation including Mex67-Mtr2 and the poly-A binding protein Nab2 (Figure 1.2) (37). Removal of Mex67-Mtr2 from exported mRNPs prevents retro-grade transport and maintains concentration gradients that drive vectoral mRNP movement.

Immunoelectron microscopy studies propose that Dbp5 binds mRNA during nuclear processing at which point the Dbp5-mRNP complex transverses the NPC central channel as a whole. Dbp5 ATPase (and mRNA remodeling) is subsequently activated by Gle1 and Nup159 at the NPC cytoplasmic face (scaffold model; Figure 1.3) (13). Although Dbp5 shuttles between the nucleus and cytoplasm (14) it is unclear whether distinctly functional nuclear, NPC bound, and cytoplasmic pools of Dbp5 exist. Indeed, Dbp5 has been implicated in transcription (15) and translation termination (38) in addition to mRNA export. Alternatively, the “ratchet” model of mRNP export proposes (39) that Dbp5, Nup159, and Gle1 bound to the cytoplasmic face of the NPC continually remodel mRNA following export (Figure 1.3). These models are not necessarily mutually exclusive and both may occur *in vivo*. However, recent characterization of Dbp5s role in tRNA export demonstrates that nuclear-cytoplasmic shuttling of Dbp5 is

not necessary for mRNA export (40), providing further support for the ratchet model.

Dbp5 ATPase activity is required for mRNA export (5) as are interactions between Dbp5, Nup159, and Gle1 (5,16). The native Dbp5 ATPase cycle is slow and likely not sufficient to drive mRNA export alone as interaction times between Dbp5 and RNA during a single ATP turnover in the absence of regulatory factors is ~ 400 milliseconds (25), far longer than the average mRNP export times observed *in vivo*. Therefore, acceleration of the native Dbp5 ATPase by Nup159 and/or Gle1 is necessary for sustained mRNA nuclear export. mRNP remodeling, and subsequent Mex67-Mtr2 dissociation, is likely driven by one or more steps in the Dbp5 ATPase cycle and probably occurs during the terminal “dwell” stage of mRNP export at the cytoplasmic face of the NPC. Consequently, a detailed understanding of how Nup159, Gle1, and RNA modulate Dbp5 steady-state ATP hydrolysis kinetics is critical to understanding mRNP export as a whole.

ATPase cycle of DEAD-box proteins

DBPs play an important role in nearly all aspects of RNA metabolism (34,41). All DBPs consist of a motor domain core with two RecA-like domains containing 12 conserved amino acid sequence motifs involved in ATP binding/hydrolysis (motifs Q, I, II, and VI), RNA binding (motifs Ia, Ib, Ic, IV, IVa, and V), or coupling between these sites (motifs III and Va) (34) (Figure 1.4). Because of their conserved structural traits, DBPs are believed to function

through similar cycles of ATP binding, hydrolysis, and subsequent ADP/Pi release (42) in RNA binding/remodeling.

The ATP hydrolysis cycle is critical to the *in vivo* function of all DBPs and is intimately linked to RNA remodeling (42). The minimum intrinsic ATPase cycle is described by at least 4 distinct biochemical transitions including ATP binding, chemical cleavage (hydrolysis) of ATP to form ADP & P_i, and subsequent release of P_i followed by ADP (top pathway of Scheme 1.1). RNA can further stimulate the ATPase cycling kinetics of DBPs (bottom pathway of Scheme 1.1) by providing an alternative pathway that avoids kinetically or thermodynamically unfavorable steps in the native ATPase cycle. In this way, RNA accelerates the overall maximum steady-state ATPase (k_{cat}) of DBPs. Any one (or more) of these biochemical transitions may be coupled to RNA remodeling.

Contrary to popular belief, the ATP hydrolysis step itself is not necessarily coupled to work output but ensures vectoral cycling through nucleotide states. Each of the nucleotide states within the DBP ATPase cycle possesses a unique RNA affinity. By cycling through various nucleotide states, DBPs are able to vectorially cycle through low and high RNA affinity structures. Importantly, this allows DBPs to bind their respective RNA substrate, execute RNA remodeling, and eventually release the remodeled RNA.

Interestingly, many DBPs perform seemingly distinct functions (34,41) from RNA clamping (43) (Mss116) to RNA chaperone activity (44) (DbpA). How can this highly conserved DEAD-box family spawn such functional diversity? The De La Cruz lab has demonstrated that two functionally distinct DBPs, Mss116

and DbpA, differ in their intrinsic rate constants for RNA-stimulated ATPase cycling and consequently, the nucleotide state occupied most often *in vivo* (43,44).

The ATPase cycles of DbpA and Mss116 are both limited by slow ATP hydrolysis and even slower subsequent P_i release. Under *in vitro* conditions, this maintains both DBPs in the predominantly ADP-P_i state during steady-state ATPase cycling. The steady-state distribution of populated intermediates shifts under *in vivo* conditions. Mss116 remains predominantly in the ADP-P_i state, while DbpA becomes mostly ADP bound. Both the ATP and ADP-P_i states are considered strong RNA binding or “high RNA affinity” states, although the exact RNA affinities can shift depending on the DBP (42). Alternatively, the *apo* (no nucleotide) and ADP bound states are canonically weak RNA binders. Mss116 is thought to function as a molecular “clamp”, stabilizing splicing intermediates for group I and group II introns (42). Population of high RNA affinity structures would promote prolonged Mss116-RNA interactions, thereby facilitating the cellular role of Mss116 as an RNA stabilization factor. DbpA on the other hand, functions as a molecular chaperone to remodel misfolded ribosomal RNA (rRNA) (42). Only a small fraction of rRNA (misfolded) would require intervention from DbpA at any given time (under normal cellular conditions). By populating the weak RNA affinity state, DbpA would facilitate release of remodeled rRNA and limit competition with other rRNA binding partners.

The predominant nucleotide state, and in turn RNA binding properties, of Mss116 and DbpA are consistent with their respective *in vivo* functions. Some

DBPs, such as Dbp5, possess an ancillary method of modulating their ATPase kinetics, and in turn cellular functions, in the form of protein regulators (Nup159 and Gle1 for Dbp5). Therefore, determining native and regulated ATPase kinetics can yield insight into the cellular function and mechanism of DBPs. Because DBP structural conservation is high (34), studies investigating specific DBP activity and regulation will help elucidate other DBP function and regulation.

Overview of *Saccharomyces cerevisiae* Dbp5 and its role in mRNA export

Dbp5 (Rat8) was initially identified in a temperature-sensitive (TS) screen of yeast mutants defective in poly-A RNA export (6). Dbp5 is essential in both yeast and humans (DDX19 in humans) (5-7), advocating the physiological importance of Dbp5 function. Multiple studies have identified localized populations of Dbp5 to the cytoplasm with a strong concentration around the nuclear rim (5-7), specifically to the cytoplasmic fibrils of the NPC (16). Dbp5 localizes to the NPC via a conserved interaction with Nup159 (NUP214 in humans) (5,14,17), where it also interacts with Gle1 (14,16) bound to Nup42 (16). Yeast mutants deficient in Dbp5-Gle1 or Dbp5-Nup159 binding display mRNP export defects (14,20), illustrating the significance of these interactions for cell viability. Although Dbp5 possesses helicase activity, dsRNA unwinding is dependent upon unidentified cellular factor(s) (5,7). Given the single-stranded nature of mRNA (45) and the specificity of Dbp5 for it (5), Dbp5 likely removes mRNA bound proteins subsequent to nuclear export at the cytoplasmic face of the NPC (40). Indeed, it has been proposed that Dbp5 removes the mRNA

binding proteins Mex67 (46) and Nab2 (47), both of which translocate with RNA from the nucleus to the cytoplasm (10,48). Given Mex67s paramount role in binding phenylalanine-glycine repeats in NPC nuclear porin proteins (FG-Nup) (49) and mRNA export (50,51), Dbp5-mediated removal of Mex67 (and other mRNA binding proteins) likely confers unidirectionality to mRNP export (10,16,17,48).

Dbp5 ATPase activity is important for *in vivo* function as Dbp5 mutants defective in ATP binding/hydrolysis display mRNA specific export defects when injected into *Xenopus laevis* oocytes (5). Although Dbp5 displays innate ATPase activity, it is insufficient for efficient mRNP remodeling *in vivo (21)* as mRNA export times are in the few hundred millisecond range (36,52), while the interaction time between Dbp5 and RNA during a single ATP turnover is at least 0.4 seconds in the absence of Nup159 or Gle1. Gle1 has been shown to enhance both innate and RNA-stimulated Dbp5 ATPase activity about 5-fold (18,20,21). Inclusion of the small molecule $InsP_6$ intensifies these effects and promotes Dbp5-Gle1 association (18,20,21) by conjugating two positively charged pockets along the Dbp5-Gle1 binding interface (23). Clearly, Gle1 along with $InsP_6$ accelerates a rate-limiting step along both the native and RNA-stimulated steady-state ATPase cycle of Dbp5 (18,20,21).

Previous structural studies (22,53) have identified an N-terminal extension of the human Dbp5 homolog DDX19, that is conserved in yeast (23) and may operate with Gle1 to adjust Dbp5 ATPase activity. The N-terminal extension forms an α-helix that inserts between the tandem RecA-like domains of DDX19

and contacts the ribose moiety of the bound nucleotide, precluding formation of a hydrolysis competent active site (53). Structures of RNA-Dbp5-ADPNP complex reveal that RNA binding dislocates the N-terminal extension from the active site, allowing ATP hydrolysis to occur (53). Consistent with this finding, removal of the DDX19 N-terminal extension accelerates RNA-stimulated ATPase activity. Therefore, the N-terminal extension of DDX19/Dbp5 likely acts as an autoinhibitory switch, slowing ATP hydrolysis in the absence of RNA (53). Gle1, when bound to Dbp5, will clash with a portion of the N-terminal helix inserted within the nucleotide binding cleft (23). Thus, Gle1 may displace the autoinhibitory extension, partially accounting for higher steady-state ATPase activity (20,21,23).

Alternatively, Dbp5 ATPase kinetics are marginally influenced (17) or even slowed by Nup159 (22,23) independent of RNA, although inhibition can be overcome by excess Gle1 (23). Nevertheless, Nup159 does not appear to accelerate any rate-limiting step in Dbp5's steady-state ATPase cycle (±RNA). Interestingly, when the Dbp5 binding domain of Nup159 is deleted, yeast display mRNA export defects that can be completed rescued by Dbp5; additionally, Dbp5 mislocalizes from the NPC (14). Furthermore, overexpression of the Dbp5 binding domain of Nup159 in yeast results in nuclear accumulation of mRNA. However, this defect can be rescued by complementary Dbp5 overexpression (14). Further, surface plasmon resonance (SPR) analysis suggests Nup159 preferentially binds *apo*Dbp5 over Dbp5-nucleotide complexes (22). *Taken*

*together, these results indicate that Nup159 may provide a docking site for apo*Dbp5 *to increase the local concentration at the NPC.*

Overview of mRNA export models

Two major models for Dbp5-mediated mRNP remodeling have been proposed (Figure 1.5) (23,24). The Wente & Cole model is based on cell biology and biochemical data (24) [discussed below], while the Weis & Berger model is predicated upon x-ray crystal structures of various Dbp5-regulator complexes (23).

In the Wente & Cole model, Gle1 is purported to aid ATP binding, priming Dbp5 for subsequent RNA remodeling. After RNA binding, ATP hydrolysis occurs followed by RNA and Pi release. Nup159 is then required to dissociate ADP from Dbp5 (function as a nucleotide exchange factor or NEF) in order to recycle Dbp5 for continued mRNP remodeling (Figure 1.5). Several lines of evidence support the Wente & Cole model. First, Dbp5-ADP binding requires several hours to equilibrate as measured through filter binding assays of radioactive nucleotide (Figure 1A in (24)). Wente & Cole (24) also demonstrate that Nup159 is able to specifically promote ADP release from Dbp5, following 24-hour Dbp5-ADP incubation (Figure 1 C, D, E in (24)). As further evidence, Wente & Cole (24) report that a Dbp5 mutant ($Dbp5^{RR}$) unable to bind Nup159 possesses a lower ADP affinity, has accelerated ADP release, and demonstrates no TS growth defects in yeast lacking the Dbp5 binding domain of Nup159, while WT Dbp5 has

diminished growth at 37°C (Figure 3; 4 in (24)). The authors speculate that *in vivo,* Nup159 NEF activity is negated by the accelerated ADP release of $Dbp5^{RR}$. Wente & Cole invoke these and other results to compose the model presented in Figure 1.5.

Weis & Berger (23) suggest that following ATP hydrolysis, Gle1 promotes Pi and RNA dissociation. *Gle1 stimulated Pi release is consistent with the observations that phosphate release is rate limiting (±RNA) (25) and that Gle1 accelerates steady-state Dbp5 ATPase cycling independent of RNA (18,20,21,23).* Subsequent to Pi dissociation, Nup159 is proposed to bind the Gle1-Dbp5-ADP complex, at which point ADP release occurs. Comparisons between x-ray crystal structures of RNA-Dbp5-ADP·BeF_3 and Gle1-Dbp5-ADP suggests that Gle1 binding induces a conformational change of Dbp5, separating the two RecA-like domains (Figure 1E in (23)). Moreover, the vacant RNA binding site of the Gle1-Dbp5-ADP structure exhibits a considerably reduced, almost neutral surface charge in addition to a more open structure (Figure 1F in (23)). Together, these data suggest Gle1 may promote RNA and Pi release from Dbp5. Indeed, RNA release from an ATP bound, hydrolysis incompetent Dbp5 mutant is accelerated by WT Gle1, as monitored by fluorescence polarization (Figure 2F in (23)). The two subdomains of Dbp5's helicase motor core are further separated in Nup159-Gle1-Dbp5-ADP complex structures, indicating that Nup159 may function in conjunction with Gle1 to promote ADP release (23). It is important to note that most structures and experiments performed by Weis & Berger (23) employ a mutant Dbp5 to stabilize Gle1 binding.

Thesis Overview

The two models proposed in the previous section (Figure 1.5) make inherently kinetic arguments regarding the influence of Nup159 and/or Gle1 on the ATPase and RNA binding rate constants of Dbp5. Ultimately, the mechanism of how Gle1 and Nup159 regulate Dbp5-RNA binding throughout the Dbp5 ATPase cycle is dictated by the preferred pathway Dbp5 uses to transverse the entire potential Nup159 and Gle1 regulated ATPase and RNA binding matrix (Figure 1.6). This preferred pathway is dictated by the relative probabilities of each potential step, which are proportional to the rate constants defining each potential transition. Therefore, by determining the rate constants defining this reaction matrix, we can identify the mechanism of Dbp5 mediated RNA export and the regulatory nucleoporins mediated this interaction. A thorough explanation of the predictions made by each model can be found in the preceding paragraph.

FIGURES

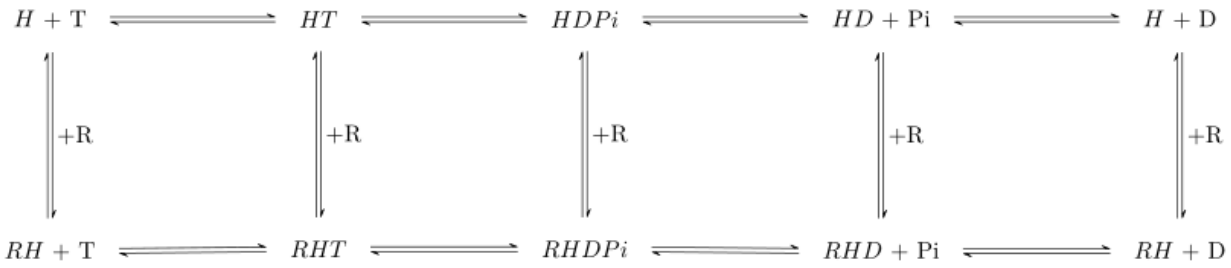

Scheme 1.1. Minimum reaction scheme for the native (top pathway) and RNA simulated (bottom pathway) ATPase cycle of Dbp5. H = Dbp5, T = ATP, D = ADP, P_i = inorganic phosphate, R = RNA.

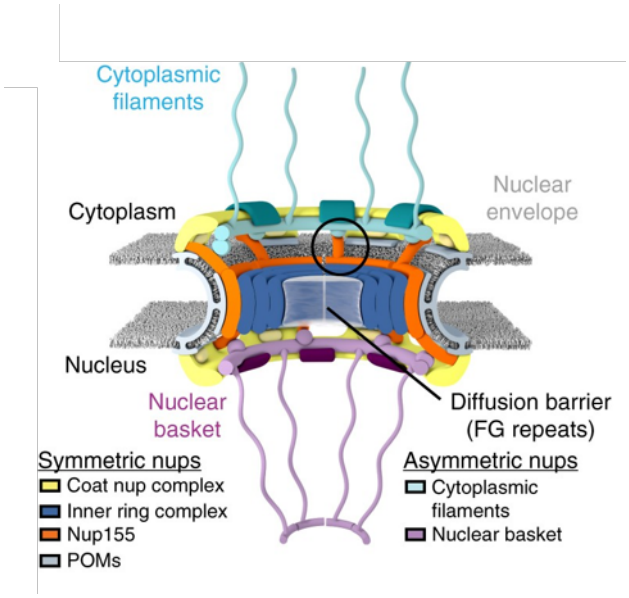

Figure 1.1. Molecular Diagram of Nuclear Pore Complex. NPCs act as diffusive barriers preventing free entry of molecules larger than ~ 40 kDa. NPCs are large multiprotein complexes that span the entirety of the nuclear envelope and help maintain the specialized microenvironment with the nucleus. Figure modified from reference (54).

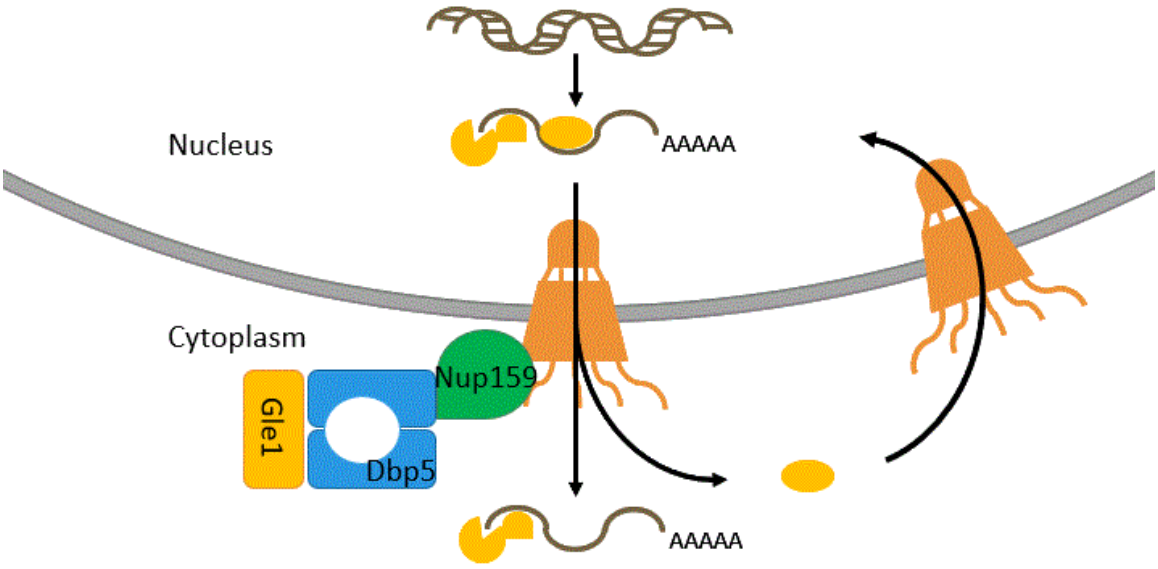

Figure 1.2. Dbp5 mediated mRNA remodeling mechanism. Dbp5 is thought to function in conjunction with Nup159 and Gle1 to remodel exported mRNA by removing certain protein components (such as Mex67-Mtr2 or Nab2) required for translocation through the NPC central pore. Removal of these factors following export prevents retro-grade diffusion of mRNA back into the nucleus and maintains the concentration gradient driving vectoral mRNP export.

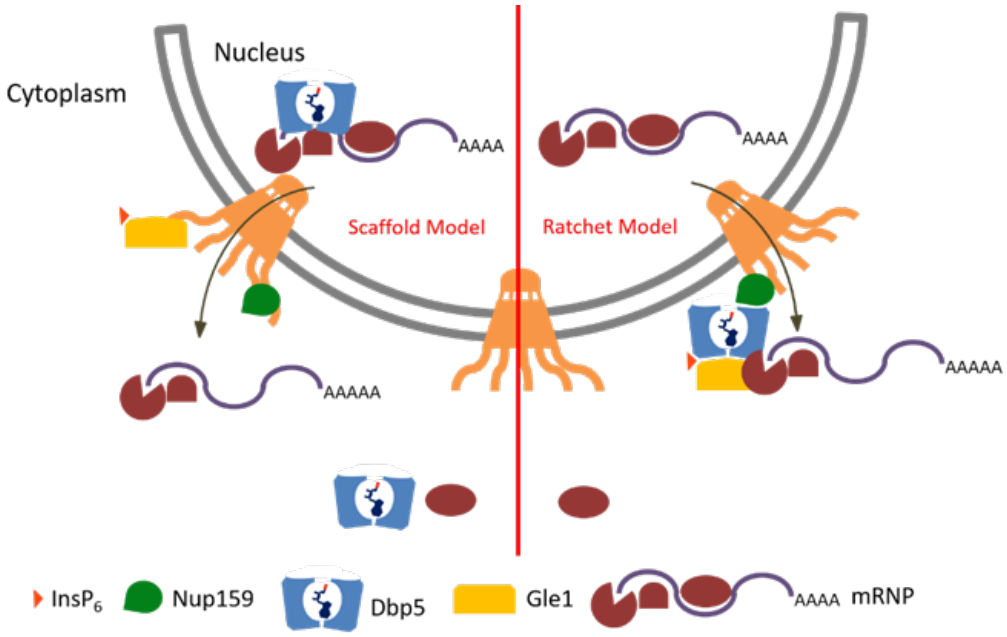

Figure 1.3. Ratchet vs Scaffold model of Dbp5 mediated mRNA export. Two models have been proposed for Dbp5 mediated mRNA export. The “Scaffold” model proposes that Dbp5 forms as part of the mRNP complex prior to export and transverses the NPC central channel to the cytoplasm at which point Nup159 and/or Gle1 activate mRNA remodeling by promoting ATP hydrolysis. Alternatively, the ratchet model asserts that Dbp5 remains attached to the cytoplasmic fibrils bound to Nup159 and/or Gle1 and facilitates mRNP remodeling following export.

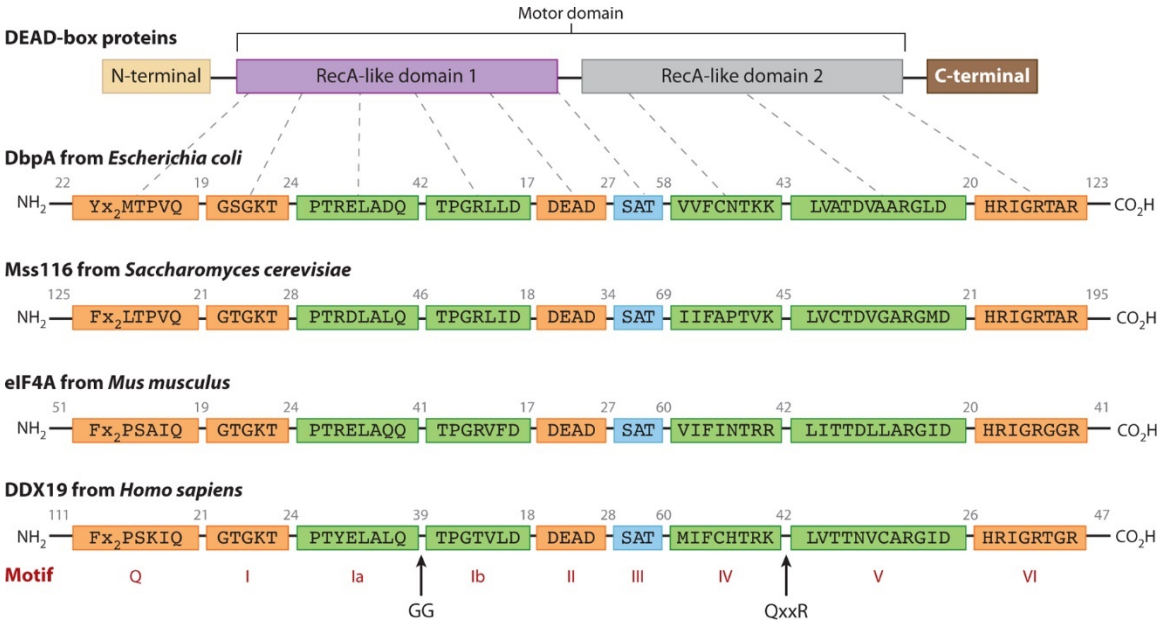

Figure 1.4. Sequence motifs of DEAD-box proteins. DEAD-box proteins display a high degree of conservation in amino acid sequence motifs involved in ATP binding (orange), RNA binding (green), and coupling between the two sites (teal). Figure modified from reference (42).

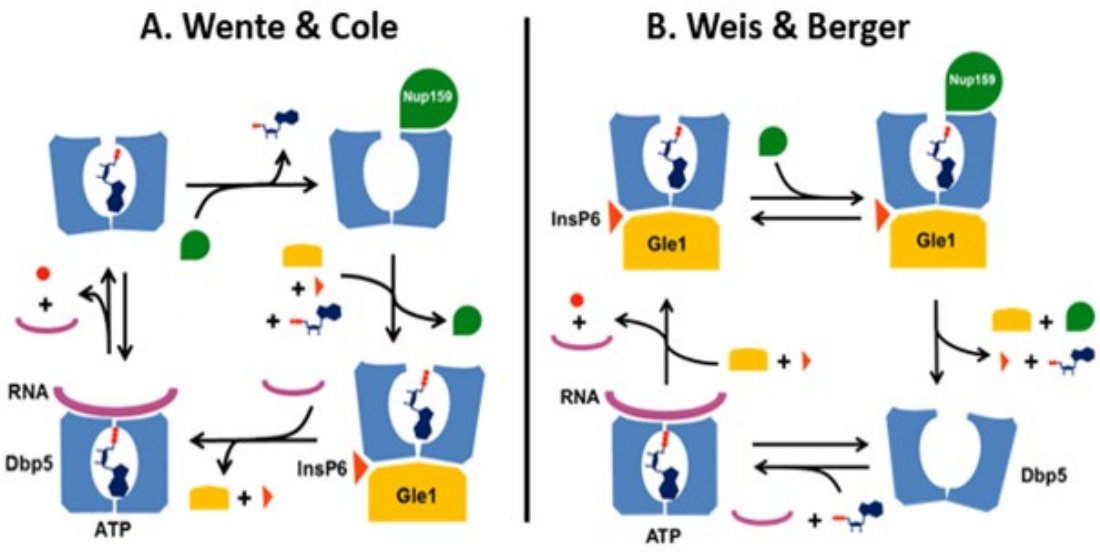

Figure 1.5. Two major models for how Nup159 and Gle1 influence the ATPase and RNA binding kinetics of Dbp5. A.) The Wente & Cole model (24) is based on a combination of genetic and biochemical data. B.) The Weis & Berger model is based upon x-ray crystal structures of various Dbp5, Nup159, Gle1, RNA, and nucleotide complexes (23).

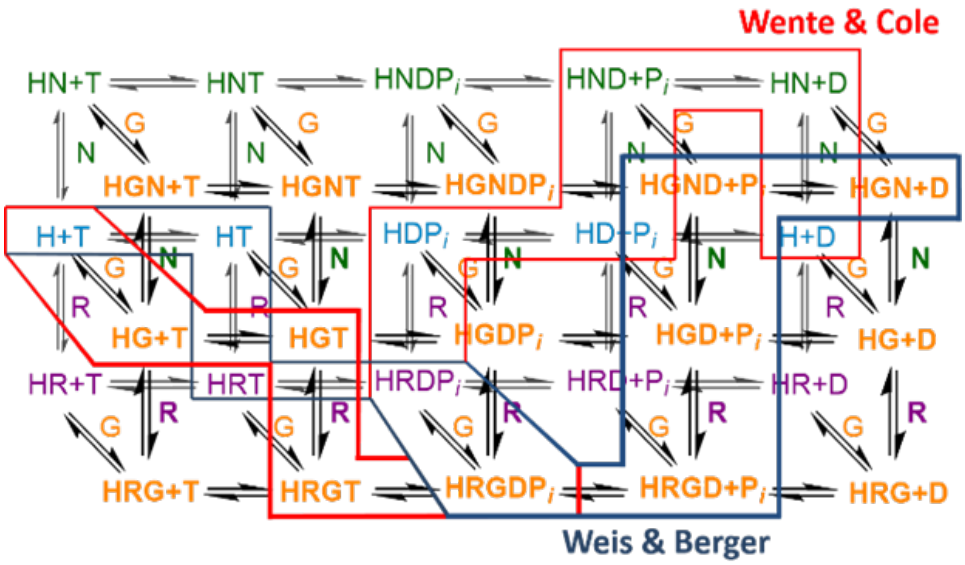

Figure 1.6. Preferred ATPase pathways of the two schematics models shown in Figure 1.5. Each of the models presented schematically in Figure 1.5 represents a preferred pathway through the entire potential Nup159 and Gle1 regulated ATPase and RNA binding matrix. H = Dbp5, T = ATP, D = ADP, P_i = inorganic phosphate, R = RNA, G = Gle1, N = Nup159.

CHAPTER 2: Influence of Mg^{2+} of Dbp5-regulator interactions and ATPase

Published as *Wong EV, *Gray SG, Cao W, Montpetit R, Montpetit B, De La Cruz EM (2018) Nup159 Weakens Gle1 Binding to Dbp5 But Does Not Accelerate ADP Release. *Journal of Molecular Biology* **430**, 2080-2095

* Indicates co-first authorship

This manuscript was a collective effort. I worked very closely with Emily V. Wong, a previous graduate student in the lab, in the data collection, analysis, and manuscript writing. We worked closely with a senior research scientist Wenxiang Cao and our research mentor Enrique M. De La Cruz in analyzing the data. All four of us wrote the manuscript with Ben Montpetit. Ben Montpetit supplied purified proteins for the data in Chapter 2.

ABSTRACT

Dbp5, DDX19 in humans, is an essential DEAD-box protein involved in mRNA export, which has also been linked to other cellular processes, including rRNA export and translation. Dbp5 ATPase activity is regulated by several factors, including RNA, the nucleoporin proteins Nup159 and Gle1, and the endogenous small molecule inositol hexakisphosphate ($InsP_6$). To better understand how these factors modulate Dbp5 activity and how this modulation relates to *in vivo* RNA metabolism, a detailed characterization of the Dbp5 mechanochemical

cycle in the presence of those regulators individually or together is necessary. In this study, we test the hypothesis that Nup159 controls the ADP-bound state of Dbp5. In addition, the contributions of Mg^{2+} to the kinetics and thermodynamics of ADP binding to Dbp5 were assessed. Using a solution based *in vitro* approach, Mg^{2+} was found to slow ADP and ATP release from Dbp5 and increased the overall ADP and ATP affinities, as observed with other NTPases. Further, Nup159 did not accelerate ADP release, while Gle1 actually slowed ADP release independent of Mg^{2+}. These findings are not consistent with Nup159 acting as a nucleotide exchange factor to promote ADP release and Dbp5 ATPase cycling. Instead, in the presence of Nup159, the interaction between Gle1 and ADP-bound Dbp5 was found to be reduced by ~18-fold, suggesting that Nup159 alters the Dbp5-Gle1 interaction to aid Gle1 release from Dbp5.

INTRODUCTION

Members of the DEAD-box protein (DBP) family couple energy from cycles of ATP binding, hydrolysis, and product release to RNA and RNP remodeling (34,55,56). RNA binding activates the intrinsic ATPase activity of many DBPs (20,42,57,58) by accelerating rate limiting step(s), e.g. ATP hydrolysis and/or product release (43,44). Numerous regulatory proteins also tune DBP ATPase rates through modulating ATPase cycle transitions and DBP interactions, which includes promoting conformations that favor nucleotide loading, RNA binding, relieve auto-inhibition, or alter product release (53,59-61). In turn, the

conformations and interactions of a DBP with binding partners are often linked to the chemical states of the bound nucleotide (34,42).

Dbp5, DDX19 in humans, is an essential DBP first described in *Saccharomyces cerevisiae* as being involved in mRNA export from the nucleus (6,7). Subsequent work has shown that Dbp5 is modulated by several regulatory factors, including RNA, the nucleoporin proteins Nup159 and Gle1, and the endogenous small molecule inositol hexakisphosphate ($InsP_6$) (5,14,16-18,20,21,23,24,62-64). The resulting phenotypic, genetic, biochemical, and structural data provides potential models by which these regulators may control Dbp5 ATPase activity and mRNA export *in vivo* (65). However, Dbp5 has also been linked to other cellular processes, including rRNA export and translation (38,64,66), complicating the interpretation of genetic and phenotypic data, and providing for the possibility of context-dependent regulation to facilitate multiple independent Dbp5 functions in RNA metabolism. Consequently, a detailed characterization of the Dbp5 mechanochemical cycle, and how this cycle is altered by regulators alone or in combination, is necessary to test and extend models of Dbp5 function. In other words, by determining the ATPase cycle rates and equilibrium constants in the presence of regulators, we can define the relevant events along the ATP hydrolysis pathway that represent control points for modulating Dbp5 activity *in vivo* and describe how regulators alter these events.

Towards this goal, our recent work showed that Dbp5 steady-state cycling (k_{cat}) in the presence and absence of RNA is most limited by inorganic phosphate (P_i) release, and that ATP affinity for Dbp5 is approximately 10-fold weaker than ADP

affinity (25). This detailed *in vitro* analysis identified P_i release and nucleotide exchange as potential biochemical transitions within the Dbp5 ATPase cycle that may be modulated *in vivo*. In line with this, it has been proposed that Nup159 and Gle1 influence the Dbp5 nucleotide bound state, specifically by Nup159 aiding ADP release and Gle1 promoting ATP binding (24). This model of Dbp5 regulation is consistent with high resolution structures showing that the two RecA-like domains of Dbp5 adopt an open configuration when bound by Gle1 and Nup159 (23), which may promote nucleotide exchange (i.e. ADP release and/or ATP loading).

Overall, the reported activities and structural data to date are supportive of Nup159 and Gle1 acting to alter the nucleotide state of Dbp5. One class of regulatory proteins, nucleotide exchange factors (NEFs), achieve this by accelerating the release of a protein bound nucleotide, often by disrupting coordination of the nucleotide-associated magnesium cation (67,68). Eviction of the nucleotide-bound cation, which mediates several key interactions between nucleotide and protein, enables rapid dissociation of the nucleotide (e.g. ADP) from the active site, subsequent binding of nucleotide (e.g. ATP), and an additional round of ATPase cycling. This mechanism of regulation has not been well described for DBPs, but Mg^{2+}-based NEFs have been shown to regulate several GTPase proteins (69-72), actin (73), kinesin (74,75) and myosin motor proteins (76,77). One exception is the *S. cerevisiae* NEF, Ypt1p, which accelerates nucleotide release from the TRAPPI GTPase through a Mg^{2+} independent pathway (78). Consequently, it is unknown whether DBPs also

employ Mg^{2+}-based NEFs, or whether Nup159 or Gle1 act as NEFs through Mg^{2+} to regulate Dbp5 activity.

Here, we test the hypothesis that Nup159 and Gle1 control the ADP-bound state of Dbp5, and further assess the contributions of Mg^{2+} to the kinetics and thermodynamics of ADP binding to Dbp5. We report that Mg^{2+} slows mantADP and mantATP release from Dbp5, as observed with other NTPases (71,75,76), and increased the overall ADP and ATP affinities (~3-fold for mantADP, 2-fold for ADP, ~6-fold for mantATP, and 3-to-5-fold for ATP). We find that Nup159 does not accelerate mantADP or Mg^{2+}-mantADP release, while Gle1/$InsP_6$ slowed mantADP release ~2-fold independent of Mg^{2+}. These findings are inconsistent with Nup159 or Gle1 acting as a NEF. Finally, binding affinity of Gle1 for the mantADP-bound Dbp5 complex was reduced ~18-fold in the presence of Nup159, suggesting that Nup159 may function *in vivo* to modulate the interaction between Dbp5 and Gle1.

MATERIALS AND METHODS

Reagents - All reagents were of the highest purity commercially available. ATP (Sigma, A7699) and ADP (Sigma, 01879) concentrations were determined by absorbance using ε259 = 15,400 M-1 cm-1. mantATP (Jena Biosciences, NU-202 and Invitrogen, M12417) and mantADP (Jena Biosciences, NU-201 and Invitrogen, M12416) concentrations were determined by absorbance using ε255 = 23,300 M-1 cm-1. Inositol hexakisphosphate (phytic acid) was purchased from

Santa Cruz Biotechnology (SC-253276). Buffers were made with either DEPC treated water (American Bio, AB021028) or Millipore MilliQ® distilled deionized water that had been filtered through a 0.2 μm filter. Experiments were performed at 25 °C in assay buffer: 30 mM Hepes (pH 7.5), 100 mM KCl, and 2 mM DTT, supplemented with the indicated [MgCl2] or [EDTA]. For all experiments, the free Mg2+ concentration ([Mg2+]free) was determined using the program WebMaxC Standard (version - 12/31/03; http://web.stanford.edu/~cpatton/webmaxcS.htm).

Protein purification - Dbp5, Gle1, and Nup159 were purified as described [43].

Transient kinetic assays - Transient kinetic measurements were performed on an Applied Photophysics SX20 stopped-flow instrument thermostatted at 25 ± 0.1 ºC. mant-nucleotide binding to Dbp5 was monitored by FRET between excited tryptophans (λex = 280 nm) in Dbp5 and the bound mant-labeled nucleotide. Fluorescence intensity was measured at 90º relative to excitation light after passing through a 400 nm long-pass colored glass filter. Inner filter effects are minimal in the mant-labeled nucleotide concentration range employed (69,79). Time courses shown are averages of at least two traces. Fitting was performed by nonlinear least-squares regression, and uncertainties of quantities determined from fits are given as standard errors in the fits.

mantADP dissociation kinetics - Irreversible dissociation of mantADP bound to Dbp5 was achieved by mixing with a large excess of unlabeled ADP to prevent mantADP rebinding. mantADP dissociation from Dbp5 in solution was measured as a function of [Mg2+]free using two approaches. First, Dbp5-mantADP was pre-formed in the presence of saturating Mg2+ by pre-equilibrating 4 μM Dbp5

and 60 μM mantADP in assay buffer containing 2 mM MgCl2 prior to initiating mantADP dissociation by rapidly mixing with a solution of 20 mM ADP supplemented with either 40 mM (for no Mg2+ only) or 3 mM EDTA, and a range of [MgCl2] to generate 0.057-2000 μM final [Mg2+]free after mixing and accounting for EDTA, mantADP and ADP chelation. Alternatively, Dbp5-mantADP was pre-formed in the absence of Mg2+ with assay buffer containing 4 mM EDTA to ensure no free Mg2+ at the start of the reaction, before being mixed with 20 mM ADP and a range of MgCl2 to generate 0.051-2000 μM [Mg2+]free after mixing. The final concentrations after mixing are 2 μM Dbp5, 30 μM mantADP and 10 mM competing unlabeled ADP.

[Nup159]-dependent Mg2+mantADP dissociation, with saturating Mg2+ (2 mM) in solution throughout the reaction, was monitored by mixing a pre-equilibrated solution of 4 μM Dbp5 and 40 μM mantADP in assay buffer containing 2 mM MgCl2 with equal volumes of a range of [Nup159] in assay buffer supplemented with 8 mM MgCl2 and 6 mM ADP (2 mM Mg2+ in solution after ADP chelation). [Nup159]-dependent mantADP dissociation without Mg2+ was monitored by mixing pre-equilibrated solutions of 2 μM Dbp5 and 80 μM mantADP in assay buffer containing 11.05 mM EDTA with equal volumes of assay buffer containing 20 mM ADP, 11.05 mM EDTA (ca. 27 nM [Mg2+]free after mixing), and various concentrations of Nup159. [Gle1]-dependent Mg2+-mantADP (saturating Mg2+ in solution) and mantADP (no Mg2+) dissociation were measured identically to Nup159, with the modification that the assay buffer in both syringes included 15 μM InsP6. Mg2+-mantADP dissociation from Nup159-Gle1-Dbp5 complex with

saturating Mg2+ in solution was performed by mixing a pre-equilibrated solution of 5 μM Nup159, 4 μM Dbp5, 40 μM mantADP, and 15 μM InsP6 with an equal volume solution of 6 mM Mg2+ADP and 15 μM InsP6 pre-equilibrated with varying concentrations of Gle1. The assay buffer in both syringes for Mg2+-mantADP dissociation from the Nup159-Gle1-Dbp5 complex included an additional 2 mM MgCl2 in excess of the nucleotide concentration.

mant-labeled nucleotide association kinetics - The kinetics of mantADP binding to Dbp5 in the absence of Mg2+ was monitored by mixing Dbp5 (final concentration after mixing is 1 μM) with various concentrations of mantADP, in assay buffer containing 10 mM EDTA. Time courses were fitted to a single exponential and the [mantADP]-dependence of the observed pseudo-first order rate constants was fitted to a linear equation to extract bimolecular binding on- and off- rate constants from the slope and y-intercept, respectively.

mantATP binding was performed identically to mantADP binding experiments, but the time courses were fitted to three exponentials. The [mantATP]-dependence of the two fastest observed rate constants were globally fitted to Equation 2.2 in the text (25,44) to determine fundamental rate constants. The third observed phase for mantATP binding while in the absence of Mg2+ is very slow (0.1 s-1) compared to the two fast observed phases and may represent a downstream process or off-pathway reaction. As in our previous analysis of mantATP binding in the presence of Mg2+ (25), we have not included this phase in our reaction schemes, since it is too slow to influence the two faster processes.

Competition of mantADP and unlabeled nucleotide - Dbp5 (final concentration after mixing is 1 μM in ADP containing reactions; 2 μM in ATP containing reactions) was rapidly mixed with 40 μM mantADP (final after mixing) and varying concentrations of unlabeled nucleotide, in assay buffer containing 1.5 mM (ADP reactions) or 2.5 mM (ATP reactions) EDTA. Time courses of FRET signal change from mantADP binding to Dbp5 in the presence of varying amounts of unlabeled ATP or ADP followed double exponentials (Figure 2.3A). The slow phase occurring at 0.1 – 0.6 s-1 has a small amplitude compared to the fast phases in both ATP and ADP competition cases and has no well-defined dependence on [ATP] or [ADP]. Since the processes presented by the slow phases in both cases are temporally well-separated from the initial event involving mantADP binding competition with unlabeled nucleotides, we analyzed only the fast, [ADP] or [ATP]-dependent observed rate constant without interference from the slow phase.

RESULTS

Removal of [Mg^{2+}] from Dbp5 accelerates mantADP release

Prior to testing regulators for Mg^{2+}-based NEF activity, it was necessary to determine how Mg^{2+} influences nucleotide exchange and binding. To evaluate the impact of magnesium on nucleotide-Dbp5 interactions (Scheme 2.1), time courses of Dbp5-mantADP dissociation in the presence of saturating Mg^{2+} and absence (i.e. with excess EDTA) of Mg^{2+} were collected (Figure 2.1A). The

resulting data are best fit by single exponentials where the observed rate constant depends hyperbolically on $[Mg^{2+}]_{free}$ (Figure 2.1B), yielding a mantADP dissociation rate constant ($k_{-mD(+Mg)}$) of 2.4 ± 0.01 s^{-1} in the presence of Mg^{2+}, and four-fold more rapid mantADP dissociation in the absence of Mg^{2+} with a rate constant ($k_{-mD(-Mg)}$) of 10.0 ± 0.4 s^{-1} (Figure 2.1A, Table 2.1). We interpret these and other related results with the assumption that the impact of Mg^{2+} on nucleotide binding arises from its direct association with the nucleotide at the Dbp5 active site, though contributions from Mg^{2+} binding to secondary sites on Dbp5 cannot be ruled out. Identical results are obtained when starting with a preformed Dbp5-Mg^{2+}-mantADP complex (in the presence of excess $MgCl_2$) or with a preformed Dbp5-mantADP complex in the absence of Mg^{2+} (excess EDTA present in buffer prior to mixing; Figure 2.1B) before rapidly mixing with excessive competing unlabeled ADP and varying concentration of $MgCl_2$. These results indicate that Mg^{2+} rapidly equilibrates between the Dbp5 active site and bulk solution on a timescale much greater than that of mantADP dissociation.

We fitted the $[Mg^{2+}]_{free}$-dependent observed dissociation rate constant as a weighted average of Mg^{2+}-mantADP and mantADP dissociation according to Equation 2.1:

$$\begin{aligned} k_{obs} &= k_{-mD(-Mg)}\frac{[HmD]}{[HmD]+[HMgmD]} + k_{-mD(+Mg)}\frac{[HMgmD]}{[HmD]+[HMgmD]} \\ &= k_{-mD(-Mg)} + \left(k_{-mD(+Mg)} - k_{-mD(-Mg)}\right)\frac{[HMgmD]}{[HmD]+[HMgmD]} \\ &= k_{-mD(-Mg)} + \frac{k_{-mD(+Mg)} - k_{-mD(-Mg)}}{K_{Mg,HmD}+[Mg]}[Mg] \end{aligned} \tag{2.1}$$

where $k_{-mD(+Mg)}$ and $k_{-mD(-Mg)}$ are the mantADP dissociation rate constants with and without Mg^{2+}; [*HMgmD*] and [*HmD*] are Dbp5-mantADP complex with and without Mg^{2+}; [Mg] is $[Mg^{2+}]_{free}$, and $K_{Mg,HmD}$ is the equilibrium dissociation constant for Mg^{2+} binding to Dbp5-mantADP. The simplified hyperbolic form of the *HMgmD* species is used since the total Mg^{2+} concentration in the titration range available to bind *HmD* complex >> total [*HmD*]. Using Equation 2.1, the best fit of the data for both sets of measurements in Figure 2.1B yields a Mg^{2+} affinity for Dbp5-mantADP ($K_{Mg,HmD}$) of ~ 164 μM (Table 2.1) with a mantADP dissociation rate constant of ~ 2.4 s^{-1} with Mg^{2+} and ~ 9 s^{-1} without Mg^{2+}, indicating that Mg^{2+} occupancy slows mantADP release.

Mg^{2+} modifies kinetics of mant nucleotide binding to Dbp5

To measure the kinetics of mantADP binding in the absence of Mg^{2+} (Scheme 2.1), time courses of FRET signal change upon mantADP association were collected following rapid mixing of Dbp5 with mantADP. In the absence of Mg^{2+}, mantADP binding traces are well-described by single exponentials with observed rate constants that depend linearly on the mantADP concentration (Figure 2.2A). The association rate constant in the absence of Mg^{2+} ($k_{+mD(-Mg)}$) determined from the slope of the best linear fit of the data is 1.0 ± 0.1 μM^{-1} s^{-1}, while the dissociation rate constant ($k_{-mD(-Mg)}$) estimated from the y-intercept is 15 ± 2 s^{-1} (Figure 2.2B, Table 2.1), slightly faster than the value of ~9-10 s^{-1} determined from irreversible dissociation measurements (Figure 2.1). The mantADP affinity in the absence of Mg^{2+} ($K_{mD(-Mg)}$) calculated from the ratio of dissociation and association rate constants is 15 ± 2.5 μM.

We previously observed multi-step mantADP binding in the presence of Mg^{2+} (25), as indicated by the apparent hyperbolic [mantADP] concentration-dependence of the observed rate constant with a weak affinity of K_{mD0} ~100 μM for the fast binding step. In the mantADP titration range that satisfies the condition [*mD*] < K_{mD0} ~100 μM, the hyperbolic [mantADP] concentration-dependence of the observed rate constant approximates to linear (80,81)_ENREF_43, and the overall on- and off rate constants for the combined two step binding can be approximately estimated by fitting this data (25) to a linear function, yielding Mg^{2+}mantADP association ($k_{+mD(+Mg)}$) and dissociation ($k_{-mD(+Mg)}$) rate constants of 0.58 ± 0.07 $\mu M^{-1}\,s^{-1}$ and 2.9 ± 0.9 s^{-1}, respectively. The ratio of association and dissociation rate constants yields a Mg^{2+}mantADP affinity of 5 ± 2 μM. Thus, Mg^{2+} slows mantADP dissociation and to a lesser extent mantADP association, explaining the overall weaker Dbp5-mantADP binding affinity (~ 2-3 fold) in the absence of Mg^{2+}.

In the case of mantATP, time courses of binding to Dbp5 in the absence of Mg^{2+} are well-fitted by three exponentials (Figure 2.2C), similar to binding measured in the presence of Mg^{2+} (25). We assume that the two fastest [mantATP]-dependent transitions occur in series and the first observed phase is from mantATP binding, while the second observed phase is a combined/overall step that involves downstream ATPase reactions, including ATP hydrolysis (44). Therefore, the two observed fast phases can be globally fitted to Equation 2.2 to determine rate constants in the ATPase reaction scheme (25,44).

$$k_{1,2obs} = \frac{1}{2}\left(k_{+1}[mT] + k_{-1} + k_{+2} + k_{-2} \pm \sqrt{(k_{+1}[mT] + k_{-1} + k_{+2} + k_{-2})^2 - 4(k_{+1}[mT]k_{+2} + k_{-1}k_{-2} + k_{+1}[mT]k_{-2})}\right) \quad (2.2)$$

In Equation 2.2, [mT] is the total mantATP concentration , k_{+1} and k_{-1} are the fundamental forward and reverse rate constants for step 1 (mantATP binding), and k_{+2} and k_{-2} are the forward and backward rate constants for combination step 2 (including mantATP hydrolysis) (25,44). The mantATP association rate constant in the absence of Mg^{2+} determined from the fit is 3 ± 1 μM^{-1} s^{-1} (Figure 2.2D, Table 2.1) and is comparable to the rate constant measured in the presence of Mg^{2+} (1.63 μM^{-1} s^{-1} from (25)). In contrast, the mantATP dissociation rate constant is an order of magnitude faster in the absence of Mg^{2+} (~125 s^{-1}; Figure 2.2D; Table 2.1) as compared to the presence of Mg^{2+} (~11.9 ± 0.7 s^{-1} from (25)). As in our previous analysis of mantATP binding in the presence of Mg^{2+} (25), we have not included the third phase in our reaction schemes, since it is too slow to influence the two faster processes (see Materials and Methods). Together, these measurements show that Mg^{2+} has a strong effect on mantATP dissociation, which is ~4 fold greater than the impact of Mg^{2+} on mantADP dissociation.

Mg^{2+} tightens unlabeled ADP and ATP binding to Dbp5

To extend and validate these measurements, the affinity of Dbp5 for unlabeled nucleotides in the absence of Mg^{2+} was determined by kinetic competition experiments between mant-labeled and unlabeled nucleotides (Figure 2.3), as previously done in the presence of Mg^{2+} (25,79). ADP or ATP competition slows

the observed fast mantADP binding phase (Figure 2.3B and 2.3C), indicating that the [ADP]- or [ATP]-dependent mantADP observed rate constants can be fitted by Equation 2.3 below (25,82), derived specifically for cases in which the unlabeled competitor binds in rapid equilibrium in advance of labeled ligand binding.

$$k_{obs} = k_{obs,\mathrm{inf}} + \frac{k_{k_{obs,0}} - k_{obs,\mathrm{inf}}}{1 + \frac{[ADP]}{K_D}} \tag{2.3}$$

In Equation 2.3, K_D is the unlabeled ADP equilibrium binding constant. $k_{obs,0}$ and $k_{obs,\mathrm{inf}}$ (with unit s^{-1}) are the observed mantADP rate constant at 0 and saturating unlabeled [ADP], i.e. $k_{obs,0} = k_{+\mathrm{mD}}$ [*mD*]+$k_{-\mathrm{mD}}$ and $k_{obs,\mathrm{inf}} = k_{-\mathrm{mD}}$. To analyze ATP competition data, replace [ADP] and K_D by [ATP] and K_T, respectively. Fitting the [ADP] or [ATP]-dependence of the observed mantADP binding rate constant in Figure 2.3B or 2.3C to Equation 2.3 gives the apparent ATP affinity ($K_{\mathrm{T(-Mg)}}$ = 15 ± 4 mM) or ADP affinity ($K_{\mathrm{D(-Mg)}}$ = 0.8 ± 0.1 mM) in the absence of Mg^{2+} (Table 2.1), and a mantADP dissociation ($k_{-\mathrm{mD(-Mg)}} = k_{obs,\mathrm{inf}}$ ~ 6 - 10 s^{-1}) and association rate constant ($k_{+\mathrm{mD(-Mg)}}$ ~ 1.2 - 1.4 μM^{-1} s^{-1}) (Table 2.1). The equilibrium constant (15 mM) for unlabeled ATP binding to Dbp5 is ~3-5-fold weaker than the 3 - 6 mM affinity of Mg^{2+}-ATP (25), and unlabeled ADP (0.8 mM) binding is ~2-fold weaker than that of Mg^{2+}-ADP (Table 2.1) (25,83). These data obtained here by ADP and ATP competition are consistent with the mantADP binding and irreversible dissociation measurements made in the absence of Mg^{2+} in Figure 2.1 and 2.2 (see Table 2.1).

A similar procedure for the derivation of Equation 2.3 can be performed without imposing the assumption of unlabeled competitor binding in rapid equilibrium by solving differential equations describing the competitive binding of labeled and unlabeled ligands for protein to yield Equation 2.3', below:

$$k_{obs} = 2\frac{k_{obs,\mathrm{inf}}[ADP] + K_D k_{obs,0}}{\frac{k_{obs,0}}{k_{+D}} + [ADP] + K_D + \sqrt{\left(\frac{k_{obs,0}}{k_{+D}} + [ADP] + K_D\right)^2 - 4\frac{k_{obs,\mathrm{inf}}[ADP] + K_D k_{obs,0}}{k_{+D}}}} \quad (2.3')$$

In Equation 2.3', the symbols are the same as in Equation 2.3 with an additional parameter, k_{+D}, which is the unlabeled ADP bimolecular association rate constant expressed with identical concentration units as the equilibrium binding constant K_D. Under conditions where

$$K_D + [ADP] >> \frac{k_{+mD}[mD] \pm k_{-mD}}{k_{+D}} = \frac{k_{obs,0} \text{ or } k_{obs,0} - 2k_{obs,\mathrm{inf}}}{k_{+D}}$$

, the quadratic form of Equation 2.3' is simplified to a hyperbolic form given in Equation 2.3. Equation 2.3 and 2.3' and the conditions and discussions above apply to ATP competition as well, while replacing [ADP] and K_D by [ATP] and K_T, respectively. Compared to Equation 2.3, Equation 2.3' is more general and does not need the presumption of unlabeled competitor binding in rapid equilibrium. Moreover, Equation 2.3' further permits determination of unlabeled nucleotide binding rate constants (k_{+D}) to provide a sense of the timescale of unlabeled nucleotide binding, though it is an approximation and subject to large error due to the rapid equilibration of unlabeled competitor.

In the absence of Mg^{2+}, unlabeled ADP and ATP competition data in Figures 2.3B and C are fitted equally well to Equation 2.3' and Equation 2.3, even though the parameter k_{+D} (k_{+T}) has a large error. The results for the remaining parameters are essentially the same for both equations. The best fit curves generated by the two equations are indistinguishable. Fitting results by Equations 2.3' estimate an ADP association rate constant ($k_{+D(-Mg)}$) of ~ 2 μM^{-1} s^{-1} and an ATP association rate constant ($k_{+T(-Mg)}$) that is even faster. We estimate from these association rate constants and binding affinities that ADP dissociates ($k_{-D(-Mg)}$) at ~1600 s^{-1} and ATP dissociates ($k_{-T(-Mg)}$) at > 30000 s^{-1} (Table 2.1). These extremely rapid rate constants are subject to large uncertainty and may only provide lower estimates of dissociation rate constants. However, these data highlight the fact that ADP and ATP binding to Dbp5 are in extremely fast equilibrium, similar to binding in the presence of Mg^{2+} (25), which suggests that a NEF would not be necessary to accelerate nucleotide exchange.

Nup159 does not accelerate mantADP release from Dbp5

Previous work has provided evidence for Nup159 accelerating ADP release from Dbp5 (24). Structural work has further shown that Nup159 binds Dbp5 in a manner mutually exclusive with RNA (22,23), and may allow separation of the two RecA-like domains of Dbp5 to facilitate nucleotide exchange. The interactions of Nup159 with Dbp5-ADP and -Mg^{2+}ADP relevant to potential Nup159 NEF activity are shown in the top half of Scheme 2.2, where N represents Nup159. To detail these interactions, time courses of mantADP dissociation from Dbp5 were collected in the presence of saturating Mg^{2+} upon

rapid mixing with Nup159 and excess competing unlabeled ADP. These data followed single exponentials (Figure 2.4A), with observed rate constants that slow in a weakly [Nup159]-dependent manner over the range examined (0-14 μM; Figure 2.4B). The observed rate constant of Mg^{2+}-mantADP dissociation decreased from 2.7 ± 0.1 s^{-1} ($k_{-mD(+Mg)}$) to 2.0 ± 0.2 s^{-1} ($k_{-mD(+Mg),\,N}$) in the presence of excess Nup159 (Figure 2.4B). Fitting [Nup159]-dependent observed rate constants of mantADP dissociation in the presence of Mg^{2+} to Equation 2.4, a population weighted average of Nup159 (N) bound and un-bound mantADP-Dbp5 complexes:

$$k_{obs} = k_{-mD}\frac{[HmD]}{[HmD]+[NHmD]} + k_{-mD,N}\frac{[NHmD]}{[HmD]+[NHmD]}$$
$$= k_{-mD} + \left(k_{-mD,N} - k_{-mD}\right)\frac{[HmD]_{tot} + [N]_{tot} + K_N - \sqrt{([HmD]_{tot} + [N]_{tot} + K_N)^2 - 4[HmD]_{tot}[N]_{tot}}}{2[HmD]_{tot}} \quad (2.4)$$

yields an affinity ($K_{N(+Mg)}$) of ~ 0.3 ± 0.8 μM for Nup159 binding to Dbp5-Mg^{2+}mantADP, where k_{-mD} and $k_{-mD,N}$ are mantADP dissociation rate constants from Dbp5 without and with bound regulator Nup159 , and K_N is the equilibrium constant of Nup159 binding to Dbp5-mantADP (*HmD*). $[HmD]_{tot}$ = [*HmD*] + [*NHmD*] by mass balance. Time courses of mantADP dissociation from Dbp5 upon rapid mixing with Nup159 and excess competing unlabeled ADP in the absence of Mg^{2+} also followed single exponentials, with no observable [Nup159] dependence in the rate constants (~11 ± 2 s^{-1} Figure 2.4C and 2.4D). Together, these measurements do not support a role for Nup159 in accelerating ADP release from Dbp5.

Gle1 slows mantADP release from Dbp5

Crystal structures of the Gle1-$InsP_6$-Dbp5-ADP complex showed that Gle1 contacts both RecA-like domains and orients them in a partially open conformation (23), and thus considered the possibility that this domain orientation may promote nucleotide exchange. The possible relationships between Gle1 and Dbp5-ADP and -Mg^{2+}ADP interactions are detailed in the bottom half of Scheme 2.2. As with Nup159, time courses were collected of irreversible [Gle1]-dependent mantADP release from Dbp5-$InsP_6$ in the presence (Figure 2.5A) and absence of Mg^{2+} (Figure 2.5C). Data are well-fitted by single exponentials, with observed rate constants that depend hyperbolically on the [Gle1] (Figure 2.5B, 2.5D). In the absence of Mg^{2+} there is a slow increase in background signal due to Gle1 itself, independent of binding, that was accounted for by an additional exponential. Under excess Gle1 conditions, mantADP release from Dbp5 slowed about two-fold from 2.4 ± 0.1 s^{-1} to 1.3 ± 0.3 s^{-1} in the presence of Mg^{2+} and from 10.5 ± 0.1 s^{-1} to 6.3 ± 0.2 s^{-1} in the absence of Mg^{2+} (Table 2.2). Fitting the [Gle1]-dependence of the observed rate constants to Equations 2.4 (substituting *N* with *G* (Gle1)) yields a Gle1 affinity for the $InsP_6$-Dbp5-ADP complex of 0.1 ± 0.3 μM with Mg^{2+} ($K_{G(+Mg),\,HmD}$) and 0.3 ± 0.1 μM without Mg^{2+} ($K_{G(-Mg),\,HmD}$), suggesting the impact of Mg^{2+} is minimal given the measurement uncertainties. Based on these measurements, Gle1 does not accelerate ADP release from Dbp5.

Nup159 weakens Gle1 affinity for Dbp5-Mg^{2+}mantADP complex

Current models propose that Dbp5 is regulated at nuclear pore complexes in a series of interactions with RNA, Gle1-$InsP_6$ and Nup159 to facilitate mRNA

export (23,24,65). One component of these models is that Dbp5 sequentially interacts with Gle1 and Nup159 to spatially modulate the Dbp5 ATPase cycle. Moreover, structural work has shown that binding of Nup159 to a Gle1-$InsP_6$-Dbp5-ADP complex induces solvent accessible separation of the two RecA-like domains of Dbp5 (23), which may favor nucleotide exchange. Consequently, to investigate the possibility that NEF activity emerges in the presence of both regulators, time courses of irreversible Mg^{2+}-mantADP dissociation from Dbp5 in buffer containing 2.5 μM Nup159 and 15 μM $InsP_6$ were measured upon rapid mixing with varying concentrations of Gle1 and excessive competing ADP. These data fit single exponentials (Figure 2.6A), where the observed rate constant of Mg^{2+}-mantADP dissociation slowed monotonically with [Gle1] (Figure 2.6B). The best fit of the observed rate constant to Equation 2.4 gives the affinity of Dbp5-mantADP for Gle1 in the presence of Nup159 and $InsP_6$ ($K_{G(+Mg),HNmD}$) as 1.8 ± 3.2 μM (Figure 2.6B), ~18 times weaker than that in the absence of Nup159 (0.1 ± 0.3 μM). The fit also yields a mantADP dissociation rate constants of 2.2. ± 0.1 s^{-1} in the presence of Nup159 ($k_{-mD(+Mg),N}$) and $InsP_6$ (no Gle1) and 0.8. ± 0.9 s^{-1} in the presence of Nup159, $InsP_6$ and Gle1 ($k_{-mD(+Mg),GN}$), similar to the mantADP dissociation rate constants with Gle1 and $InsP_6$ (no Nup159; $k_{-mD(+Mg)}$ =2.4 ± 0.1 s^{-1} and $k_{-mD(+Mg),GN}$ = 1.3 ± 0.3 s^{-1}; Figure 2.5). These results indicate that binding of Nup159 to Dbp5 significantly alters the association between Dbp5 and Gle1, but still has minimal impact on mantADP release from Dbp5 in the presence of Gle1- $InsP_6$.

DISCUSSION

Genetics, cell biology, biochemistry and structural biology have significantly contributed to the understanding of Dbp5, including regulation of the Dbp5 ATPase cycle, leading to various models of Dbp5 mediated mRNA export (39,65,84-87). Here we present quantitative kinetic and thermodynamic data that provides evidence for an alternative model of Nup159–mediated regulation of Dbp5, achieved by mediating the interaction of Dbp5 with Gle1.

Note that the complexes and data presented here do not include RNA, which may alter Nup159 and Gle1 activities in regulating ADP release as NEFs. However, previous studies suggest that potential NEF activity from Nup159 or Gle1 binding to the Dbp5-ADP complex occurs after RNA release (23,24). Still, it is possible that transient co-binding of RNA, Gle1 and ADP during steady-state ATPase cycling (i.e. following hydrolysis and Pi release) may provide the opportunity for RNA to influence nucleotide and regulator interactions. For this reason, we limit our discussions and conclusions to ADP-bound complexes formed in the absence of RNA.

Mg^{2+}-Nucleotide binding linkage in Dbp5

Although many NTPases require a Mg^{2+} cofactor for hydrolysis of the phosphodiester bond (88), persistence of Mg^{2+} in the post-hydrolysis active site can inhibit NDP dissociation and therefore recycling of the enzyme. In the Ras superfamily of small GTPases, the presence of Mg^{2+} contributes to extremely tight GDP binding affinities with dissociation constants that can be in the

subnanomolar range (89,90). Consequently, by altering Mg^{2+} binding and accelerating off rates, NEFs are able to spatially and temporally regulate a vast number of cellular processes (91). Like the Ras family and other NTPases, Mg^{2+} is also an important cofactor for nucleotide binding and hydrolysis by DBPs (34,92). A previous study had identified Mg^{2+}-mediated inhibition of helicase activity for Dbp5, and another DBP Sub2, but the mechanism of inhibition was not identified and may be multifaceted given the duplex unwinding readout, which encompasses all steps of the ATPase cycle, as well as Mg^{2+}-sensitive protein-RNA and RNA-RNA interactions (93). Therefore, it is not known if Mg^{2+} is a target for regulators that function to control discrete transitions within the DBP ATPase activity.

In these studies, Mg^{2+} was found to bind Dbp5-mantADP with an affinity of ~164 μM. The presence of Mg^{2+} slowed mantADP dissociation ~4-6 fold and decreased mantADP association, which resulted in a modest tightening of mantADP binding affinity for Dbp5 (3-fold) from ~15 μM to ~5 μM (Table 2.1). Unlabeled ADP binding affinity was also observed to tighten 2-fold from 0.8 to 0.36 mM in the presence of Mg^{2+} using kinetic competition assays with mantADP (Figure 3 and (25)). Mg^{2+} tightened the affinity of Dbp5 for mantATP ~6-fold (42 to 7.3 μM, K_{1mT} or K_{mT} comparison, Table 2.1 and (25)) and unlabeled ATP ~3 - 5-fold (15 to 3 - 6 mM, Table 2.1 and Figure 2.3) as well. We assume these Mg^{2+} effects originate from a Mg^{2+} cation bound to the nucleotide in the active site of Dbp5, although Mg^{2+} may interact with secondary regulatory sites on Dbp5. Under this assumption, the affinity of Mg^{2+} for Dbp5-ADP or -ATP can be

estimated to be ~113 and 17 μM, respectively (Table 2.1). These values are calculated using literature values for affinity of Mg^{2+}ADP of ~676 μM and Mg^{2+}ATP of 87 μM under our experimental conditions (94,95) and using the subsequent detailed balance of Scheme 2.1, where in the case of ATP, ADP (D) is replaced by ATP. The ~7-fold tighter affinity of Mg^{2+} for Dbp5-ATP (17 μM) as compared to Dbp5-ADP (113 μM) might be expected from the presence of the gamma phosphate, which helps coordinates the cation in the pre-hydrolysis active site.

To our knowledge, this is the first study to investigate the role of Mg^{2+} in stabilizing the nucleotide-bound state of a DBP and may prove to be a more general model for DBP-nucleotide interactions given the evidence for Mg^{2+}-linked nucleotide associations in other NTPase families (67-70,72-78,96), including the superfamily I helicases (97). Notably, *S. cerevisiae* intracellular $[Mg^{2+}]_{free}$ is estimated to be 0.1-1 mM (94), and is known to fluctuate throughout the cell cycle and in response to environmental conditions (94,98). As such, Dbp5-ADP is potentially responsive to these cellular fluctuations in Mg^{2+}, raising the possibility that Dbp5 activity may be modified by environmental factors in addition to known protein regulators (14,16,18,20,64).

The impact of Gle1 on the Dbp5-ADP complex

Gle1 slowed the dissociation of mantADP(±Mg^{2+}) from Dbp5 approximately two-fold and displayed a similar binding affinity within error for Dbp5-mantADP in the presence and absence of Mg^{2+} (0.1 ± 0.3 vs 0.3 ± 0.1 μM, Table 2.2). Although it is a trivial difference within error of the Gle1 affinity measurements, this 3-fold

change produces an apparent difference in Mg^{2+} affinity of Gle1-$InsP_6$-Dbp5-mantADP (55 μM) vs. Dbp5-mantADP (164 μM, Table 2.1) calculated from detailed balance of Scheme 2.2. However, the difference in Mg^{2+} affinity for the Dbp5-mantADP complex (±Gle1) is also not significant due to the large error propagated from the uncertainties in the Gle1 affinity measurements. Therefore, these data suggest that Gle1 has a minimal impact on interactions among Mg^{2+}, Dbp5, and mantADP and does not act as a NEF under these solution conditions. Therefore, Gle1 stimulation of Dbp5 ATPase activity (±RNA) (20,23) arises from a transition other than acceleration of nucleotide exchange. Given that Pi release limits both the RNA-stimulated and intrinsic Dbp5 steady-state ATPase activity (25), Gle1 presumably accelerates Pi release.

The impact of Nup159 on the Dbp5-ADP complex

It has been reported that Nup159 stimulates ADP release from Dbp5, assayed using an *in vitro* filter-binding assay (24). Using rapid solution based kinetic and thermodynamic assays, we found that Nup159 did not accelerate dissociation of Mg^{2+}mantADP or mantADP from Dbp5, nor did Nup159 alter mantADP release in the presence of Gle1 (i.e. mantADP release from Gle1-$InsP_6$-Dbp5 is the same with and without Nup159; Table 2.2). We also did not observe long-lived ADP states in our mantADP release time courses through unlabeled ADP competition and Dbp5 ATPase cycling. Finally, we note that ADP release is not rate-limiting for Dbp5 ATPase activity in the presence or absence of RNA (25) and a reported slow (i.e. minutes) Nup159 stimulated ADP release (24) is unlikely to be relevant to the kinetics of mRNA export *in vivo*, which occurs in the sub-second time scale

(36,99-101). Accordingly, we conclude from these data that Nup159 and Gle1 do not function as NEFs for Dbp5.

The affinity of Dbp5 for mantADP relative to unlabeled ADP is significantly tighter due to hydrophobic interaction between the mant fluorophore and three residues of Dbp5 (25). Thus, it is conceivable that strong interactions between Dbp5 and the mant fluorophore could potentially alter the effects of Nup159 and Gle1 in our studies. However, for the mant moiety to mask possible NEF activity of the regulators, putative NEF binding would have to enhance mant interactions with Dbp5 to an extent that the favorable interactions exceed (since mantADP release is actually slowed) the net perturbations in ADP binding. In other words, assuming the ADP dissociation activation energy is reduced to near zero following NEF perturbation (to allow for immediately release), the dissociation activation energy of the mant moiety alone must exceed the total dissociation activation energy of mantADP (both mant and ATP moieties) prior to regulator association. Consequently, we do not favor a mechanism in which the mant fluorophore masks regulator NEF activity.

Instead, our findings show that Nup159 weakens Gle1 affinity for the Dbp5-mantADP complex ~18 fold (from 0.1 to 1.8 μM, Table 2.2). Crystal structures of the Nup159-Gle1-Dbp5 complex demonstrate that Nup159 and Gle1 bind separate and distinct sites on Dbp5 and do not directly compete for Dbp5 binding (23). Consequently, we expect that Nup159 likely modulates Gle1 binding to Dbp5 through an allosteric mechanism (i.e. Nup159 promotes conformational changes of Dbp5 that weaken Gle1 binding), supporting a model where Nup159

aids Gle1 release from Dbp5 to promote enzyme turnover and further rounds of ATP hydrolysis *in vivo*.

SCHEMES

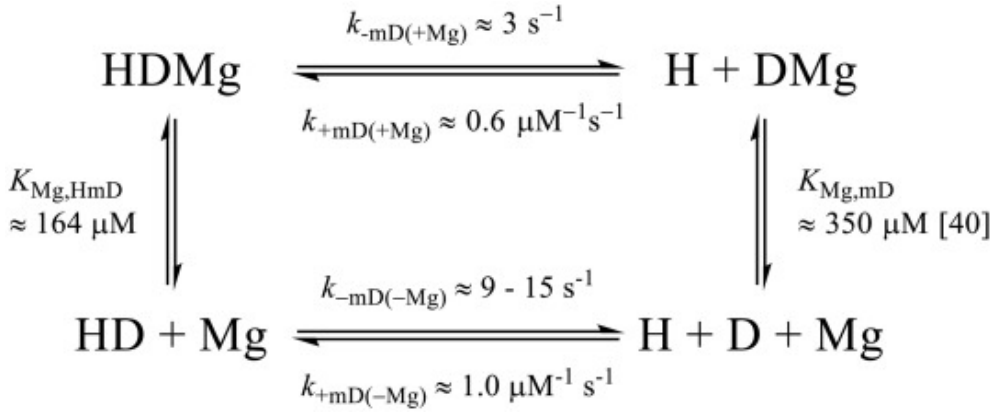

Scheme 2.1. Dbp5 catalytic cycle reaction scheme in the presence of nucleotide and magnesium. H: Dbp5; R: RNA; D: ADP; Mg: magnesium.

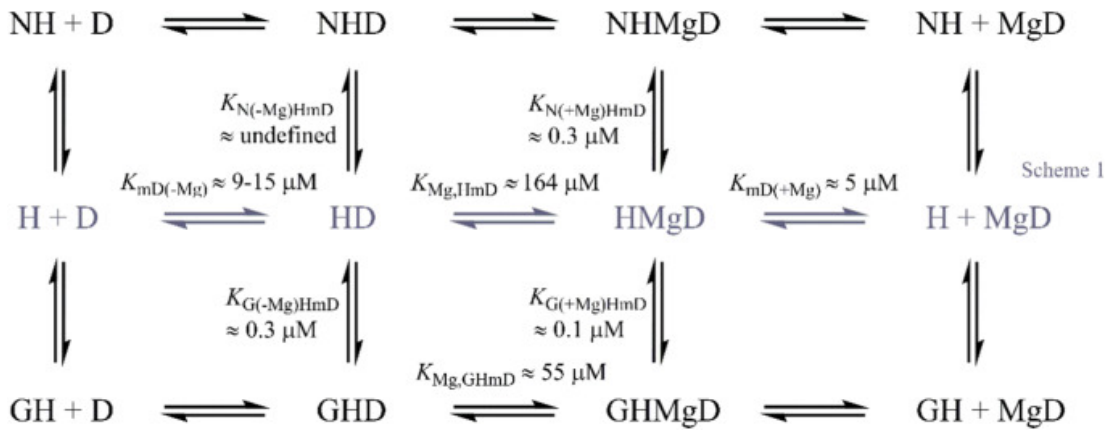

Scheme 2.2. Dbp5 catalytic cycle reaction scheme in the presence of Gle1, Nup159, nucleotide, and magnesium. H: Dbp5; R: RNA; G: Gle1; N: Nup159; D: ADP; Mg: magnesium.

FIGURES

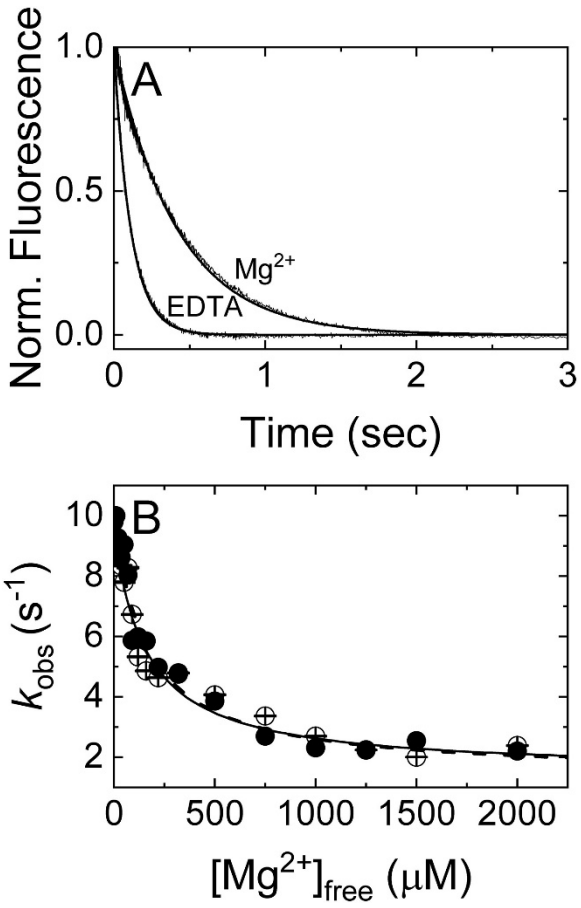

Figure 2.1. Mg^{2+} slows mantADP dissociation from Dbp5. (A) Time courses of FRET signal changes in pre-equilibrated solutions of Dbp5 and mantADP with 2 mM $MgCl_2$ (Mg^{2+} curve) or 4 mM EDTA (EDTA curve) upon rapid mixing with an equal volume of 20 mM ADP in assay buffer containing either 2 mM $[MgCl_2]_{free}$ (Mg^{2+} curve) or 0 mM $[MgCl_2]_{free}$ (EDTA curve). Continuous lines through the data represent best fits to single exponentials, yielding $k_{-mD(-Mg)}$ = 10.0 ± 0.4 s^{-1} and $k_{-mD(+Mg)}$ = 2.4 ± 0.009 s^{-1}. (B) $[Mg^{2+}]_{free}$ dependence of the observed rate constants of mantADP dissociation from a pre-formed Dbp5-mantADP (no Mg^{2+}, filled circles) or Dbp5-Mg^{2+}mantADP complex (open circles). The solid and dashed lines through the data represent the best fits of the data

starting with Dbp5-mantADP (filled circles) or Dbp5-Mg^{2+}mantADP (open circles) to Equation 2.1, yielding the two $K_{Mg(HmD)}$ values (160 ± 40 – filled circles and 165 ± 26 μM – open circles) for Mg^{2+} binding to Dbp5-mantADP complex as well as the fundamental dissociation rate constants for mantADP ($k_{-mD(-Mg)}$ ≈ 10 and 9 s^{-1}, no Mg^{2+}) or Mg^{2+} mantADP ($k_{-mD(+Mg)}$ ≈ 2.4 and 2.2 s^{-1}, saturating Mg^{2+}). Uncertainty bars represent standard errors of the fits and are contained within the data points.

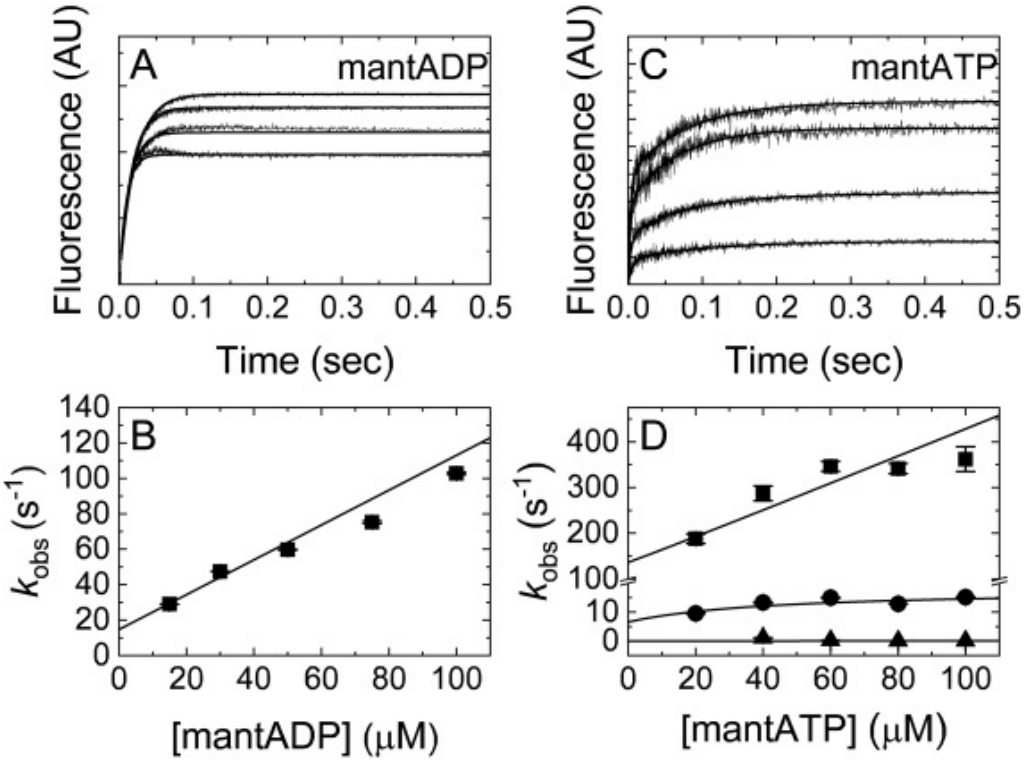

Figure 2.2. mant nucleotide–Dbp5 binding kinetics in the absence of Mg^{2+}. (A) Time courses of FRET signal change after mixing Dbp5 with varying [mantADP] in 10 mM EDTA. Final concentrations after mixing are 1 μM Dbp5 and (lower to upper) 30, 50, 75, or 100 μM mantADP. Best fits to single exponentials are illustrated by smooth lines through the data. (B) [mantADP] dependence of observed rate constants obtained from exponential fits in A. The line through the data represents the best linear fit, giving the fundamental association rate constants ($k_{+\,mD(-\,Mg)}$ = 1.0 ± 0.1 $\mu M^{-1}\,s^{-1}$) for divalent cation-free mantADP binding to Dbp5, and fundamental dissociation rate constant, $k_{-\,mD(-Mg)}$ = 15 ± 2 s^{-1}. (C) Time courses of FRET signal change after mixing Dbp5 with varying [mantATP], in buffer with 10 mM EDTA. Final concentrations after mixing are 1 μM Dbp5 and (lower to upper) 20, 40, 60 or 80 μM mantATP. Best fits to three

exponentials are illustrated by continuous lines through the data. (D) [mantATP] dependence of observed rate constants. $k_{1mT(-Mg),obs}$ and $k_{2mT(-Mg),obs}$ were globally fit to Equation 2.2 (44) and the resulting kinetic rate constants are listed in Table 2.1. $k_{3mT(-Mg),obs}$ ~ 0.1 s^{-1} and is [mantATP]-independent over the range titrated. The [mantATP] dependence of the fastest phase observed rate constants was not fitted to a hyperbolic function given the uncertainty associated with k_{obs} values that approach the instrument dead time. Moreover, when these values are fitted to an unconstrained hyperbolic function, an unwarranted, large negative *y*-intercept value results. Therefore, we fitted to the simplest mechanism/model. Uncertainty bars represent standard errors of the fits and are contained within the data points.

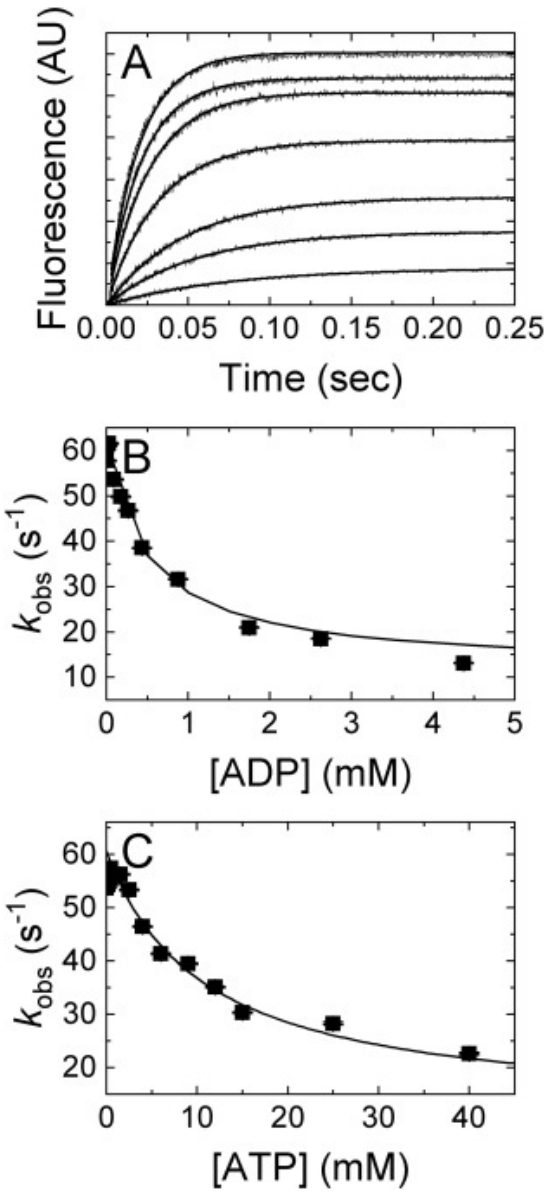

Figure 2.3. Determination of unlabeled nucleotide affinity in the absence of Mg2+ by kinetic competition with mantADP. (A) Time courses of FRET signal change after mixing 1 μM Dbp5 with an equal volume solution of 40 μM mantADP and (upper to lower) 0, 0.00875, 0.0625, 0.0875, 0.175, 0.2625, 0.4375, 0.875, 1.75, 2.625, or 4.375 mM ADP in assay buffer containing excess EDTA. Concentrations are final after mixing. The lines through the data represent best fits to double exponentials. (B) [ADP]-dependence of the fast observed rate

constants from the double exponential fits in Panel A. (C) [ATP] dependence of the fast observed rate constant of two exponential fits after mixing 2 μM Dbp5 with 40 μM mantADP and excess EDTA supplemented with either 0, 0.2, 0.5, 0.9, 1.5, 2.5, 4, 6, 9, 12, 15, 25, or 40 mM ATP. Concentrations are final after mixing. The lines through the data in panels B and C represent the best fits to Equation (2.3) and yield apparent affinities: $K_{D(-Mg)}$ = 0.8 ± 0.1 mM and $K_{T(-Mg)}$ = 15 ± 4 mM. Uncertainty bars represent standard errors of the fits and are contained within the data points.

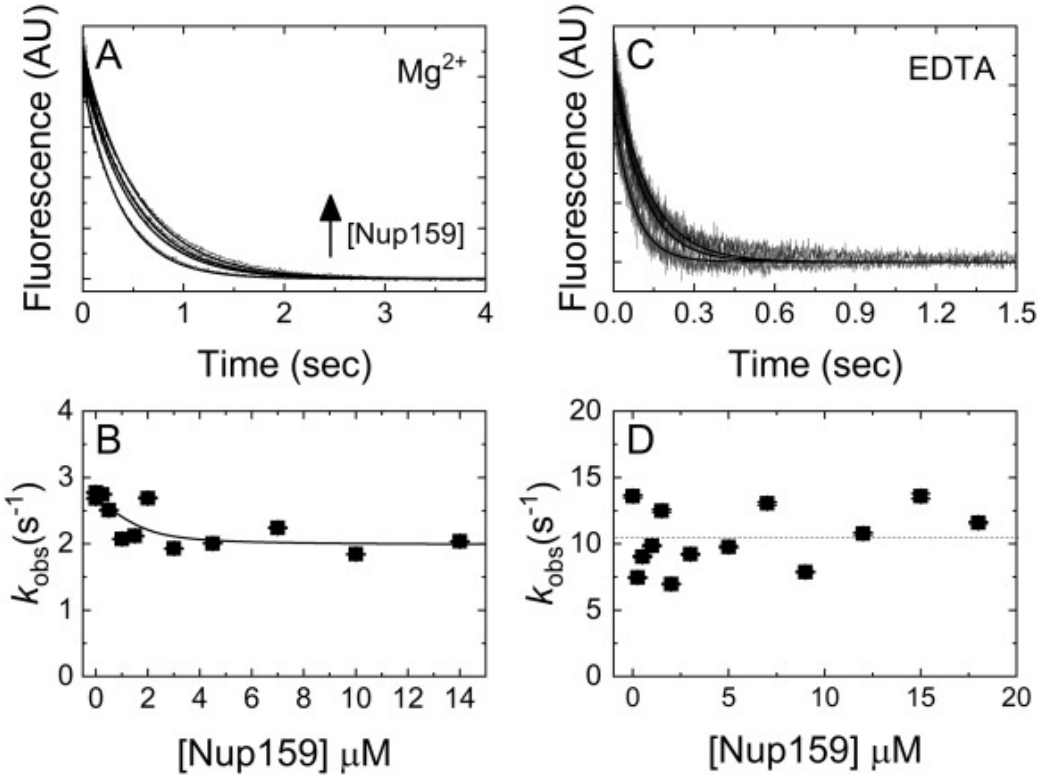

Figure 2.4. Nup159 minimally affects mantADP(± Mg^{2+}) dissociation kinetics. (A) Time courses of irreversible Mg^{2+} mantADP dissociation from a pre-incubated solution of Dbp5 (2 μM) and Mg^{2+} mantADP (20 μM) upon mixing with 3 mM Mg^{2+} ADP and (from lower to upper) 0, 1.5, 4.5, or 10 μM Nup159 in assay buffer containing excess $MgCl_2$. Concentrations are final after mixing. Smooth lines through the data represent best fits to single exponentials. (B) [Nup159] dependence of the observed rate constants obtained from panel A. The line through the data represents the best fit to Equation 2.4, yielding $K_{N(+\,Mg)HmD}$ of 0.3 ± 0.8 μM, $k_{-\,mD(+\,Mg)}$ = 2.7 ± 0.1 s^{-1} and $k_{-\,mD(+Mg),N}$ = 2.0 ± 0.2 s^{-1}. (C) Time courses of FRET signal change after mixing pre-equilibrated solutions of 1 μM Dbp5 and 40 μM mantADP with an equal volume of (lower to upper) 0, 3, or 9 μM

Nup159 and 10 mM ADP in assay buffer containing excess EDTA (ca. 27 nM $[Mg^{2+}]_{free}$ after mixing). The concentrations are final after mixing. Continuous lines through the data represent best fits to a single exponential. (D) [Nup159] dependence of the mantADP dissociation observed rate constants obtained from exponential fits in panel (C) ANOVA analysis suggests that the dependence is insignificant and the average dissociation rate constant is ~ 11 s^{-1} indicated by a horizontal dashed line. Uncertainty bars represent standard error of the fits and are contained within the data points.

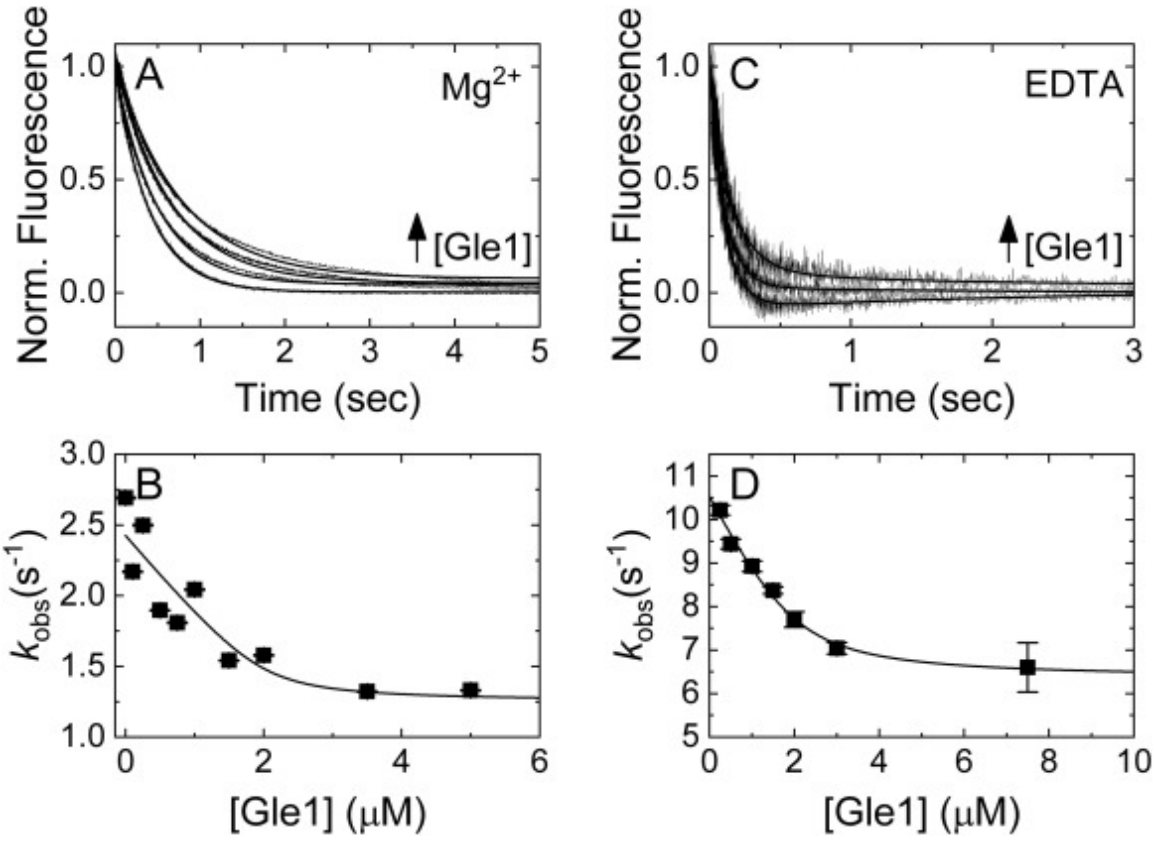

Figure 2.5. Gle1 slows mantADP(± Mg^{2+}) dissociation from Dbp5. (A) Time courses of FRET signal shift upon mixing pre-equilibrated mixtures of 2 μM Dbp5 and 20 μM Mg^{2+} mantADP with equal volumes of (lower to upper) 0, 1, 2, or 3.5 μM Gle1 and 3 mM Mg^{2+}-ADP. Concentrations are final after mixing. The assay buffer in both syringes before mixing contains 15 μM $InsP_6$ and an extra 2 mM $MgCl_2$. Continuous lines through the data represent best fits to single exponential. (B) [Gle1] dependence of the observed rate constant from exponential fits in A. The continuous line through the data represents the best fit to Equation 2.4, yielding an affinity of Gle1 for the Dbp5–Mg^{2+} mantADP complex of 0.1 ± 0.3 μM, $k_{-\,mD(+\,Mg)}$ = 2.4 ± 0.1 s^{-1}, and $k_{-\,mD(+\,Mg),G}$ = 1.3 ± 0.3 s^{-1}. (C) Time courses of FRET signal change after mixing pre-equilibrated solutions of 1

μM Dbp5 and 40 μM mantADP with an equal volume of (lower to upper) 0, 0.5, or 3 μM Gle1 and 10 mM ADP. Concentrations are final after mixing. The assay buffer in both syringes before mixing contains 15 μM $InsP_6$ and 10.64 mM EDTA (ca. 44 nM $[Mg^{2+}]_{free}$ after mixing). The time courses were fitted mainly by single exponential with an additional exponential to fit the slightly increasing part after 0.5–0.8 s (continuous lines through the data) due to the slow background signal increase by Gle1 alone that is not related to the binding process. (D) [Gle1] dependence of the mantADP dissociation observed rate constant obtained from exponential fits in C. The smooth line through the data represents the best fit to Equation 2.4, yielding an affinity ($K_{G(-Mg)}$) of 0.3 ± 0.1 μM, $k_{-mD(-Mg)}$ = 10.5 ± 0.1 s^{-1}, and $k_{-mD(-Mg),G}$ = 6.3 ± 0.2 s^{-1}. Uncertainty bars represent standard error of the fits.

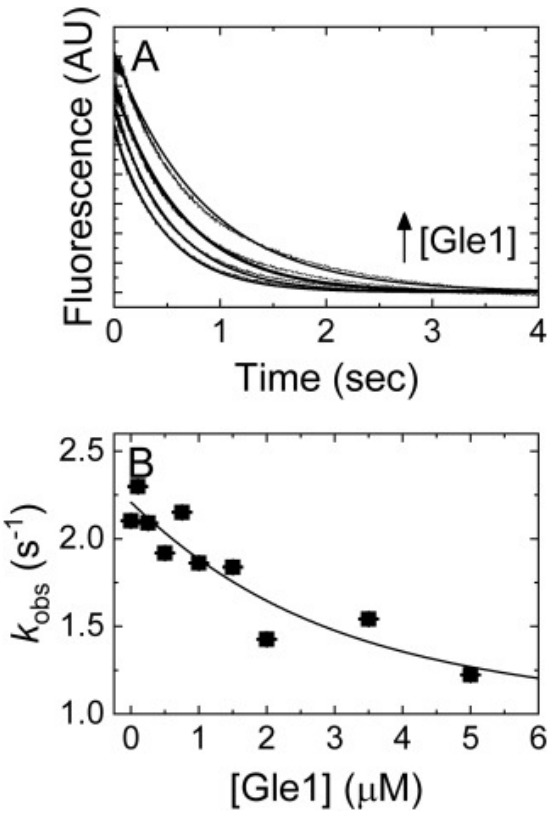

Figure 2.6. Nup159 has no significant effect on Gle1-mediated Mg^{2+}–mantADP dissociation. (A) Time courses of FRET signal change upon mixing Dbp5 (2 μM) pre-incubated with Mg^{2+} mantADP (30 μM), Nup159 (2.5 μM) and $InsP_6$ (15 μM) with excess unlabeled Mg^{2+} ADP (3 mM) and (lower to upper curves) 0, 1, 3.5, or 5 μM Gle1 in assay buffer with excess $MgCl_2$. The concentrations are final after mixing. Smooth lines through the data represent best fits to single exponential. (B) [Gle1] dependence of the observed rate constant of Mg^{2+} mantADP dissociation from the exponential fit in panel A. Continuous lines through the data represent the best fit of the observed rate constant to Equation 2.4, giving a $K_{G(+\,Mg),HNmD}$ of 1.8 ± 3.2 μM, $k_{-\,mD(+\,Mg),N}$ = 2.2 ± 0.1 s^{-1}, and $k_{-mD(+\,Mg),GN}$ = 0.8 ± 0.9 s^{-1}. Error bars represent standard error of the fits and are contained within the data points.

TABLES

Table 2.1. Mg2+ dependence of Dbp5–mant nucleotide interaction

Parameter	Value	Units	Assay
Mg^{2+}affinity for Dbp5–mantADP			
	165 ± 40	μM	Dissociation from initial HMmD (Figure 2.1)
$K_{Mg,HmD}$	160 ± 27	μM	Dissociation from initial HmD (Figure 2.1)
	164 ± 25	μM	Global fitting of HMmD and HmD data (Figure 2.1)
Mg^{2+} affinity for Dbp5–ADP			
$K_{Mg,HD}$	~ 113	μM	Detailed balance of Scheme 2.1 and $K_{Mg,D}$ ~ 676 μM (102)
Mg^{2+} affinity for Dbp5–ATP			
$K_{Mg,HT}$	~ 17	μM	Detailed balance of Scheme 2.1 (modified for ATP) and $K_{Mg,T}$ ~ 87 μM (102)
Unlabeled nucleotide affinity			
$k_{+\,D(-\,Mg)}$	~ 2	s^{-1} μM^{-1}	Estimated from competition with mD (Figure 2.3B)
$k_{-\,D(-\,Mg)}$	~ 1600	s^{-1}	Estimated from competition with mD (Figure 2.3B)
$K_{D(-\,Mg)}$	0.8 ± 0.1	mM	Kinetic competition with mD (Figure 2.3B)
$K_{D(+\,Mg)}$	0.36 ± 0.05	mM	Kinetic competition with mD (69)
$k_{+\,T(-\,Mg)}$	> 2	s^{-1} μM^{-1}	Estimated from competition with mD (Figure 2.3C)
$k_{-\,T(-\,Mg)}$	> 30000	s^{-1}	Estimated from competition with mD (Figure 2.3C)
$K_{T(-\,Mg)}$	15 ± 4	mM	Kinetic competition with mD (Figure 2.3C)

Parameter	Value	Units	Assay
$K_{T(+ Mg)}$	3–6 ± 0.4–2	mM	Kinetic competition with mD (69)
Mg^{2+}–mantADP binding			
$K_{mD(+ Mg)}$	5 ± 2	μM	$k_{- mD(+ Mg)}/k_{+ mD(+ Mg)}$ from linear fit of Mg^{2+} mantADP binding in ref. (69)
$k_{+ mD(+Mg)}$	0.58 ± 0.07	$\mu M^{-1} s^{-1}$	Linear fit of Mg^{2+} mantADP binding in ref. (69)
	2.4 ± 0.009	s^{-1}	MgmD dissociation from HMmD (Figure 2.1)
$k_{- mD(+Mg)}$	2.2 ± 0.012	s^{-1}	MgmD dissociation from HmD (Figure 2.1)
	2.9 ± 0.9	s^{-1}	Linear fit of Mg^{2+} mantADP binding in ref. (69)
mantADP binding			
$k_{+ mD(- Mg)}$	1.0 ± 0.1	$\mu M^{-1} s^{-1}$	mD binding (Figure 2.2)
	15 ± 2	s^{-1}	mD binding (Figure 2.2)
$k_{- mD(- Mg)}$	9 ± 0.02	s^{-1}	mD dissociation from HMmD (Figure 2.1)
	10 ± 0.4	s^{-1}	mD dissociation from HmD (Figure 2.1)
$K_{mD(- Mg)}$	15 ± 2.5	μM	$k_{-mD}/k_{+ mD}$ (Figure 2.2)
mantATP binding			
$k_{+ 1mT(- Mg)}$	3 ± 1	$\mu M^{-1} s^{-1}$	mT binding global fit (Figure 2.2D)
$k_{- 1mT(- Mg)}$	125 ± 77	s^{-1}	mT binding global fit (Figure 2.2D)
$K_{1mT(- Mg)}$	42 ± 32	μM	$k_{-mT1}/k_{+ mT1}$
$k_{+ 2mT(Mg)}$	11 ± 4	s^{-1}	mT binding global fit (Figure 2.2D)

Parameter	Value	Units	Assay
$k_{-2mT(-Mg)}$	7 ± 3	s^{-1}	mT binding global fit (Figure 2.2D)
$K_{2mT(-Mg)}$	0.7 ± 0.2		k_{-mT2}/k_{+mT2}
$k_{-3mT,obs(-Mg)}$	~ 0.1	s^{-1}	mantATP binding (Figure 2.2D)

Table 2.2. Regulator dependence of mantADP dissociation

Parameter	Value	Units	Assay
Nup159-mediated Mg^{2+}–mantADP dissociation			
$\boldsymbol{k}_{-\,mD(+\,Mg)}$	2.7 ± 0.1	s^{-1}	mD dissociation, Nup free (Figure 2.4B)
$\boldsymbol{k}_{-\,mD(+\,Mg),N}$	2.0 ± 0.2	s^{-1}	mD dissociation, Nup saturating (Figure 2.4B)
$\boldsymbol{K}_{N(+\,Mg)HmD}$	0.3 ± 0.8	μM	[Nup159] dependence of $k_{obs(+\,Mg)}$ (Figure 2.4B)
Nup159-mediated mantADP dissociation			
$\boldsymbol{k}_{-\,mD(-\,Mg),N}$	11 ± 2	s^{-1}	mD dissociation, all [Nup] (Figure 2.4D)
$\boldsymbol{K}_{N(-\,Mg)HmD}$	undetermined	μM	[Nup159] dependence of $k_{obs(-\,Mg)}$ (Figure 2.4D)
Gle1-mediated Mg^{2+}–mantADP dissociation			
$\boldsymbol{k}_{-\,mD(+\,Mg)}$	2.4 ± 0.1	s^{-1}	mD dissociation from HMmD, Gle1 free (Figure 2.5B)
$\boldsymbol{k}_{-\,mD(+\,Mg),G}$	1.3 ± 0.3	s^{-1}	mD dissociation from HMmD, Gle1 saturating (Figure 2.5)
$\boldsymbol{K}_{G(+\,Mg)HmD}$	0.1 ± 0.3	μM	[Gle1] dependence of $k_{obs(+\,Mg)}$ (Figure 2.5B)
Gle1-mediated mantADP dissociation			
$\boldsymbol{k}_{-\,mD(-\,Mg)}$	10.5 ± 0.1	s^{-1}	mD dissociation from HMmD, Gle1 free (Figure 2.5D)

Parameter	Value	Units	Assay
$\boldsymbol{k}_{-\text{mD}(-\text{Mg}),\text{G}}$	6.3 ± 0.2	s^{-1}	mD dissociation from HmD, Gle1 saturating (Figure 2.5D)
$\boldsymbol{K}_{\text{G}(-\text{Mg})\text{HmD}}$	0.3 ± 0.1	μM	[Gle1] dependence of $k_{\text{obs}(-\text{Mg})}$ (Figure 2.5)
Mg^{2+} affinity for Gle1–Dbp5–mantADP			
$\boldsymbol{K}_{\text{Mg,GHmD}}$	55 ± 159	μM	Calculated from detailed balance of Scheme 2.2
Gle1-mediated Mg^{2+}–mantADP dissociation in the presence Nup159			
$\boldsymbol{k}_{-\text{mD}(+\text{Mg}),\text{N}}$	2.2 ± 0.1	s^{-1}	mD dissociation from Nup-HMmD, Gle1 free (Figure 2.6B)
$\boldsymbol{k}_{-\text{mD}(+\text{Mg}),\text{GN}}$	0.8 ± 0.9	s^{-1}	mD dissociation from Nup-HMmD, Gle1 saturating (Figure 2.6B)
$\boldsymbol{K}_{\text{G}(+\text{Mg}),\text{HNmD}}$	1.8 ± 3.2	μM	[Gle1] dependence of $k_{\text{obs}(-\text{Mg})}$-Nup (Figure 2.6B)

CHAPTER 3: The Nucleoporin Gle1 Activates DEAD-box Protein 5 (Dbp5) by Promoting ATP Binding and Accelerating Rate Limiting Phosphate Release

Published as Gray S, Cao W, Montpetit B, De La Cruz EM (2022) The Nucleoporin Gle1 Activates DEAD-box Protein 5 (Dbp5) by Promoting ATP Binding and Accelerating Rate Limiting Phosphate Release. *Nucleic Acids Research.* 50(7)

This worked was a collaborative effort. I collected and analyzed the data. The initial manuscript was writing by myself, a senior research scientist Wenxiang Cao, and my research mentor Enrique De La Cruz. All three of us worked alongside Ben Montpetit to edit the manuscript for final submission.

ABSTRACT

The DEAD-box protein Dbp5 is essential for RNA export, which involves regulation by the nucleoporins Gle1 and Nup159 at the cytoplasmic face of the nuclear pore complex (NPC). Mechanistic understanding of how these nucleoporins regulate RNA export requires analyses of the intrinsic and activated Dbp5 ATPase cycle. Here, kinetic and equilibrium analyses of the S. cerevisiae Gle1-activated Dbp5 ATPase cycle are presented, indicating that Gle1 and ATP, but not ADP-Pi or ADP, binding to Dbp5 are thermodynamically coupled. As a result, Gle1 binds Dbp5-ATP >100-fold more tightly than Dbp5 in other nucleotide

states and Gle1 equilibrium binding of ATP to Dbp5 increases >150-fold via slowed ATP dissociation. Second, Gle1 accelerated Dbp5 ATPase activity by increasing the rate-limiting Pi release rate constant ~20-fold, which remains rate limiting. These data show that Gle1 activates Dbp5 by modulating ATP binding and Pi release. These Gle1 activities are expected to facilitate ATPase cycling, ensuring a pool of ATP bound Dbp5 at NPCs to engage RNA during export. This work provides a mechanism of Gle1-activation of Dbp5 and a framework to understand the joint roles of Gle1, Nup159, and other nucleoporins in regulating Dbp5 to mediate RNA export and other Dbp5 functions in gene expression.

INTRODUCTION

DEAD-box proteins (DBPs) are ATPases that typically unwind and structurally reorganize RNA and ribonucleoprotein (RNP) complexes. As a large protein family in eukaryotes, bacteria, and archaea, DBPs support nearly all aspects of RNA metabolism(42), including ribosome biogenesis, mRNA splicing(43), RNA transport, translation(42), and RNA decay. DBPs are members of the SF2 family of helicases and defined by an enzymatic core formed by two RecA-like domains and a conserved Asp-Glu-Ala-Asp (D-E-A-D) amino acid sequence motif. The two RecA-like domains form a unit capable of binding ATP, RNA, and ATP hydrolysis, which is supported by the DEAD motif and 10 other characteristic sequence motifs within the helicase core(42).

Many DBPs are activated by RNA binding with an overall RNA-activated ATPase reaction cycle mechanism that appears to be conserved among DBP family members (42). During an ATPase cycle of ATP binding, hydrolysis, and product release there are a series of conformational states with distinct RNA binding properties (e.g., affinity, specificity). The functional diversity of DBPs is achieved through enzymatic adaptation of ATPase cycle kinetics and through interactions with specific regulatory proteins (43), which is coupled to specific biochemical activities (e.g., RNA duplex unwinding, protein displacement) and the individual physiological functions of the DBP.

Dbp5 (DDX19 in humans) is an essential *Saccharomyces cerevisiae* DBP required for mRNA export *(5-7,16),* with less defined roles in both ncRNA export and translation (38,40,66). Dbp5 is dynamically bound to the cytoplasmic face of a nuclear pore complex (NPC) via interaction with the nucleoporins Nup159 (Nup214 in humans) and Gle1, with a significant fraction of Dbp5 present in the cytoplasm and nucleoplasm (5,6,14,16). The interaction of Dbp5 and Nup159 occurs through an interaction with the β-propeller domain of Nup159 and the N-terminal RecA-like domain of Dbp5, which occludes RNA binding to Dbp5 (17,22,23,103,104). Nup214 binds DDX19 with the highest affinity in the absence of nucleotide (22) and therefore may act to dynamically increase the local concentration of Dbp5. Recent works have furthered provided insight into the context of these protein interactions at NPCs that addresses positioning of Dbp5/DDX19 via Nup159/Nup214 with respect to the transport channel (35,37,105).

Gle1 activates the intrinsic steady-state Dbp5 ATPase and is required for Dbp5-mediated mRNA nuclear transport (14,16) which is mediated in part by the endogenous small molecule inositol hexakisphosphate ($InsP_6$) (18,20). Structural studies have shown that Gle1 engages both RecA-like domains of Dbp5 in the presence of ADP to orient the domains in an open conformation that is incompatible with RNA binding (23). A conformation that may organize the two RecA-like domains to facilitate ATP loading and/or release of inorganic phosphate (P_i) and ADP. In vitro assays indicate that Gle1 accelerates the maximum Dbp5 ATPase cycling rate constant (k_{cat}) and lowers the Michaelis constant (K_M) for ATP (18,20,23,24). Binding studies of an ATPase deficient Dbp5 mutant further suggest that Gle1 may promote both the binding of ATP by Dbp5 and release of a bound RNA substrate from Dbp5 (23,24).

In this work, transient kinetic analyses were used to elucidate the basis of Dbp5 ATPase activation by Gle1in the presence of $InsP_6$. By measuring the effects of Gle1 on nucleotide binding, hydrolysis, and product release from Dbp5, it is demonstrated that Gle1 maximally activates the Dbp5 ATPase (k_{cat}) by accelerating P_i product release and promoting ATP binding by slowing ATP dissociation. These results provide a kinetic scheme for the regulation of the Dbp5 ATPase by Gle1. Importantly, this work establishes a framework for developing a mechanistic description and functional understanding of Dbp5 regulation via Gle1-$InsP_6$, Nup159 and other nucleoporins in the presence of RNA during nuclear export.

MATERIALS AND METHODS

Reagents – All reagents were of the highest purity commercially available. ATP (Sigma, A7699) concentrations were determined by absorbance using ε_{259} =15,400 $M^{-1}cm^{-1}$. mantADP (Jena Biosciences, NU-201) concentrations were determined by absorbance using ε_{255} = 23,300 $M^{-1}cm^{-1}$. Inositol hexakisphosphate (phytic acid) was purchased from SantaCruz Biotechnology (SC-253276). Full length Dbp5 and a soluble truncated Gle1(a.a. 244-538) were purified as described (23) (Figure S3.4). Note that $InsP_6$ is included in all experiments at an equimolar concentration with Gle1. The affinity is high between Gle1- $InsP_6$ (~ 120 nM (20)), as such it is treated as a single species in this study and referred to as just Gle1 throughout the text. Gle1 (i.e., without Dbp5) did not demonstrate any significant ATPase activity. Buffers were made with either DEPC treated water (American Bio, AB021028) or Millipore MilliQ® distilled deionized water (ddH_2O) that had been filtered through a 0.2-μm filter. Experiments were performed at 25 °C in assay buffer: 30 mM HEPES (pH 7.5), 100 mM KCl, and 2 mM DTT, 2 mM $MgCl_2$. Equimolar magnesium ($MgCl_2$) was added to all nucleotide stocks unless otherwise noted. The solution ionic strength changes <2-fold throughout the range of [ATP] examined (0-15 mM) without affecting the results (**Supplementary Information**, section **S5**).

Transient kinetic assays – Transient kinetic measurements were performed on an Applied Photophysics SX20 stopped-flow instrument thermostatted at 25 ± 0.1 °C. mant-nucleotide binding to Dbp5 was monitored by FRET between excited tryptophans (λ_{ex} = 280 nm) in Dbp5 and the bound mant-labeled nucleotide.

Fluorescence intensity was measured at 90° relative to excitation light after passing through a 400-nm long-pass colored glass filter. Inner filter effects are minimal in the mant-labeled nucleotide concentration range employed (69,79). Time courses shown are averages of at least two traces. Fitting was performed by nonlinear least-squares regression, and uncertainties of quantities determined from fits are given as standard errors in the fits. All assays utilizing Gle1 include equimolar InsP6 in solution (18,20). Dbp5 and Gle1 were incubated for at least 2 hours at room temperature in all assays utilizing preformed Gle1-Dbp5 complex.

mantADP dissociation kinetics – Irreversible dissociation of mantADP bound Dbp5 was achieved by mixing with a large excess of unlabeled ADP to prevent mantADP rebinding. mantADP dissociation from Dbp5 was measured as a function of Gle1 concentration ([Gle1]) by incubating 2 μM Dbp5, 40 μM mantADP, and various concentrations of Gle1 (0, 2, 4, 6, 10, 20, 60, 88 μM) for at least 2 hours at room temperature in assay buffer before mixing with 20 mM ADP. Final concentrations after mixing are 1 μM Dbp5, 20 μM mantADP, 10 mM ADP, and 0, 1, 2, 3, 5, 10, 30, 44 μM Gle1. Time courses of dissociation were fitted to single (0 μM Gle1) or double (2, 4, 6, 10, 20, 60, 88 μM Gle1) exponential functions. The [Gle1]-dependance of both the slow and fast phase observed rate constants were fitted to Equation 3.1 and Equation 3.2, respectively.

mantADP binding kinetics – mantADP binding to Dbp5 in the presence varying concentration of [Gle1] was measured by incubating 2 μM Dbp5 with various concentrations of Gle1 (0, 2, 6, 10, 20 μM) for at least 2 hours at room

temperature and subsequently mixed with 200 μM mantADP. Final concentrations after mixing are 1 μM Dbp5, 100 μM mantADP, and 0, 1, 3, 5, and 10 μM Gle1. The [Dbp5] and [Gle1] employed in this experiment (Figure 3.3) precludes an analytical solution to Scheme 3.1 with reasonable approximations. Therefore, unknown rate constants were not determined analytically. Rather, an upper limit of Gle1 binding affinity for Dbp5 was estimated from a trend in the data (see Results). The [Gle1]-dependence of the slow phase k_{obs} was overlaid on top with a rectangular hyperbola to aid visualization.

MantADP binding to preformed Gle1-Dbp5 complex was measured as a function of [mantADP] by incubating 1 μM Dbp5 with 20 μM Gle1 for at least 2 hours at room temperature and subsequently mixed with various concentrations of mantADP (10, 20, 30, 40, 60, 80, 100, 140 μM). Final concentrations after mixing are 0.5 μM Dbp5, 10 μM Gle1, and 5, 10, 15, 20, 30, 40, 50, 70 μM mantADP. Time courses of mantADP binding were fitted to double exponential functions and the [mantADP]-dependance of the observed rate constants, raw, total, and fractional amplitudes were globally fitted to the analytical solution of a two-step binding model (76).

Competition of mantADP and unlabeled ATP – Binding of ATP to Gle1-Dbp5 complex was measured as a function of [ATP] by incubating 2 μM Dbp5 with 20 μM Gle1 for at least 2 hours at room temperature and subsequently mixed with 40 μM mantADP with various concentrations of ATP (0, 20, 40, 60, 100, 140, 200, 600 μM). Final concentrations after mixing are 1 μM Dbp5, 10 μM Gle1, 20 μM mantADP, and 0, 10, 20, 30, 50, 80, 100, 300 μM ATP. Time courses of

FRET signal change from mantADP binding to Dbp5 in the presence of varying amount of unlabeled nucleotide were fitted to a MATLAB simulation of Scheme 3.2. Time courses of mantADP binding were also fitted to a sum of two or three exponential functions. The resulting observed rate constants were globally fitted to Equation A (S3.18, S3.19 and S3.24) with equilibrium and fundamental rate constants corresponding to Scheme 3.2 shared across λ_1, λ_2, and λ_3. mantADP binding rate constants were fixed to values determined previously (Figure 3.2-3.4).

Quench Flow – ATP hydrolysis by Gle1-Dbp5 complex was measured as a function of time at two different ATP concentrations by incubating 36 μM Dbp5 with 120 μM Gle1 for at least 2 hours at room temperature and subsequently mixing with 76 or 340 μM ^{32}P labeled ATP, aging for various times, and quenching with 5 M Formic Acid. Samples were spotted (0.5 μL) onto Cellulose F TLC plates (EMD Millipore, Billerica, MA) and resolved in 0.6 M KH_2PO_4 (pH 3.4) for 30 min. Plates were exposed to phosphor screen, read using Amersham™ Typhoon™ imager (GE Healthcare), and quantitated using Fiji(106) software. Time courses of hydrolyzed P_i (free and enzyme bound) were fitted to Equation 3.5 combined with Equations 3.6 and 3.7 (44). ATP binding and dissociation rate constants (k_{47} and k_{74}, respectively) were constrained to 0.2 μM^{-1} s^{-1} and 4.1 s^{-1} as determined from kinetic competition of ATP and mantADP binding (Figure 3.4).

Phosphate Binding Protein – P_i release by Gle1-Dbp5 complex was measured from the eight-fold increase in fluorescence (λ_{ex} = 436 nm, 463 nm long pass

emission filter) of MDCC-labeled P_iBP upon binding phosphate. P_iBP binds P_i rapidly and with a tight affinity (K_d = 0.1 μM) providing real time detection of transient and steady-state P_i release(107). 1 μM Dbp5 was incubated with 20 μM Gle1 for at least 2 hours at room temperature and subsequently mixing with 0, 10, 20, 30, 40, 100, 200 μM ATP with 6 μM MDCC labeled P_iBP for single mixing experiments. Contaminating P_i was removed from the buffers and instrument with a "P_i mop" consisting of 0.5 mM 7-methylguanosine and 0.01 U/mL purine nucleoside phosphorylase. P_iBP fluorescence was converted to [P_i] using a phosphate standard calibration curve. P_iBP fluorescence was converted to [P_i] using a P_i standard curve.

MATLAB Fitting – Global fits to the mantADP binding time courses (Figure 3.3A, 4A) were carried out using a custom MATLAB program in which the concentrations of all species in Scheme 3.1 were solved for at each time step using the relevant differential equations and a built-in ordinary differential equation solver (*ode45* or *ode15s*) Global parameter optimization was achieved by minimizing the total sum of squares for all experiments, i.e. simulated time courses of mantADP binding (Figure 3.3A, 3.4A) and dissociation (Figure 3.2A) using a built-in, non-linear least squares solver (*lsqcurvefit*). Briefly, residuals between the experimental and simulated data were calculated during each fitting iteration and *trust-region-reflective* algorithm was employed to modify open parameters until the total sum of squares is below the default cut-off value. Quench flow data was fitted similarly to an ATP hydrolysis reaction scheme (44) where the sum of [P_i] and [EP] were used in the fit.

RESULTS

Previous work from others has shown that Dbp5 has a low intrinsic ATPase rate in the absence of RNA or other regulatory factors (18,20,23,25) (k_{cat} ~0.03 s^{-1}, $K_{M,ATP}$ ~2 mM) and Gle1 stimulates the maximum Dbp5 ATPase rate 3-5 fold (18,20,23) with an "apparent K_M" (K_{Gle1}; the [Gle1] needed for half maximum activation) of ~0.4 μM (20). To validate the purified protein components used and experimental conditions that vary from previous work with respect to solution conditions, these parameters were again measured here. Consistent with previous determinations (18,20,23), Gle1 activated Dbp5 ATPase activity 5-fold from 0.03 s^{-1} to 0.16 s^{-1} with a K_{Gle1} of 0.3 ± 0.1 μM in the presence of saturating ATP (Figure 3.1).

Assays for measuring nucleotide binding to Dbp5

Within the Dbp5 ATPase cycle, Gle1 is proposed to regulate ATP binding and RNA release (23,24), the latter being an activity that is directly influenced by changes in nucleotide binding status. Unfortunately, binding of unlabeled nucleotides (ADP or ATP) to Dbp5 yields no detectible spectroscopic signal, so nucleotide binding must be measured in kinetic competition with the fluorescent nucleotide, mantADP (79,102,108,109). The kinetics of mantADP binding to Dbp5 are significantly different from those of ADP, mostly due to the additional hydrophobic interaction provided by the mant moiety (25). However, since mantADP is only used as a signal source to assess Gle1 binding Dbp5 or ATP binding Gle1-Dbp5 any difference in binding kinetics caused by the mant moiety are trivial. The minimum reaction scheme considered for Dbp5, Gle1, and

(mant)ADP binding involves six biochemical intermediates of Dbp5 with transitions defined by seven equilibrium and fourteen rate constants (Scheme 3.1). In the absence of Gle1 (top pathway of Scheme 3.1), mantADP binds Dbp5 following a two-step mechanism with the initial binding step in rapid equilibrium (k_{12} [mantADP] + k_{21} > 1000 s^{-1}) with a Dbp5-(mant)ADP complex (HmD) that isomerizes (HmD*) (25). Gle1 binding to Dbp5 (64) and Dbp5-(mant)ADP (26) is then accounted for in the bottom pathway of Scheme 3.1.

Gle1 binds Dbp5-mantADP with an affinity ~ 1 μM.

The first part of Scheme 3.1 measured was the Gle1 affinity for Dbp5-(mant)ADP, which was estimated from the effect of Gle1 on (irreversible) mantADP release. A pre-equilibrated sample of 20, 1 μM Dbp5, and a range of Gle1 concentrations ([Gle1] = 0, 1, 2, 3, 5, 10, 30, 44 μM) was rapidly mixed with 10 mM ADP. Time courses of fluorescence change, corresponding to mantADP dissociation, followed single exponentials in the absence of Gle1, while they followed double exponentials in the presence of Gle1 (Figure 3.2A). The effects of Gle1 on mantADP release are saturated at [Gle1] ≥ 10 μM (Figure 3.2B, C). Note that this analysis assumes that Gle1 binds Dbp5-(mant)ADP in a rapid equilibrium (i.e., Gle1 binding equilibrates faster than nucleotide is released). If this condition were not fulfilled, (at least) three exponentials would be observed in time courses of irreversible mantADP dissociation at sub-saturating [Gle1] ([Gle1] < K_{d52}, K_{d63}; Scheme 3.1, Figure 3.2A). The observed biphasic dissociation time courses are consistent with Gle1 binding of Dbp5-(mant)ADP in rapid equilibrium.

The fast and slow phases of mantADP dissociation are well separated in time, such that the rapid exponential decay is completed before the slower exponential decay appears. mantADP also dissociates more slowly when [Gle1] is saturating. Under these conditions, the two decays differ by an order of magnitude (fast observed rate constant is ~ 25 s^{-1} and the slow observed rate constant is ~ 2.2 s^{-1}), providing temporal separation of these events and allowing independent analysis of the two phases. The fast phase of the dissociation time courses corresponds to mantADP dissociation from GHmD (Gle1-Dbp5-(mant)ADP) and HmD (Scheme 3.1). The slow phase originates from isomerization of GHmD* and HmD* to GHmD and HmD prior to release. The [Gle1]-dependence of the fast and slow observed mantADP dissociation rate constants ($k_{obs,\ fast}$ and $k_{obs,\ slow}$) were fitted to the following equations accounting for the weighted population average of the parallel dissociation pathways (Scheme 3.1) (26):

$$k_{obs,fast} = k_{obs,fast(-G)} + \frac{(k_{obs,fast(+G)} - k_{obs,fast(-G)})[G]}{K_{d52} + [G]} \quad (3.1),$$

$$k_{obs,slow} = k_{obs,slow(-G)} + \frac{(k_{obs,slow(+G)} - k_{obs,slow(-G)})[G]}{K_{d63} + [G]} \quad (3.2),$$

where $k_{obs,\ fast(-G)}$ is the fast observed rate constant in the absence of Gle1, $k_{obs,\ fast(+G)}$ is the fast observed rate constant at saturating Gle1, [G] is the Gle1 concentration, K_{d52} is the affinity of Gle1 for HmD, and K_{d63} is the affinity of Gle1 for HmD*. The fast observed rate constant in the absence of Gle1 ($k_{obs,\ fast(-G)}$) completed in the 1.2 msec instrument dead-time and was therefore constrained to 500 s^{-1} in fits to Equation 3.1. The best fits to Equation 3.1 and Equation 3.2

yield $k_{obs,\ fast(+G)}$ = 19.8 ± 6.0 s^{-1}, K_{d52} = 0.2 ± 0.1 μM, $k_{obs,\ slow(-G)}$ = 2.2 ± 0.2 s^{-1}, $k_{obs,\ slow(+G)}$ = 1.3 ± 0.1 s^{-1}, and K_{d63} = 1.1 ± 0.6 μM (Table 3.1), indicating that Gle1 binds Dbp5-(mant)ADP with an affinity ~1 μM. Therefore at [Gle1] ≥ 10 μM, HmD and HmD* are bound to Gle1 and mantADP dissociation occurs exclusively through the bottom pathway of Scheme 3.1. The observed rate constants of mantADP dissociation are related to the fundamental (mant)ADP dissociation (k_{54}) and isomerization (k_{56}, k_{65}) rate constants according to the following equations (76,110):

$$k_{obs,\ fast(+G)} \sim k_{54}, \tag{3.3}$$

$$k_{obs,slow(+G)} = k_{65}\left(\frac{k_{54}}{k_{56}+k_{54}}\right) \geq k_{65} \tag{3.4}.$$

the values of k_{54} (19.8 ± 6.0 s^{-1}) and k_{65} (≥ 1.3 ± 0.1 s^{-1}) approximated in Equation 3.3 and Equation 3.4, respectively, are consistent with more accurate determinations obtained from mantADP binding to Gle1-Dbp5 (discussed below, Figure 3.4; Table 3.1).

Gle1 binds Dbp5 (no nucleotide) with an affinity < 1 μM.

To measure the binding affinity of Gle1 for the nucleotide free form of Dbp5, the effect of Gle1 on mantADP binding to Dbp5 was used. A solution of 1 μM Dbp5 was equilibrated with a range of [Gle1] (0, 1, 3, 5, 10 μM) and rapidly mixed with 100 μM mantADP in a stopped flow apparatus and the time course of fluorescence change monitored. Time courses of mantADP binding under these pseudo first-order conditions ([mantADP] >> [Dbp5] and [Gle1-Dbp5]) followed a

single exponential in the absence of Gle1 and double exponentials in the presence of Gle1 (Figure 3.3A).

In the absence of Gle1, mantADP binds Dbp5 following a two-step mechanism with the first step rapidly equilibrating within the dead time of the stopped flow instrument such that time courses of mantADP binding followed single exponentials (25). Gle1 slowed mantADP binding to Dbp5, which allows both binding phases to be observed (Figure 3.3). Due to the temporal separation of the two observed mantADP binding phases, it is assumed the first step for mantADP binding Gle1-Dbp5 equilibrates before the second step occurs. Therefore, the slow mantADP binding phase was analyzed independent of the fast phase. The [Dbp5] and [Gle1] employed preclude an analytical solution to Scheme 3.1 with reasonable approximations; moreover, little change in the [Gle1]-dependent k_{obs} of both fast and slow phases occurs at > 3-5 μM Gle1 (Figure 3.3B). Dbp5-(mant)ADP is saturated when [Gle1] ≥ 10 μM (Figure 3.2) indicating the affinity of Gle1 for Dbp5 in the absence of nucleotides (K_{d41}) is ≤ 1 μM (Table 3.1). Consequently, at [Gle1] ≥ 10 μM mantADP binding proceed exclusively through the bottom pathway in Scheme 3.1, defining experimental conditions under which nucleotide binding to the Gle1-Dbp5 complex could be measured.

mantADP binds Gle1-Dbp5 following a two-step binding mechanism

The preceding section established that Gle1 binds Dbp5 and Dbp5-(mant)ADP with affinities ≤ 1 μM, defining experimental conditions under which nucleotide binding to the Gle1-Dbp5 complex could be measured, specifically when

maintaining [Gle1] ≥ 10 μM. Using this condition, the kinetics of mantADP binding to the Gle1-Dbp5 complex (bottom pathway of Scheme 3.1) was measured by rapidly mixing mantADP (5-70 μM) with an equilibrated mixture of 0.5 μM Dbp5 and 10 μM Gle1. Time courses of mantADP binding were best fitted by a sum of double exponential functions (Figure 3.4A, solid lines).

The [mantADP]-dependence of the observed rate constants (k_{obs}) were globally fitted to a two-step binding model(76) (Figure 3.4B), yielding the rate and equilibrium constants for mantADP binding to Gle1-Dbp5 (k_{45} = 1.8 ± 0.14 μM^{-1} s^{-1}, k_{54} = 47 ± 4.3 s^{-1}, K_{d54} = 26 ± 3.2 μM, Table 3.1) and subsequent isomerization of the Gle1-Dbp5-(mant)ADP complex (k_{56} = 24 ± 1.7 s^{-1}, k_{65} = 2.1 ± 0.3 s^{-1}, K_{d65} = 0.09 ± 0.01, Table 3.1). The overall mantADP affinity for Dbp5 is ~2 μM (25) and ~2.2 μM for Gle1-Dbp5 (Table 3.1), indicating that Gle1 has a modest effect on the (mant)ADP binding affinity. Measurements with unlabeled ADP yield a similar conclusion (discussed below; Figure S3.3).

Globally fitting the mantADP binding and release data (Figures 3.2-3.4) to the reaction matrix outlined in Scheme 3.1 via a custom MATLAB program yielded a shared parameter set consistent with those determined from independent analysis of the individual experimental data sets (**Supplemental Information,** section **S1;** Figure S3.1).

Gle1 promotes ATP binding to Dbp5

Unlabeled ATP binding to Gle1-Dbp5 complex was then measured by kinetic competition between mantADP and ATP. A solution of 1 μM Dbp5 was incubated

with 10 μM Gle1 and rapidly mixed with 20 μM mantADP and various concentrations of ATP (0 - 300 μM). Time courses of mantADP binding in the presence of ATP were best fitted by a sum of three exponentials. Since mantADP binds rapidly and equilibrates before any significant ATP hydrolysis occurs (see below), ATP hydrolysis was uncoupled from binding and the time courses reflect only competitive binding of the two nucleotides (Scheme 3.2). Kinetic competition time courses were fitted to Scheme 3.2 with numerical analysis using a custom MATLAB program (Figure 3.5A, dashed lines; Figure S3.2).

Best fits of the data yield association (k_{47}) and dissociation (k_{74}) rate constants of 0.2 ± 0.1 μM^{-1} s^{-1} and 4.1 ± 2.5 s^{-1} for ATP binding to the Gle1-Dbp5 complex (Table 3.1). Similar values for ATP binding and dissociation to Gle1-Dbp5 were obtained from an approximate analytical solution of Scheme 3.2 (**Supplemental Information,** section **S2-2**). Together these data suggest that the presence of Gle1 in complex with Dbp5 slows both the dissociation and binding of ATP. However, the much larger effect on ATP dissociation from Dbp5 by nearly 3-orders of magnitude, results in Gle1 effectively increasing the ATP affinity of Dbp5 ~150-fold.

Gle1 accelerates ATPase activity of Dbp5 by increasing the P_i release rate constant

The increased ATP binding affinity of the Gle1-Dbp5 complex allowed for the direct measurement of both the rate and equilibrium constants for ATP hydrolysis by Gle1-Dbp5 using chemical quench-flow (Figure 3.6). The weak

ATP affinity (~3 mM (25)) of Dbp5 alone previously precluded such measurements (25). An equilibrated solution of 18 μM Dbp5 and saturating (60 μM) Gle1 was rapidly mixed with either 38 or 170 μM ATP containing trace amounts of radioactive ^{32}P-labeled ATP, aged for various times, and quenched with formic acid. Time courses of P_i (enzyme bound and free) production by Gle1-Dbp5 reveal a rapid burst followed by a linear phase (Figure 3.6). The burst represents the first turnover of ATP hydrolysis, and the linear phase represents steady-state hydrolysis. Neither 20 μM Dbp5 nor 60 μM Gle1 alone generated detectable hydrolysis of ATP (50 μM) within this time range examined. All hydrolyzed ATP can therefore be attributed to the Gle1-Dbp5 complex. Time courses of P_i production were fitted to the following equation (44,111) (Figure 3.6, continuous lines), which accounts for reversible ATP binding and hydrolysis, and irreversible P_i release from Gle1-Dbp5 (bottom pathway of Scheme 3.3):

$$[EP]+[P_i]=\beta\left(\frac{1}{k_{89}}+\exp(-\lambda_2 t)\left(\frac{\lambda_1(k_{89}-\lambda_2)}{k_{89}\lambda_2(\lambda_1-\lambda_2)}\right)-\exp(-\lambda_1 t)\left(\frac{\lambda_2(k_{89}-\lambda_1)}{k_{89}\lambda_1(\lambda_1-\lambda_2)}\right)-\frac{\lambda_1+\lambda_2}{\lambda_1\lambda_2}+t\right) \quad (3.5),$$

where formation and loss of Gle1-Dbp5-ADP-P_i state are given by two observed exponential terms (eigenvalues λ_1 and λ_2, respectively):

$$\lambda_{1,2}=\frac{1}{2}\left(\begin{array}{l}k_{47}[ATP]+k_{74}+k_{78}+k_{89}\pm\\ \sqrt{\left(k_{47}[ATP]+k_{74}+k_{78}+k_{89}\right)^2-4\left(k_{47}[ATP](k_{87}+k_{89}+k_{78})+k_{74}(k_{87}+k_{89})+k_{78}k_{89}\right)}\end{array}\right)$$

(3.6),

and the steady-state ATP hydrolysis (slope of linear phase) is given by:

$$\beta = \frac{k_{47}[ATP]k_{78}k_{89}}{k_{47}[ATP](k_{87}+k_{89}+k_{78})+k_{74}(k_{87}+k_{89})+k_{78}k_{89}} \quad (3.7).$$

The best fit of the data (Figure 3.6) with unconstrained ATP binding (k_{47}, k_{74}), hydrolysis (k_{78}), resynthesis (k_{87}), and P_i release (k_{89}) parameters indicate that Gle1 promotes ATP resynthesis (k_{87}) and accelerates P_i release (k_{89}) from Dbp5 ~20-fold (k_{47} = 0.09 ± 0.5 μM^{-1} s^{-1}, k_{74} = 9.7 ± 55 s^{-1}, k_{78} = 0.6 ± 0.2 s^{-1}, k_{87} = 1.0 ± 0.9 s^{-1}, k_{89} = 0.4 ± 0.1 s^{-1}, and the steady-state ATPase k_{cat} = 0.1-0.2 ATP s^{-1} and $K_{M,ATP}$ = 30-50 μM; Table 3.1). The best fit rate constants for ATP binding are consistent with those determined from kinetic competition (Figure 3.5) and the steady-state ATPase consistent with those determined from NADH assay (Figure 3.1B; Figure 3.7B) and P_i release (Figure 3.7B). Constraining k_{47} and k_{74} to values from kinetic competition results in a less than two-fold change in ATP hydrolysis and phosphate release rate constants: k_{78} = 0.6 ± 0.2 s^{-1}, k_{87} = 1.9 ± 1.3 s^{-1}, k_{89} = 0.6 ± 0.1 s^{-1} (Table 3.1). Note that fits to quench-flow time courses assume ADP release from Gle1-Dbp5 is more rapid than steady-state cycling and that phosphate release is irreversible, which hold in this system (Figure S3.3, **Supplemental Information**, section **S3-S4**). Similar rate constant values were obtained from fitting the ATP hydrolysis reaction mechanism by Gle1-Dbp5 (bottom pathway of Scheme 3.3) with numerical analysis using a custom MATLAB program.

Prior work has shown that P_i release (k_{1112} = 0.02 (±0.1) s^{-1}, Table 3.1), is a critical transition that limits Dbp5 steady-state ATP hydrolysis in the absence or presence of RNA (25). Note that uncertainty in the measurement of k_{1112} is

determined from the intercept of the best linear fit of the [ATP]-dependence of observed lag phase rate constants, but because the intercept is close to the origin, it is subject to significant experimental uncertainty (25). The quench-flow data presented above (Figure 3.6) shows that Gle1 accelerates P_i release. To directly measure the effect of Gle1 on P_i release from Dbp5, phosphate binding protein (P_iBP) read out was used (107). An equilibrated solution of 0.5 μM Dbp5 and 10 μM Gle1 was rapidly mixed with a solution containing various [ATP] (0, 5, 10, 15, 20, 50, 100 μM) and 3 μM fluorescently labeled phosphate binding protein. Time courses of P_i release from Gle1-Dbp5 were linear without a detectable burst or lag phase (Figure 3.7A), yielding steady-state ATPase cycling velocities that are comparable to those found using the NADH coupled assay (Figure 3.7B, Table 3.1) and quench flow (Figure 3.6, Table 3.1).

In these reactions, if ATP hydrolysis and P_i dissociation were rate limiting, time courses of P_i release would display a lag phase. Alternatively, if ADP release was rate limiting, time courses would show a burst of liberated P_i (112,113). The observation that time courses of P_i release are linear with [Gle1]-dependent rates indicates that P_i release solely limits the Gle1-stimulated ATPase of Dbp5 and that Gle1 accelerates P_i release from Dbp5.

A complete thermodynamic scheme of the Gle1 activated Dbp5 ATPase cycle

The majority of the rate and equilibrium constants defining the Gle1-stimulated Dbp5 ATPase (Scheme 3.3) cycle have now been determined, as presented in the preceding sections (ATPase activity of Gle1-Dbp5, bottom pathway of Scheme 3.3) and in previous studies (ATPase activity of Dbp5 alone, top

pathway of Scheme 3.3) (25,26). In those cases where equilibrium constants have not been measured (K_{d107}, K_{d118}, and K_{d129}), values can be calculated from the principles of detailed balance given that the other constants defining the cycle are known (114).

As an example, consider the cycle formed by initial mantADP binding to Dbp5 and Gle1-Dbp5 as shown in Scheme 3.1 accounting for a part of multistep mantADP binding to (Gle1-)Dbp5. In this cyclic scheme the product of equilibrium constants $K_{d52} \times {}^{1}/K_{d54} \times K_{d21} \times {}^{1}/K_{d41}$ must equal 1. Therefore:

$$\frac{K_{d52}K_{d21}}{K_{d54}} = K_{d41} \qquad (3.8),$$

allowing determination of the affinity of Gle1 binding affinity for nucleotide-free Dbp5 (K_{d41}) from the experimentally determined equilibrium constants for mantADP binding (K_{d54} and K_{d21}) and Gle1 binding to Dbp5-(mant)ADP (K_{d52}). The affinity of Gle1 binding nucleotide-free Dbp5 (K_{d41}) calculated this way is 0.8 ± 0.3 μM, consistent with the value of K_{d41} of ≤ 1 μM estimated from mantADP binding (Figure 3.3B).

Furthermore, the product of the experimentally determined equilibrium constants for mantADP isomerization (K_{d32} and K_{d65}) and Gle1 binding to the two Dbp5-(mant)ADP states (K_{d52} and K_{d63}) calculated from $K_{d52} \times {}^{1}/K_{d32} \times K_{d65} \times {}^{1}/K_{d63}$ is ~0.82, close to the expected value of unity and indicating the experimentally determined values for mantADP isomerization (K_{d32} and K_{d65}) and Gle1 binding

to the two Dbp5-(mant)ADP states (K_{d52} and K_{d63}) are thermodynamically consistent.

Similarly, the affinity of Gle1 for Dbp5 bound to unlabeled ATP (K_{d107}; Scheme 3.3) calculated from K_{d41}, K_{d74}, and K_{d101} (the affinity of ATP for Dbp5 (25)) is 2 nM; the affinity of Gle1 for Dbp5-ADP-P_i (K_{d118}, Scheme 3.3) calculated from K_{d107}, K_{d87}, and K_{d1110} (the dissociation constant for ATP hydrolysis by Dbp5 alone (25); ~0.004) is 0.8 μM, suggesting that ATP hydrolysis is coupled to conformational rearrangement of Dbp5. The affinity of Gle1 for Dbp5-ADP (K_{d129}) calculated from K_{d41}, K_{d121} (the affinity of Dbp5 for ADP(25)), and K_{d94} (the affinity of Gle1-Dbp5 for ADP; Figure S3.3) is 0.5 μM (Scheme 3.3; Table 3.1), consistent with the affinity of Gle1 for Dbp5-(mant)ADP (K_{d52}, K_{d63}) measured by mantADP binding (Figures 3.2 and 3.3; Table 3.1) and the combined affinity of the two mantADP states ($K_{d52}K_{d63}/(K_{d52}+K_{d63})$ ~ 0.17 μM).

Note that some of these calculations were carried out with parameters determined with mantADP and not unlabeled ADP. Despite the mant moiety significantly affecting ADP binding to Dbp5, the atomic-resolution structures of Dbp5-ADP and Dbp5-(mant)ADP indicate that the structure of Dbp5 is identical with both nucleotides and that the altered binding interactions with the nucleotide arise from hydrophobic contacts with the mant moiety (25). Therefore, the measured affinity of Gle1 for Dbp5-(mant)ADP is likely representative of the equilibrium constant for Gle1 binding Dbp5 bound to unlabeled ADP, which is supported by detailed balance calculations.

With these values and a complete scheme, predictions of steady-state cycling outputs can be made and compared to measured rates to validate the model. First, the measured maximum steady-state ATPase activity of Dbp5 is activated 5-fold from an intrinsic k_{cat} ~0.03 s^{-1} to a Gle1-activated k_{cat} ~0.16 s^{-1} (Figure 3.1; Figure 3.7; Table 3.1). The value of the k_{cat} predicted from the values of the Gle1-Dbp5 ATP hydrolysis rate constant (k_{78}), Gle1-Dbp5 ATP resynthesis rate constant (k_{87}), and the P_i release rate constant of Gle1-Dbp5-ADP-P_i (k_{89}) determined here and Equation 3.9 (44):

$$k_{cat} = \frac{k_{78}k_{89}}{k_{87} + k_{89} + k_{78}} \quad (3.9),$$

yield a k_{cat} value of 0.12 s^{-1} comparable to the k_{cat} of ~0.15 s^{-1} measured in steady-state ATPase assays (Figure 3.1, Figure 3.7; Table 3.1). Second, the "apparent K_M" of Gle1 (K_{Gle1}; [Gle1] for half-maximal Dbp5 steady-state ATPase) measured experimentally is 300 nM (Figure 3.1; Table 3.1). The value of the K_{Gle1} predicted from the values of the Gle1 affinity for Dbp5-ATP (K_{d107}), Gle1 affinity for Dbp5-ADP-P_i (K_{d118}), Gle1-Dbp5 ATP hydrolysis rate constant (k_{78}), Gle1-Dbp5 ATP resynthesis rate constant (k_{87}), and the P_i release rate constant of Gle1-Dbp5-ADP-P_i (k_{89}) determined here and Equation 3.10 (44):

$$K_{Gle1} = \frac{\left(k_{87} + k_{89}\right)K_{d107} + k_{78}K_{d118}}{\left(k_{78} + k_{87} + k_{89}\right)} \quad (3.10),$$

yield a K_{Gle1} value of 240 nM, comparable to the K_{Gle1} of 300 nM measured in steady-state ATPase assays (Figure 3.1; Table 3.1). Similarly, the $K_{M,ATP}$ of Gle1-

Dbp5 predicted from the association rate constant of ATP binding Gle1-Dbp5 (k_{47}), ATP release rate constant of Gle1-Dbp5-ATP (k_{74}), Gle1-Dbp5 ATP hydrolysis rate constant (k_{78}), Gle1-Dbp5 ATP resynthesis rate constant (k_{87}), and the P_i release rate constant of Gle1-Dbp5-ADP-P_i (k_{89}) determined here and Equation 3.11 (44):

$$K_{m,ATP} = \frac{k_{74}k_{87} + k_{74}k_{89} + k_{78}k_{89}}{k_{47}\left(k_{87} + k_{89} + k_{78}\right)} \quad (3.11),$$

yield a $K_{M,ATP}$ of 4-15 μM comparable to the ~20 μM measured in steady-state ATPase assays (Figure 3.1, Figure 3.7; Table 3.1). The consistency between the predicted and measured Gle1 stimulated Dbp5 steady-state cycling parameters ($k_{cat,}$ $K_{M,ATP}$, K_{Gle1}) indicate that the applied model and analysis are valid, and that the experimentally determined rate and equilibrium constants are consistent with the overall steady-state ATPase cycling behavior of Dbp5.

DISCUSSION

The use of transient kinetic analyses in this work has allowed for insight into the basis of Dbp5 ATPase activation by Gle1 with $InsP_6$. Considering the effects of Gle1 on nucleotide binding, hydrolysis, and product release from Dbp5, these data provide a model of Dbp5 activation by Gle1 that includes Gle1 accelerating Pi release and promoting ATP binding. Moreover, the kinetic scheme detailing Gle1 regulation of Dbp5 supplies an important foundation for developing a

complete kinetic description and functional understanding of Dbp5 regulation within the gene expression pathway via regulation by Gle1-$InsP_6$ and Nup159.

Gle1 stimulated ATP hydrolysis by Dbp5

Previous work has shown that the intrinsic Dbp5 steady-state ATPase cycling rate constant (k_{cat}) is slow (~0.03 s^{-1}) and limited by near-irreversible P_i release (25). Dbp5 also has a relatively weak affinity for ATP ($K_{M,ATP}$ of 1.3 – 1.9 mM) with RNA acting in the ATPase cycle to accelerate P_i release (25). Here, in the absence of RNA, it is demonstrated that Gle1 activates Dbp5 ATPase activity by accelerating P_i release. Although in the presence of Gle1, like RNA (25), P_i release remains the rate limiting step in the Dbp5 ATPase cycle. It is not currently known if this limitation is fully relieved when both Gle1 and RNA are present.

High resolution crystal structures indicate that Gle1 binds both RecA-like domains of Dbp5 to alter the positioning of these two domains and the nucleotide binding site (23). Gle1-induced rearrangements also include displacement of an auto-inhibitory helix in an ATP or ADP bound auto-inhibited form of DDX19 (human homolog of Dbp5) to promote an RNA-binding competent state (54). The accelerated release of phosphate reported here is consistent with these previously observed Gle1-induced rearrangements in Dbp5 that may act to weaken coordination of bound P_i and enable dissociation from Dbp5 post-hydrolysis. This Gle1activity is expected to transition Dbp5 from a high (Dbp5-ADP-P_i) to low (Dbp5-ADP) affinity RNA binding state, or resolve an auto-

inhibited state, which may be critical for Dbp5 function and/or efficient recycling of Dbp5 after an ATP hydrolysis event.

A second finding of this work is that Gle1 promotes ATP binding ~150-fold and lowers the $K_{M,ATP}$ 75-fold from ~1.5 mM to ~20 μM (Figure 3.7, Table 3.1) during Gle1 stimulated steady-state Dbp5 ATPase cycling. Previous studies reported a $K_{M,ATP}$ for Gle1 stimulated Dbp5 ATPase of about 100 μM (20), considerably weaker than the 20 μM reported here. The [Dbp5] and [Gle1] utilized in those measurements were not saturating, so the measured $K_{M,ATP}$ reflects a population weighted average of free and Gle1 bound Dbp5 steady-state turnover, yielding a significantly weaker $K_{M,ATP}$.

The ability of Gle1 to affect phosphate release and ATP binding (this work), and to promote RNA-release from Dbp5 and bind a Dbp5-ADP complex (23), suggests that Gle1 engages Dbp5 in multiple configurations. Note that the full N-terminus of Dbp5/DDX19 has not been modeled by structural data with Gle1 bound, which may be engaged by Gle1 to regulate Dbp5/DDX19 activity since it harbors an autoinhibitory function (23) (54). Overall, it is envisioned that Gle1 may act within the same ATPase cycle to engage Dbp5 to promote cycling by multiple modes of action based on nucleotide state. For example, following Gle1 stimulated phosphate release, the continued binding and organization of both RecA-like domains of ADP bound Dbp5 by Gle1 may subsequently promote ATP binding by limiting the conformational flexibility of the two domains (23). In this way, enzyme recycling would be mediated by Gle1 linking ADP, P_i, and RNA release to binding of ATP. Alternatively, only a single function of Gle1 may occur

in each Dbp5 ATPase cycle based on context, including the binding of other regulators, the presence and type of RNA substrate (e.g., mRNA, pre-rRNA, or tRNA) and process being directed (e.g., RNA export vs. translation regulation).

Implications for mRNA export models

Biochemical, structural, and genetic data strongly support a role for Gle1 in regulating Dbp5 activity to mediate mRNA export through NPCs. Several models have been presented (19,39,65,115) for individual aspects of the Dbp5 ATPase cycle given the available data. The kinetic and equilibrium analysis presented here allows for further refinement and alignment of these models.

One proposed mRNA export model suggests that Gle1 promotes ATP binding to Dbp5 based on a combination of genetic, cell, and biochemical data (24). Another model proposes that Gle1 binding would facilitate RNA-release from Dbp5 and enzyme recycling based on structural and biochemical data (23). The kinetic analyses in this work are consistent with both proposed Gle1 activities. Specifically, Gle1 promotes ATP loading via a ~150-fold increase in ATP affinity that is achieved by slowing ATP dissociation (Table 3.1). In addition, Gle1 promotes P_i release and ATP resynthesis ~20-fold, which is expected to promote release of RNA following hydrolysis, and in turn Dbp5 recycling. In combination, the kinetic effects of Gle1 on Dbp5 would favor the Dbp5-ATP state, which has a high affinity for RNA compared to other nucleotide states (42). The net effect of Gle1 on Dbp5 would be to shift the steady-state distribution of populated intermediates from weak RNA binding states to strong RNA binding states (i.e., Dbp5-ADP and nucleotide free Dbp5 to Dbp5-ATP; Figure 3.8) and to facilitate

RNA-release and enzyme recycling (RNA-Dbp5-ADP-Pi to Dbp5-ADP), which likely involves resolving auto-inhibited Dbp5 conformations bound to both ATP and ADP (23) (54).

At NPCs, Nup159 facilitates Dbp5 localization and activity, including reports that Nup159 weakens Gle1 binding to Dbp5-ADP (26). These data, combined with the observations that Gle1 slows both ATP binding and release from Dbp5, suggest that Nup159 may play a key role at this point in the ATPase cycle to promote a weakened interaction between Gle1 and Dbp5 and enhance enzyme turnover. These activities involving Gle1 and Nup159 likely act to ensure there is an available pool of ATP bound Dbp5 at NPCs to engage RNA and facilitate export, which can maintain RNA flux from the nucleus and the kinetics of RNA export that occurs on the millisecond time scale (36,48,100,101).

Notably, Dbp5 has been linked to pre-ribosomal complex and tRNA export, as well as translation, which is suggested to involve unique enzyme activities (e.g., ATP hydrolysis appears dispensable for pre-ribosomal export but is required for mRNA export) and functions within discrete cellular compartments (15,38,40,66). This raises questions about the functionality of Dbp5 in these other roles that may be independent of Gle1 and/or dependent on different Dbp5 activities (e.g., stable RNA binding in the nucleus vs. RNA-protein remodeling at NPCs involving ATP hydrolysis). These questions involving Dbp5 functions and differential regulation of the ATPase cycle to effect different outcomes must be addressed in the context of a fully reconstituted system that involves Nup159, Gle1-$InsP_6$, and RNA, which is a goal of future work.

SCHEMES

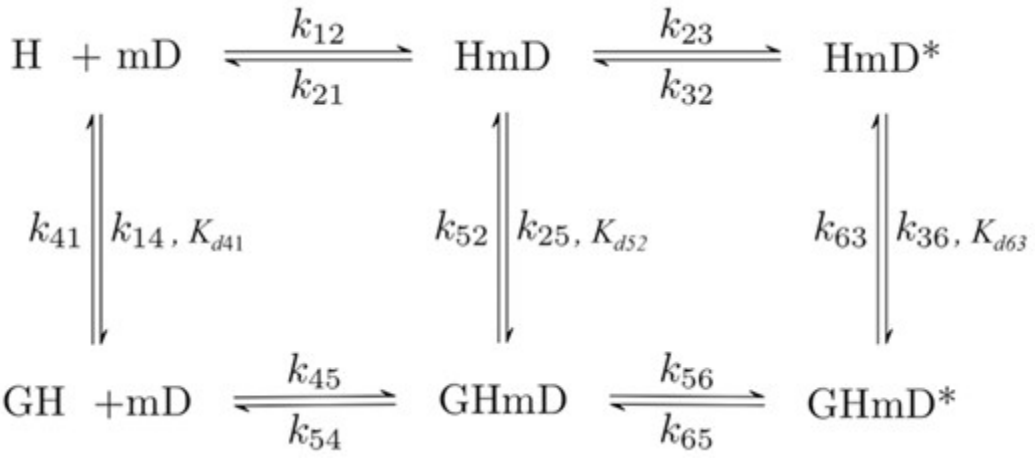

Scheme 3.1 Two-step reaction mechanism for mantADP binding to Dbp5 and Gle1–Dbp5. H = Dbp5, G = Gle1- $InsP_6$, mD = mantADP.

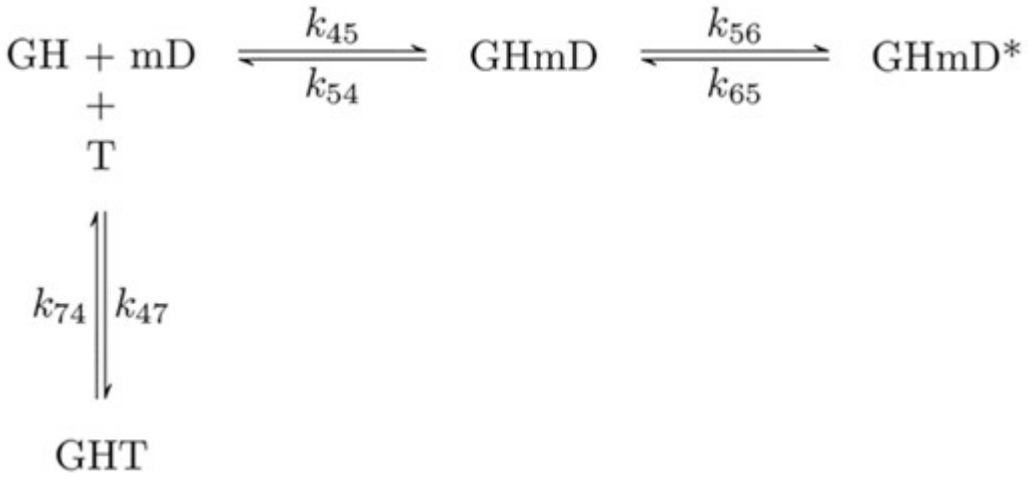

Scheme 3.2 Minimal reaction scheme for kinetic competition between mantADP and ATP binding by Gle1–Dbp5. H = Dbp5, G = Gle1-InsP6, mD = mantADP, T = ATP.

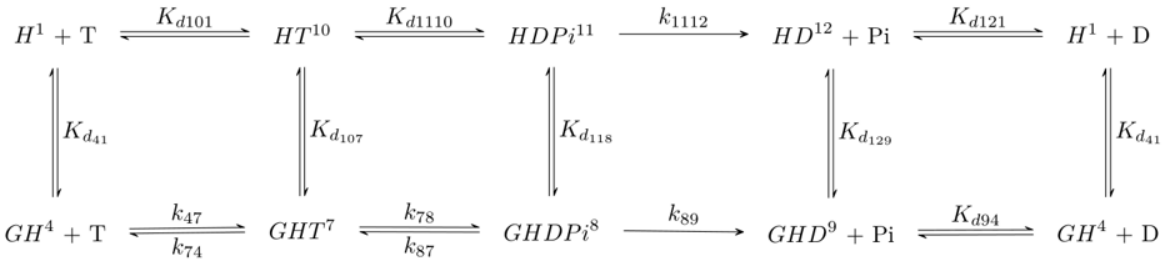

Scheme 3.3 Minimal reaction scheme for Dbp5 steady-state ATPase (±Gle1). H = Dbp5, G = Gle1-InsP_6, T = ATP, D = ADP, P_i= PO_4. Rate and equilibrium constants for Dbp5 ATPase (top pathway) have been published elsewhere (25).

FIGURES

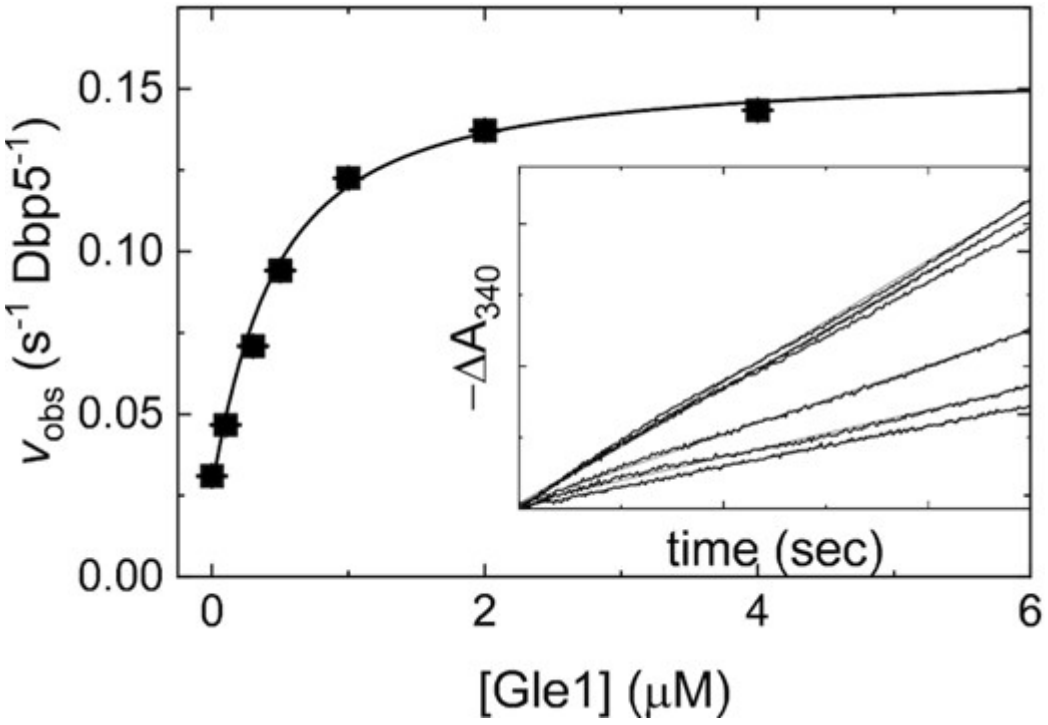

Figure 3.1 Gle1-stimulated steady-state ATPase activity of Dbp5. [Gle1]-dependance of the Gle1-stimulated Dbp5 steady-state ATPase rate (v_{obs}) per enzyme. The continuous line through the data represents the best fit to Equation (2.9) in (109) yielding the maximum observed velocity vobs per enzyme (k_{cat}= 0.16 ± 0.01 s^{-1} $Dbp5^{-1}$) from the amplitude and K_{Gle1} (apparent K_M = 0.3 ± 0.1 μM) from the [Gle1] at half-maximum velocity (Table 3.1). Uncertainty bars represent standard errors in the fits and are contained within the data points. Inset: Time courses of absorbance change at 340 nm assayed with the NADH-coupled assay after mixing 200 nM Dbp5 (100 nM after mixing) and 30 mM ATP (15 mM after mixing) with various [Gle1] (0–4 μM after mixing). The continuous lines through the data represent the best fits to linear functions, yielding the

steady-state ATPase rate from the slopes. InsP6 is included in all experiments at an equimolar concentration with Gle1.

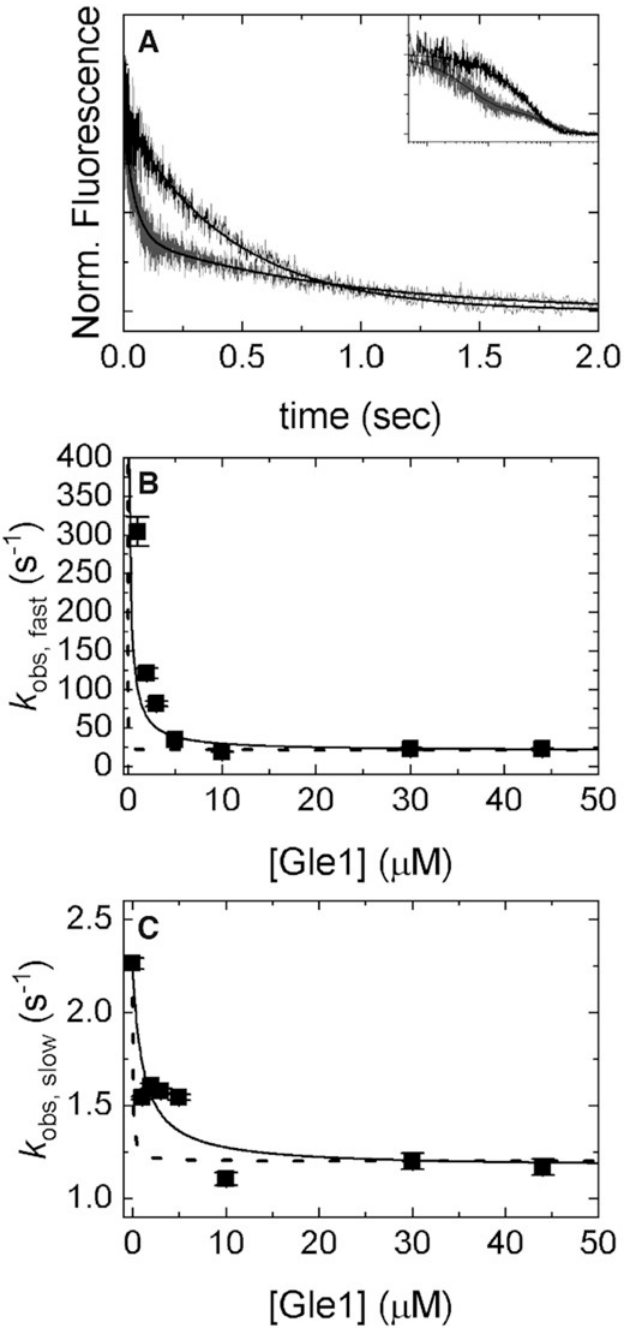

Figure 3.2. [Gle1]-dependence of mantADP dissociation from Dbp5. (A). Time courses of FRET signal changes after mixing a pre-equilibrated solution of Dbp5 (1 μM after mixing), 40 μM mantADP (20 μM after mixing), and various concentrations of Gle1 (0, 1, 2, 3, 5, 10, 30, 44 μM after mixing) with an equal volume of 20 mM ADP (10 mM after mixing). Continuous lines through the data

represent the best fits to either single (0 μM Gle1) or double ([Gle1] > 0 μM) exponentials. The inset is a log-scale depiction of the same time courses in A. (B). [Gle1]-dependence of the fast phase observed rate constants of mantADP dissociating from pre-formed Gle1-Dbp5(mant)ADP complex. Continuous lines through the data represent the best globally fits to a kinetic simulation of Scheme 3.1 with the data from Figures 3.3 and 3.4 (dashed lines) or the best fits to Equation 3.1 (continuous lines), which yields K_{d52} = 0.2 ± 0.1 μM. (C). [Gle1]-dependence of the slow phase observed rate constants of mantADP dissociating from pre-formed Gle1-Dbp5(mant)ADP complex. Continuous lines through the data represent the best globally fits to a kinetic simulation of Scheme 3.1 with the data from Figures 3.3 and 3.4 (dashed lines) or the best fits to Equation 3.2 (continuous lines) yielding K_{d63} = 1.1 ± 0.6 μM. Fundamental rate constants garnered from the global fits are: k_{45} = 1 ± 0.4 s^{-1}, k_{54} = 13 ± 6 s^{-1}, k_{56} = 8 ± 7 s^{-1}, k_{65} = 2 ± 1 s^{-1}, K_{d52} < 0.1 μM, K_{d63} < 1 μM, K_{d41} < 1 μM. Uncertainty bars represent standard error in the fits and are contained within the data points. $InsP_6$ is included in all experiments at an equimolar concentration with Gle1.

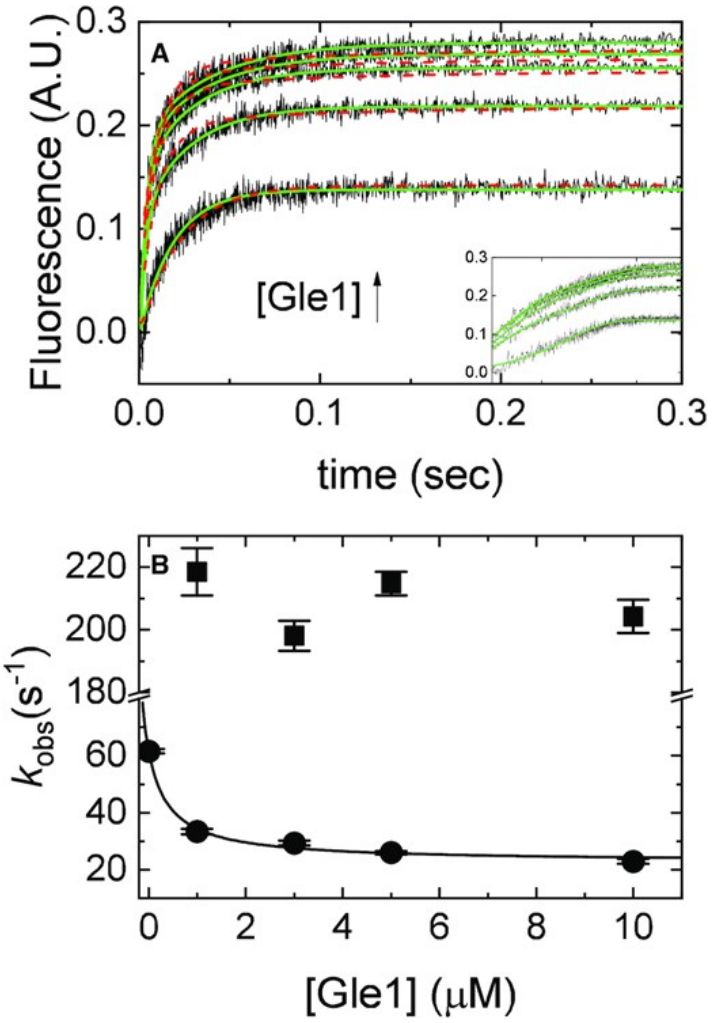

Figure 3.3. [Gle1]-dependence of mantADP binding to Dbp5. (A). Time courses of FRET signal change in pre-equilibrated solution of 2 μM Dbp5 (1 μM after mixing) with various concentrations of Gle1 ([Gle1] = 1-10 μM after mixing) upon rapid mixing with and equal volume of 200 μM mantADP (100 μM after mixing). Continuous lines through the data represent the best fits to exponential functions (solid lines) or the best global fits (with the data from Figures 3.2 and 3.4) to a kinetic simulation of Scheme 3.1 (dashed lines). The inset is a log-scale version of the same time courses in A (B). [Gle1]-dependence of the observed rate constants of mantADP binding to pre-formed Gle1-Dbp5 complex. The

continuous line through the data represents the slow phase k_{obs} (closed circles) overlaid on top with a rectangular hyperbola to aid visualization. Uncertainty bars represent standard error in the fits and are contained within the data points. $InsP_6$ is included in all experiments at an equimolar concentration with Gle1.

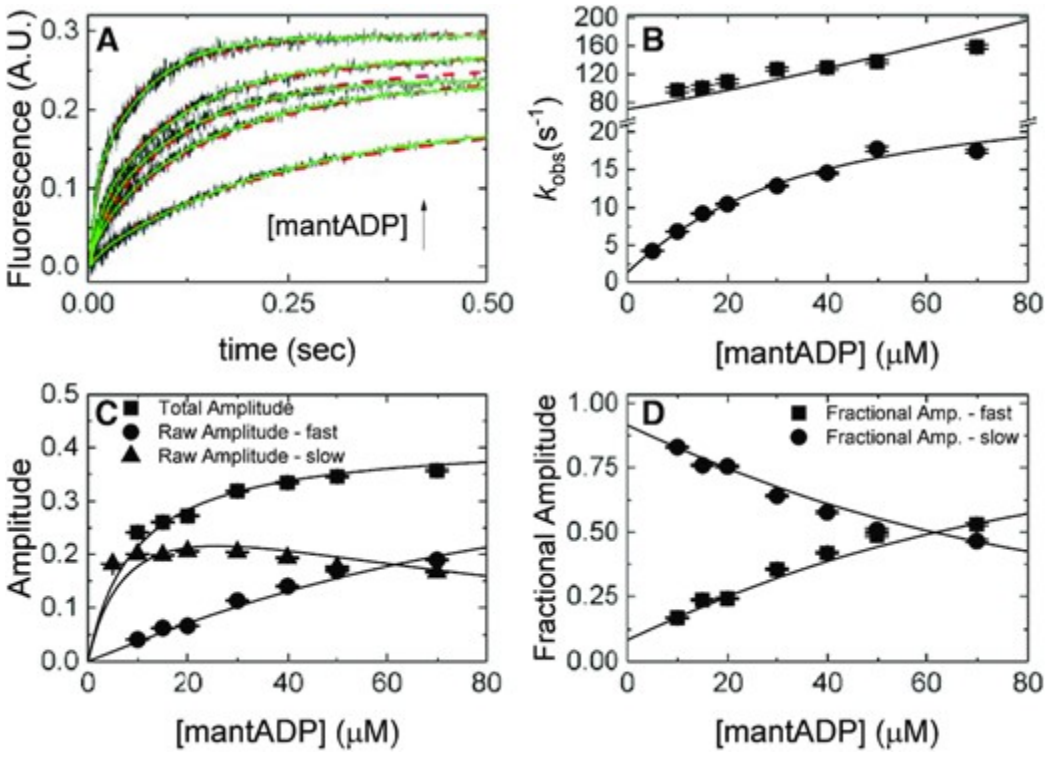

Figure 3.4. mantADP binding to Gle1-Dbp5. (A). Time courses of FRET signal changes in pre-equilibrated solution of 1 μM Dbp5 (0.5 μM after mixing) with 20 μM Gle1 (10 μM after mixing) upon rapidly mixing with an equal volume of various concentrations of mantADP (5-70 μM after mixing). Continuous lines through the data are the best fits to either double exponentials (solid lines) or global fits (with data from Figure 3.2B and Figure 3.3) to a kinetic simulation of Scheme 3.1 (dashed lines). (B). [mantADP]-dependence of the observed rate constants for mantADP binding pre-formed Gle1-Dbp5 complex. Continuous lines through the data represent the best global fits to a two-step binding model(76). Rate constants resulting from this analysis are: k_{45} = 1.8 ± 0.14 μM^{-1} s^{-1}, k_{54} = 47 ± 4.3 s^{-1}, k_{56} = 24 ± 1.7 s^{-1}, k_{65} = 2.1 ± 0.3 s^{-1}. (C). [mantADP]-dependence of the fast and slow phase raw amplitudes and total amplitude for mantADP binding pre-formed Gle1-Dbp5 complex. (D). [mantADP]-dependence

of the fast and slow phase fractional amplitudes for mantADP binding pre-formed Gle1-Dbp5 complex. Continuous lines through the data in C and D are simulated amplitudes using rate constants from fits in B. We include the amplitude data to demonstrate consistency with a two-step binding model. Uncertainty bars represent standard error in the fits and are contained within the data points. $InsP_6$ is included in all experiments at an equimolar concentration with Gle1.

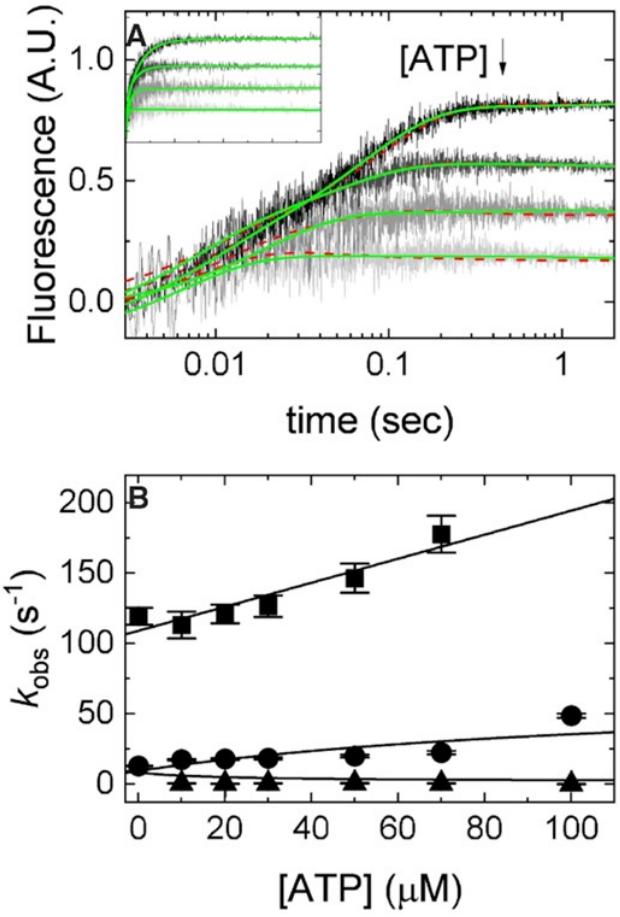

Figure 3.5. Kinetic competition between mantADP and ATP. (A). Time courses of FRET signal changes in pre-equilibrated solution of 2 μM Dbp5 (1 μM after mixing) with 20 μM Gle1 (10 μM after mixing) upon rapid mixing with an equal volume of 40 μM mantADP (20 μM after mixing) with various concentrations of ATP (from 0 to 300 μM after mixing). Continuous lines through the data are either the best fits to double or triple exponential functions (solid lines) or the best fits to a kinetic simulation of Scheme 3.2 (dashed lines). (B) [ATP]-dependence of the observed rate constants from exponential fits in A (solid lines) for mantADP binding pre-formed Gle1-Dbp5 complex. Continuous lines through the data are the best global fits to Supplemental Equations S3.18, S3.19

and S3.24. Uncertainty bars represent standard error in the fits and are contained within the data points. For both fits, rate constants for mantADP binding were held to values determined from fits in Figure 3.4B. Fundamental rate constants resulting from the fits to a kinetic simulation of Scheme 3.2 are k_{47} = 0.2 ± 0.1 μM^{-1} s^{-1} and k_{74} = 4.1 ± 2.5 s^{-1}, while fits to Equations S3.18, S3.19 and S3.24 yield k_{47} = 0.6 ± 0.1 μM^{-1} s^{-1} and k_{74} = 3.3 ± 1.1 s^{-1}. $InsP_6$ is included in all experiments at an equimolar concentration with Gle1.

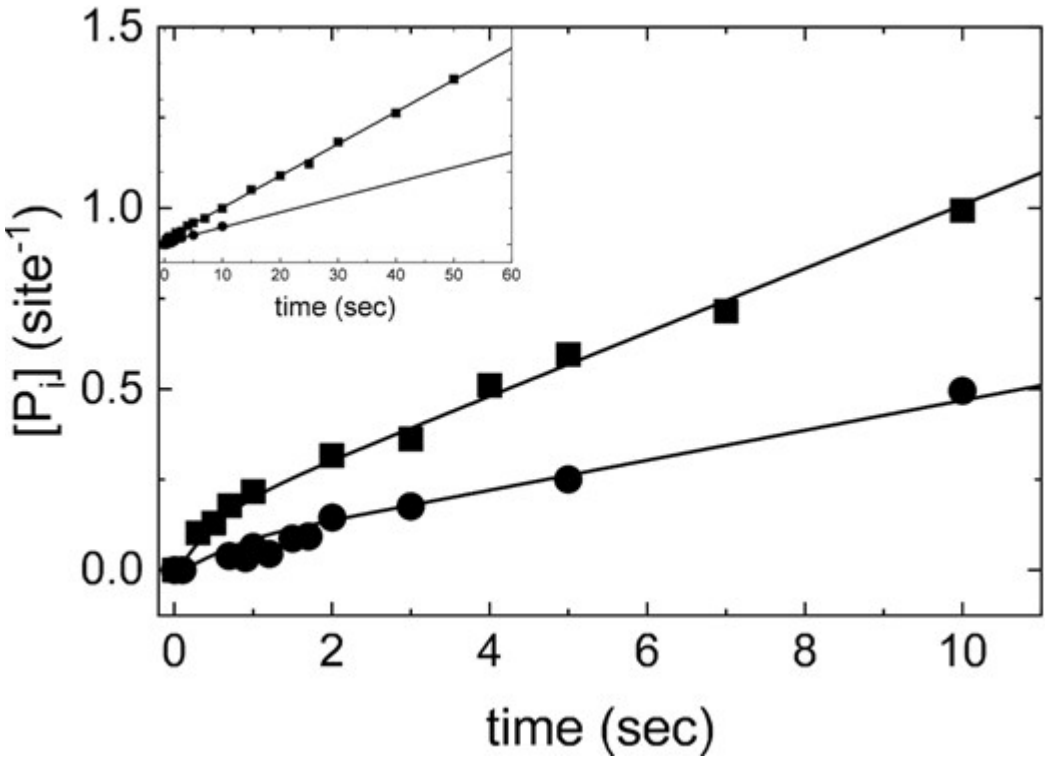

Figure 3.6. Direct measurement of ATP hydrolysis by Gle1-Dbp5 via quench flow. Time courses of phosphate production in pre-equilibrated solution of 36 μM Dbp5 (18 μM after mixing) with 120 μM Gle1 (60 μM after mixing) upon rapid mixing with either 76 μM (circles, 38 μM after mixing) or 340 μM (squares, 170 μM after mixing) ATP containing a trace of P^{32}-ATP. Continuous lines through the data are the best fits to either the analytical solution for an ATP hydrolysis reaction scheme (Equations 3.5-3.7) (44) or the best fits to a custom MATLAB program simulating ATP hydrolysis. The best fits from each method overlap. When all parameters are left unconstrained, the best fit to the analytical solution yields: k_{47} = 0.09 ± 0.5 μM^{-1} s^{-1}, k_{74} = 9.7 ± 55 s^{-1}, k_{78} = 0.6 ± 0.2 s^{-1}, k_{87} = 1.0 ± 0.9 s^{-1}, k_{89} = 0.4 ± 0.1 s^{-1}. Alternatively, fixing k_{47} and k_{74} to values determined from kinetic competition (Figure 3.5) results in a less than two-fold change in ATP hydrolysis and phosphate release rate constants: k_{78} = 0.6 ± 0.2 s^{-1}, k_{87} = 1.9 ±

1.3 s^{-1}, k_{89} = 0.6 ± 0.1 s^{-1}. Lastly, the best fit MATLAB simulation yields: k_{78} = 0.4 ± 0.2 s^{-1}, k_{87} = 1.7 ± 0.4 s^{-1}, and k_{89} = 0.6 ± 0.1 s^{-1}. Neither 20 μM Dbp5 nor 60 μM Gle1 alone generated detectable ATP hydrolysis with up to ten second incubation with 50 μM ATP. $InsP_6$ is included in all experiments at an equimolar concentration with Gle1.

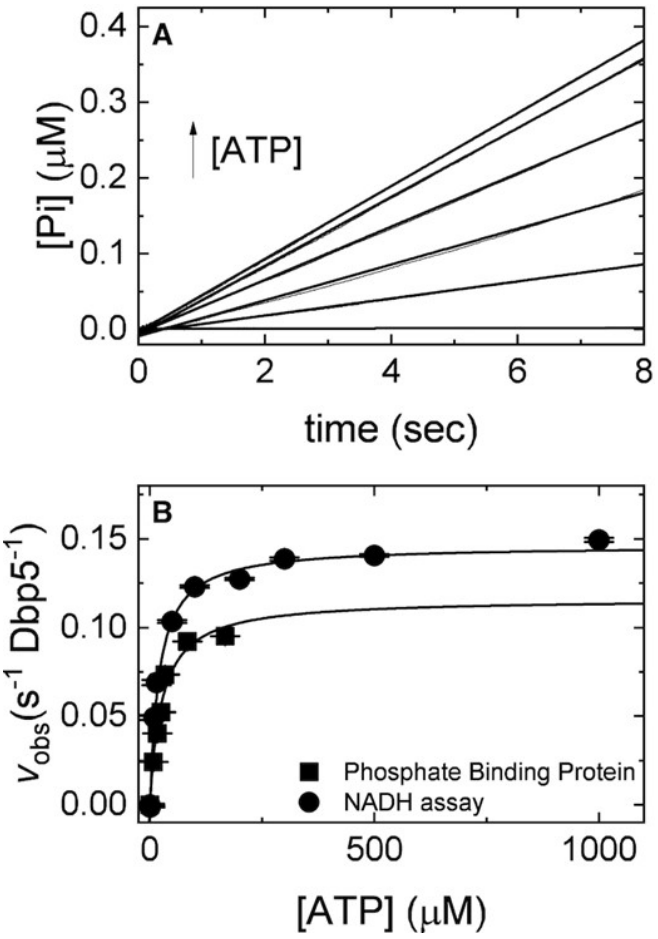

Figure 3.7. Direct measurement of Pi release from Gle1-Dbp5 via P_iBP. (A). Time courses of phosphate release in a pre-equilibrated mixture of 1 μM Dbp5 (0.5 μM after mixing) and 20 μM Gle1 (10 μM after mixing) upon rapid mixing with various [ATP] (0, 5, 10, 15, 20, 50, 100 μM after mixing) containing 6 μM P_iBP (3 μM after mixing). Continuous lines through the data are the best fits to a linear equation. (B). [ATP]-dependance of the observed steady-state P_i release in A (solid squares) or steady-state ATP hydrolysis in the presence of the NADH regenerating system (44,109,116). Continuous lines through the data are the best fits to a rectangular hyperbola yielding the maximum velocity per enzyme (k_{cat} = 0.15 ± 0.02 s^{-1} $Dbp5^{-1}$, circles; k_{cat} = 0.12 ± 0.01 s^{-1} $Dbp5^{-1}$, squares) from

the amplitude and K_M (20 ± 3 μM, circles; 26 ± 6 μM, squares) from the [ATP] at half-maximum velocity (Table 3.1). Uncertainty bars represent standard errors in the fits and are contained within the data points. $InsP_6$ is included in all experiments at an equimolar concentration with Gle1.

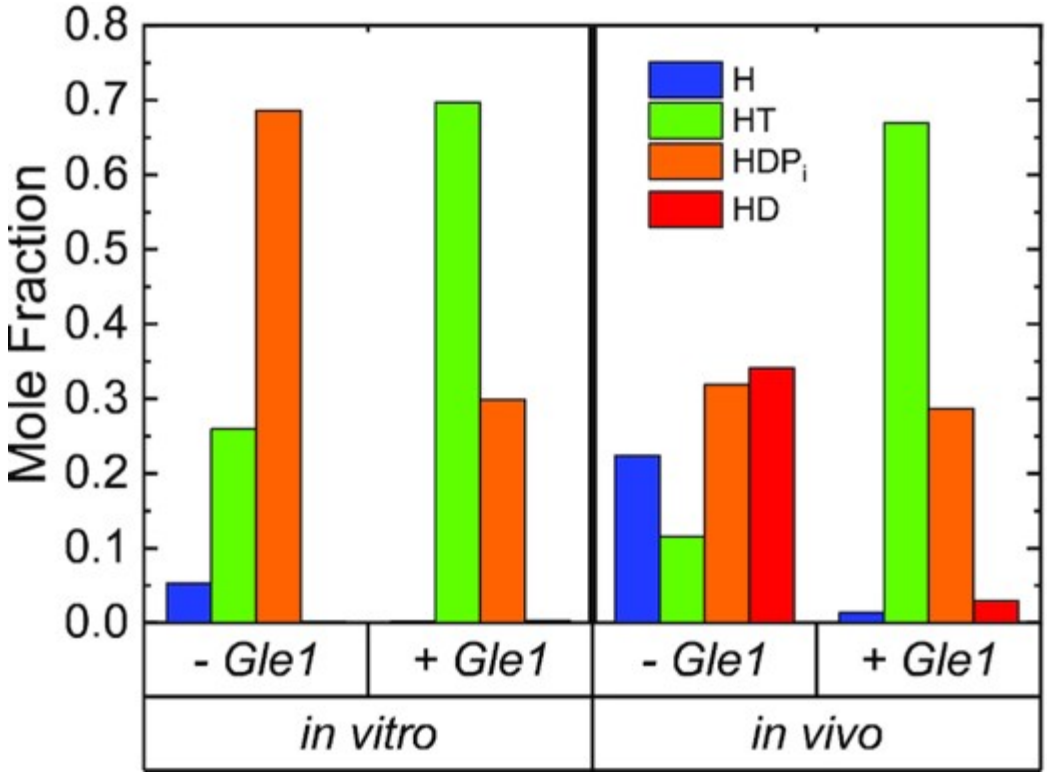

Figure 3.8. Steady-state distribution of Dbp5(±Gle1) ATPase cycle intermediates. *In vitro* conditions are 20 mM ATP, 0 mM ADP, and 0 mM P_i. *In vivo* conditions are 2.1 mM ATP (117), 470 μM ADP (117), and 2.5 mM P_i (118). $InsP_6$ is included in all experiments at an equimolar concentration with Gle1.

TABLES

Table 3.1

Parameter	Reaction	Value	Assay
Gle1 stimulated Dbp5 steady-state ATPase			
k_{cat}	Maximum Gle1 stimulated steady-state turnover rate	0.15 (± 0.03) s^{-1} $Dbp5^{-1}$	NADH assay, Fig. 3.7
		0.16 (± 0.01) s^{-1} $Dbp5^{-1}$	NADH assay, Fig. 3.1
		0.12 (± 0.01) s^{-1} $Dbp5^{-1}$	P_iBP, Fig. 3.7
		0.12 (± 0.07) s^{-1} $Dbp5^{-1}$	Predicted from individually measured rate and equilibrium constants, Eq. 3.9
$K_{M,ATP}$	[ATP] at half maximal steady-state velocity	20 (± 3) μM	NADH assay, Fig. 3.7
		26 (± 6) μM	P_iBP, Fig. 3.7
		4 (±3) μM	Predicted from individually measured rate and equilibrium constants, Eq. 3.11
		15 (±13) μM	
K_{Gle1}	[Gle1] at half maximal steady-state velocity	0.3 (± 0.1) μM	NADH assay, Fig. 3.1
		0.24 (± 0.1) μM	Predicted from individually measured rate and equilibrium constants, Eq. 3.10
mantADP binding to Dbp5			
K_{d21}	Equilibrium constant for initial binding	102 (± 21) μM	mantADP, reference (25)
k_{23}	Forward isomerization rate constant	98 (± 15) s^{-1}	
k_{32}	Reverse isomerization rate constant	2.6 (± 0.003) s^{-1}	
K_{d32}	Isomerization equilibrium constant	0.02 (± 0.003)	

$K_{mD,overall}$	Overall mantADP binding affinity, ([HmD] + [HmD*])	2 (± 0.07) μM	$\frac{K_{d21}K_{d32}}{1+K_{d32}}$
mantADP binding to Gle1-Dbp5			
k_{45}	Association rate constant	1.8 (± 0.14) μM^{-1} s^{-1}	mantADP, Fig. 3.4
k_{54}	Dissociation rate constant	47 (± 4.3) s^{-1} 19.8 (± 6) s^{-1}	mantADP, Fig. 3.2
K_{d54}	Equilibrium constant for initial binding	26 (± 3.2) μM 11 (± 3.4) μM	$\frac{k_{54}}{k_{45}}$
k_{56}	Forward isomerization rate constant	24 (± 1.7) s^{-1}	mantADP, Fig. 3.4
k_{65}	Reverse isomerization rate constant	2.1 (± 0.3) s^{-1} ≥ 1.3 (± 0.1) s^{-1} 2 (± 1) s^{-1}	mantADP, Fig. 3.2 mantADP, Global fit of Figs. 3.2-3.4
K_{d65}	Isomerization equilibrium constant	0.09 (± 0.01) ≥ 0.07 (± 0.006)	$\frac{k_{65}}{k_{56}}$
$K_{mD,overall}$	Overall mantADP binding affinity, ([GHmD] + [GHmD*])	2.2 (± 0.3) μM	$\frac{K_{d54}K_{d65}}{1+K_{d65}}$
ATP binding to Dbp5			
K_{d101}	ATP equilibrium binding affinity	3 (± 0.4) mM	Kinetic competition of ATP and mantADP, reference (25)
ATP binding to Gle1-Dbp5			
k_{47}	Association rate constant	0.2 (± 0.1) μM^{-1} s^{-1} 0.6 (± 0.1) μM^{-1} s^{-1}	Kinetic competition of ATP and mantADP, global MATLAB fit (dashed lines), Fig. 3.5A Kinetic competition of ATP and mantADP, Eq. S3.18, S3.19 and S3.24, Fig. 3.5B
k_{74}	Dissociation rate constant	4.1 (± 2.5) s^{-1}	Kinetic competition of ATP and

			mantADP, global MATLAB fits (dashed lines), Fig. 3.5A
		3.3 (± 1.1) s^{-1}	Kinetic competition of ATP and mantADP, Eq. S3.18, S3.19 and S3.24, Fig. 3.5B
K_{d74}	ATP equilibrium binding affinity	20 (± 16) μM	Ratio of rate constants from global MATLAB fits
		5.5 (± 2) μM	Ratio of rate constants from Eq. S3.18, S3.19 and S3.24
ATP Hydrolysis by Dbp5			
k_{1011}	ATP hydrolysis rate constant	0.16 (± 5 × 10^{-4}) s^{-1}	KinTek steady-state simulation, reference (25)
		2.2 (± 0.4) s^{-1}	P_iBP, reference (25)
k_{1110}	ATP resynthesis rate constant	6 × 10^{-4} (± 8 × 10^{-7}) s^{-1}	KinTek steady-state simulation, reference (25)
		2 × 10^{-4} (± 5 × 10^{-5}) s^{-1}	P_iBP and isotope exchange, reference (25)
K_{d1110}	Equilibrium constant for ATP hydrolysis	0.004 (± 5 × 10^{-4})	$\frac{k_{1110}}{k_{1011}}$
		10^{-4} (± 3 × 10^{-5})	
ATP Hydrolysis by Gle1-Dbp5			
k_{78}	ATP hydrolysis rate constant	0.6 (± 0.2) s^{-1}	Quench-flow, Fig. 3.6
k_{87}	ATP resynthesis rate constant	1.0 (± 0.9) s^{-1}	
K_{d87}	Equilibrium constant for ATP hydrolysis	1.7 (± 1.6)	$\frac{k_{87}}{k_{78}}$
P_i release from Dbp5-ADP-P_i			
k_{1112}	Rate constant for P_i release from HDP_i	0.02 (± 0.1) s^{-1}	P_iBP, reference (25)

K_{d1211}	Equilibrium constant for P_i binding HD	> 10 mM	Steady-state P_i inhibition, reference (25)
P_i release from Gle1-Dbp5-ADP-Pi			
k_{89}	Rate constant for P_i release from $GHDP_i$	0.4 (± 0.1) s^{-1}	Quench-flow, Fig. 3.6
K_{d89}	Equilibrium constant for P_i binding GHD	> 10 mM	Supplemental Information, section S4
ADP binding Dbp5			
K_{d121}	Equilibrium constant for ADP binding H	360 (± 50) μM	Kinetic competition of ADP and mantADP, reference (25)
ADP binding Gle1-Dbp5			
K_{d94}	Equilibrium constant for ADP binding GH	240 (± 15) μM	Kinetic competition of ADP and mantADP, Fig. S3.3
Gle1 binding Dbp5-ATP			
K_{d107}	Equilibrium constant of Gle1 binding to HT	1.5 (± 0.8) nM	Detailed balance of Scheme 3, **Supplemental Information** section **S6**
Gle1 binding Dbp5-ADP-P_i			
K_{d118}	Equilibrium constant for Gle1 binding to HDP_i	0.6 (± 0.2) μM	Detailed balance of Scheme 3, **Supplemental Information** section **S6**
Gle1 binding Dbp5-ADP			
K_{d129}	Equilibrium constant for Gle1 binding HD	0.5 (± 0.2) μM	Detailed balance of Scheme 3, **Supplemental Information** section **S6**
Gle1 binding to Dbp5			
K_{d41}	Equilibrium constant for G binding H	0.8 (± 0.3) μM	mantADP, Detailed balance of Scheme 1, Fig. 3.3
Gle1 Dbp5-mantADP complexes			
K_{d52}	Equilibrium constant for G binding HmD	0.2 (± 0.1) μM	mantADP, Fig. 3.2

K_{d63}	Equilibrium constant for G binding HmD*	1.1 (± 0.6) μM	
$K_{D,overall}$	Equilibrium constant for G binding Dbp5-mantADP	0.17 (± 0.15) μM	$\frac{K_{d52}K_{d63}}{K_{d52}+K_{d63}}$

CHAPTER 3: SUPPLEMENTAL INFORMATION

SECTION S1

As an independent check of the assumptions required to fit the data in Figure 3.4 to a simplified two-step binding model, the mantADP binding data from Figures 3.3A and 3.4A, along with the [Gle1]-dependance of the k_{obs} for irreversible mantADP dissociation in Figure 3.2B, were all globally fitted using a custom MATLAB program to numerically solve for unknown parameters in Scheme 3.1. The relevant rate and equilibrium constants in Scheme 3.1 were shared across all data sets. Rate and equilibrium constants were left unconstrained and randomly initialized between 0 and 500. This fit results in the following set of parameters: k_{45} = 1 ± 0.4 s^{-1}, k_{54} = 13 ± 6 s^{-1}, k_{56} = 8 ± 7 s^{-1}, k_{65} = 2 ± 1 s^{-1}, K_{d41} < 0.1 μM, K_{d52} < 0.1 μM, K_{d63} < 1 μM, which are consistent with fits to the analytical solution in Figure 3.4B. The listed uncertainties represent the ninety-five percent confidence interval of the final converged values after many fitting iterations (n = 100).

We note that occasionally, rate constants did not converge and yielded physically unrealistic values (e.g., association rate constants far exceeding the diffusion limit). However, upon plotting it is clear that these parameters cannot match the experimental data collectively and likely represent a local, but not global minimum in the total sum of squares. Rate constants for Gle1 binding *apo*Dbp5 depend on parameter initialization, although the equilibrium constant (K_{d41}) never exceeded 0.1 μM regardless of parameter initialization (Figure S3.1 A, B),

consistent with published data (64). The values of K_{d52} and K_{d63} never exceed ~ 1 μM, regardless of initialization (Figure S3.1 C-F). Together, these results validate the assumptions required for fits in Figure 3.4B.

SECTION S2

The reaction scheme for ATP and mantADP binding to Dbp5 in a kinetic competition can be described by the following general mechanism:

$$M + L_l \underset{k_{l,-1}}{\overset{k_{l,+1}}{\rightleftarrows}} (ML_l)_1 \underset{k_{l,-2}}{\overset{k_{l,+2}}{\rightleftarrows}} (ML_l)_2$$
$$M + L_{unl} \underset{k_{unl,-}}{\overset{k_{unl,+}}{\rightleftarrows}} ML_{unl}$$

Scheme S3.1

where, the unlabeled ligand L_{unl} competes to bind the macro molecule M with two-step binding of labeled ligand L_l. The time course of the reaction should follow 3 exponentials and the different equations associated with Scheme S3.1 are

$$\frac{d[ML_l]_1}{dt} = k_{l,+1}[M][L_l] - k_{l,-1}[ML_l]_1 - k_{l,+2}[ML_l]_1 + k_{l,-2}[ML_l]_2 \quad \text{(S3.1)}$$

$$\frac{d[ML_{unl}]}{dt} = k_{unl,+}[M][L_{unl}] - k_{unl,-}[ML_{unl}] \quad \text{(S3.2)}$$

To obtain meaningful form for unlabeled ligand concentration dependence of rate constant, suitable assumptions have to be made. Thus, we consider the following 3 cases:

1. Unlabeled ligand dissociates much faster than labeled ligand binding, i.e., $k_{unl,-} >> k_l[M][L_l]$. In this case, unlabeled ligand reaches fast equilibrium with macromolecule before labeled ligand binds.

Given rapid equilibration of L_{unl} and M, $[ML_{unl}] = \frac{[M][L_{unl}]}{K_{unl}}$, we assume that the $[L_{unl}]$ is always in excess over [M] such that:

$$[ML_{unl}] = \frac{[M][L_{unl}]_0}{K_{unl}}$$

This yields a mass balance relationship of:

$$M_{tot} = [M] + [ML_{unl}] + [ML_l]_1 + [ML_l]_2 = [M]\left(1 + \frac{[L_{unl}]_0}{K_{unl}}\right) + [ML_l]_1 + [ML_l]_2 \quad \text{(S3.3)}$$

Therefore, the two differential equations describing the reaction scheme are:

$$\begin{pmatrix} \frac{d[ML_l]_1}{dt} \\ \frac{d[ML_l]_2}{dt} \end{pmatrix} = \begin{pmatrix} -\left(k_{l,-1} + k_{l,+2} + \frac{k_{l,+1}[L_l]_0 K_{unl}}{[L_{unl}]_0 + K_{unl}}\right) & -\left(\frac{k_{l,+1}[L_l]_0 K_{unl}}{[L_{unl}]_0 + K_{unl}} - k_{l,-2}\right) \\ k_{l,+2} & -k_{l,-2} \end{pmatrix} \begin{pmatrix} [ML_l]_1 \\ [ML_l]_2 \end{pmatrix} + \begin{pmatrix} \frac{M_{tot} k_{l,+1} K_{unl}[L_l]_0}{[L_{unl}]_0 + K_{unl}} \\ 0 \end{pmatrix} \quad \text{(S3.4)}$$

The solution to Equaiton S3.4 will take the following form $\overrightarrow{x(t)} = Y_c + Y_p$, where Y_c is the general solution and Y_p is the special solution. Y_c will have the following form:

$$Y_c = C_1 e^{-\lambda_1 t}\overrightarrow{\eta_1} + C_2 e^{-\lambda_2 t}\overrightarrow{\eta_2}$$

To solve for $\lambda_{1,2}$,

$$\begin{vmatrix} -\left(k_{l,-1} + k_{l,+2} + \dfrac{k_{l,+1}[L_l]_0 K_{unl}}{[L_{unl}]_0 + K_{unl}}\right) - \lambda & -\left(\dfrac{k_{l,+1}[L_l]_0 K_{unl}}{[L_{unl}]_0 + K_{unl}} - k_{l,-2}\right) \\ k_{l,+2} & -k_{l,-2} - \lambda \end{vmatrix}$$

$$0 = k_{l,-1}k_{l,-2}\lambda^2 + \lambda\left(k_{l,-1} + k_{l,+2} + k_{l,-2} + \frac{k_{l,+1}[L_l]_0 K_{unl}}{[L_{unl}]_0 + K_{unl}}\right) + \frac{k_{l,+1}\left(k_{l,+2} + k_{l,-2}\right)K_{unl}[L_l]_0}{[L_{unl}]_0 + K_{unl}}$$

Solving the roots of this equation,

$$\lambda_{1,2} = -\frac{1}{2}\left(k_{l,1} + k_{l,+2} + k_{l,-2} + \frac{k_{l,+1}[L_l]_0 K_{unl}}{[L_{unl}]_0 + K_{unl}} \pm \sqrt{\left(k_{l,1} + k_{l,+2} + k_{l,-2} + \frac{k_{l,+1}[L_l]_0 K_{unl}}{[L_{unl}]_0 + K_{unl}}\right)^2 - 4\left(k_{l,-1}k_{l,-2} + \frac{k_{l,+1}k_{l,+2}K_{unl}[L_l]_0}{[L_{unl}]_0 + K_{unl}} + \frac{k_{l,+1}k_{l,-2}K_{unl}[L_l]_0}{[L_{unl}]_0 + K_{unl}}\right)}\right)$$

(S3.5)

Now we will solve for the eigen vectors, $\overrightarrow{\eta_{1,2}}$:

$$\begin{pmatrix} -\left(k_{l,-1}+k_{l,+2}+\dfrac{k_{l,+1}[L_l]_0 K_{unl}}{[L_{unl}]_0+K_{unl}}\right)-\lambda & -\left(\dfrac{k_{l,+1}[L_l]_0 K_{unl}}{[L_{unl}]_0+K_{unl}}-k_{l,-2}\right) \\ k_{l,+2} & -k_{l,-2}-\lambda \end{pmatrix}\begin{pmatrix}\eta_1\\ \eta_2\end{pmatrix}=\begin{pmatrix}0\\0\end{pmatrix}$$

$$\Rightarrow \eta_2=\eta_1\frac{k_{l,+2}}{k_{l,-2}+\lambda}$$

The eigenvector in this case is:

$$\vec{\eta}^{(1)}=\begin{pmatrix}1\\ \dfrac{k_{l,+2}}{k_{l,-2}+\lambda}\end{pmatrix}$$

Therefore,

$$Y_c=C_1e^{-\lambda_1 t}\begin{pmatrix}1\\ \dfrac{k_{l,+2}}{k_{l,-2}+\lambda_1}\end{pmatrix}+C_2e^{-\lambda_2 t}\begin{pmatrix}1\\ \dfrac{k_{l,+2}}{k_{l,-2}+\lambda_2}\end{pmatrix}$$

Now we will solve for Y_p:

$$\vec{x}'-A\vec{x}=\vec{g},\ \text{where } \vec{g}=\begin{pmatrix}\dfrac{M_{tot}k_{l,+1}K_{unl}[L_l]_0}{[L_{unl}]_0+K_{unl}}\\ 0\end{pmatrix}$$

Therefore, Y_p will be a constant vector, $\vec{B}$:

$$\vec{0}-A\vec{B}=\begin{pmatrix}\dfrac{M_{tot}k_{l,+1}K_{unl}[L_l]_0}{[L_{unl}]_0+K_{unl}}\\ 0\end{pmatrix}\Rightarrow \vec{B}=A^{-1}\begin{pmatrix}\dfrac{M_{tot}k_{l,+1}K_{unl}[L_l]_0}{[L_{unl}]_0+K_{unl}}\\ 0\end{pmatrix}$$

Therefore,

$$\vec{B} = -\frac{M_{tot} k_{l,+1} K_{unl} [L_l]_0}{k_{l,-1} k_{l,-2} \left([L_{unl}]_0 + K_{unl}\right) + k_{l,+1} [L_l]_0 K_{unl} \left(k_{l,+2} + k_{l,-2}\right)} \begin{pmatrix} k_{l,-2} \\ k_{l,+2} \end{pmatrix}$$

The general solution is:

$$\begin{pmatrix} [ML_l]_1(t) \\ [ML_l]_2(t) \end{pmatrix} = C_1 e^{-\lambda_1 t} \begin{pmatrix} 1 \\ \frac{k_{l,+2}}{k_{l,-2} + \lambda_1} \end{pmatrix} + C_2 e^{-\lambda_2 t} \begin{pmatrix} 1 \\ \frac{k_{l,+2}}{k_{l,-2} + \lambda_2} \end{pmatrix}$$
$$- \frac{M_{tot} k_{l,+1} K_{unl} [L_l]_0}{k_{l,-1} k_{l,-2} \left([L_{unl}]_0 + K_{unl}\right) + k_{l,+1} [L_l]_0 K_{unl} \left(k_{l,+2} + k_{l,-2}\right)} \begin{pmatrix} k_{l,-2} \\ k_{l,+2} \end{pmatrix} \quad \text{(S3.6)}$$

To solve for the arbitrary constants, $C_{1,2}$, in Equation S3.6 we use the initial conditions at t = 0. At equilibrium, prior to mixing (i.e., t = 0) $[ML_l]_1(0)$ and $[ML_l]_2(0)$ are described by the following reaction scheme:

$$M + L_l \underset{}{\overset{K_1}{\longleftrightarrow}} (ML_l)_1 \underset{}{\overset{K_2}{\longleftrightarrow}} (ML_l)_2$$

Where $K_1 = \frac{k_{l,-1}}{k_{l,+1}} = \frac{[M][L_l]_0}{[ML_l]_1}$ and $K_2 = \frac{k_{l,-2}}{k_{l,+2}} = \frac{[ML_l]_1}{[ML_l]_2}$ if we assume $[L_l] >> [M]_{tot}$ then, $[L_l]_{tot} \sim [L_l]_0$.

$$[ML_l]_1 + [ML_l]_2 = [ML_l]_1 + \frac{[ML_l]_1}{K_2} = \frac{1 + K_2}{K_2} [ML_l]_1$$
$$\Rightarrow [ML_l]_1 = \frac{K_2}{1 + K_2} ([ML_l]_1 + [ML_l]_2)$$
$$\Rightarrow [ML_l]_2 = \frac{1}{1 + K_2} ([ML_l]_1 + [ML_l]_2) \quad \text{(S3.7)}$$

From mass balance, $[M]_{tot} = [M] + [ML_l]_1 + [ML_l]_2$ and K_1, K_2, and Equation S3.7:

$$[M]_{tot} = \frac{K_1 K_2}{1+K_2}\frac{[ML_l]_1 + [ML_l]_2}{[L_l]_0} + [ML_l]_1 + [ML_l]_2 \quad \text{(S3.8)}$$

Solving Equation S3.8 for $[ML_l]_1 + [ML_l]_2$ yields,

$$[ML_l]_1 + [ML_l]_2 = \frac{[M]_{tot}[L_l]_0}{[L_l]_0 + K_2 + K_1 K_2} \quad \text{(S3.9)}$$

Substituting Equation S3.9 into K_1 and K_2 yields,

$$[ML_l]_1(0) = \frac{[M]_{tot}[L_l]_0 K_2}{(1+K_2)([L_l]_0 + K_2 + K_1 K_2)}$$
$$[ML_l]_2(0) = \frac{[M]_{tot}[L_l]_0}{(1+K_2)([L_l]_0 + K_2 + K_1 K_2)} \quad \text{(S3.10)}$$

Substituting Equation S3.10 into Equation S3.6 at t = 0 yields,

$$\begin{pmatrix}[ML_l]_1(0)\\ [ML_l]_2(0)\end{pmatrix} = \begin{pmatrix}\frac{[M]_{tot}[L_l]_0 K_2}{(1+K_2)([L_l]_0 + K_2 + K_1 K_2)}\\ \frac{[M]_{tot}[L_l]_0}{(1+K_2)([L_l]_0 + K_2 + K_1 K_2)}\end{pmatrix} = C_1 e^{-\lambda_1 t}\begin{pmatrix}1\\ \frac{k_{l,+2}}{k_{l,-2}+\lambda_1}\end{pmatrix} + C_2 e^{-\lambda_2 t}\begin{pmatrix}1\\ \frac{k_{l,+2}}{k_{l,-2}+\lambda_2}\end{pmatrix}$$
$$-\frac{M_{tot}k_{l,+1}K_{unl}[L_l]_0}{k_{l,-1}k_{l,-2}([L_{unl}]_0 + K_{unl}) + k_{l,+1}[L_l]_0 K_{unl}(k_{l,+2}+k_{l,-2})}\begin{pmatrix}k_{l,-2}\\ k_{l,+2}\end{pmatrix} \quad \text{(S3.11)}$$

Solving Equation S3.11 for $C_{1,2}$ yields,

$$C_1 = -\frac{M_{tot}k_{l,+1}(k_{l,-2}+\lambda_1)\lambda_2[L_l]_0([L_{unl}]_0 k_{l,-1}k_{l,+2}k_{l,-2} + k_{l,-1}k_{l,-2}(2k_{l,+2}+k_{l,-2})K_{unl} + k_{l,+1}(k_{l,+2}+k_{l,-2})K_{unl}(k_{l,-2}+2k_{l,+2}[L_l]_0))}{(k_{l,+2}+k_{l,-2})(\lambda_1-\lambda_2)([L_{unl}]_0 k_{l,-1}k_{l,-2} + k_{l,-1}k_{l,-2}K_{unl} + k_{l,+1}(k_{l,+2}+k_{l,-2})K_{unl}[L_l]_0)(k_{l,-1}k_{l,-2} + k_{l,+1}(k_{l,-2}+k_{l,+2}[L_l]_0))}$$
$$C_2 = -\frac{M_{tot}k_{l,+1}(k_{l,-2}+\lambda_2)\lambda_1[L_l]_0([L_{unl}]_0 k_{l,-1}k_{l,+2}k_{l,-2} + k_{l,-1}k_{l,-2}(2k_{l,+2}+k_{l,-2})K_{unl} + k_{l,+1}(k_{l,+2}+k_{l,-2})K_{unl}(k_{l,-2}+2k_{l,+2}[L_l]_0))}{(k_{l,+2}+k_{l,-2})(\lambda_1-\lambda_2)([L_{unl}]_0 k_{l,-1}k_{l,-2} + k_{l,-1}k_{l,-2}K_{unl} + k_{l,+1}(k_{l,+2}+k_{l,-2})K_{unl}[L_l]_0)(k_{l,-1}k_{l,-2} + k_{l,+1}(k_{l,-2}+k_{l,+2}[L_l]_0))}$$

2. Unlabeled ligand binding is comparable to the first binding step of labeled ligand, i.e., $k_{unl,+} \sim k_{l,+1,}$ and both dissociation of unlabeled ligand and the first step of labeled ligand is much faster than labeled ligand second step binding, i.e., $k_{unl,-}$, $k_{l,-1} >> [ML_l]\ k_{l,+2}$. In this case, the macromolecule reaches equilibrium with $[ML_l]_1$ and $[M_{unl}]$ before $[ML_l]_2$ is significantly populated. Therefore, in the time region after the first step of labeled ligand binding and unlabeled ligand binding reach equilibrium, but before labeled ligand second step binding significantly starts, according to mass conservation, the total macromolecule is approximated to

$$[M]_{tot} = [M] + [ML_{unl}] + [ML_l]_1 + [ML_l]_2 \sim [M] + [ML_{unl}] + [ML_l]_1 \quad \text{(S3.12)}$$

Equation S3.1 is reduced to

$$\begin{aligned}
&\frac{d[ML_l]_1}{dt} \sim k_{l,+1}[M][L_l] - \left(k_{l,-1} + k_{l,+2}\right)[ML_l]_1 \\
&= k_{l,+1}\left([M]_{tot} - [ML_l]_1 - [ML_{unl}]\right)[L_l] - \left(k_{l,-1} + k_{l,+2}\right)[ML_l]_1 \\
&= k_{l,+1}[L_l][M]_{tot} - \left(k_{l,+1}[L_l] + k_{l,-1} + k_{l,+2}\right)[ML_l]_1 - k_{l,+1}[L_l][ML_{unl}]
\end{aligned}$$

i.e.,

$$\left(\frac{d}{dt} + k_{l,+1}[L_l] + k_{l,-1} + k_{l,+2}\right)[ML_l]_1 + k_{l,+1}[L_l][ML_{unl}] = k_{l,+1}[L_l][M]_{tot} \quad \text{(S3.13)}$$

Equation S3.2 becomes

$$\begin{aligned}
&\frac{d[ML_{unl}]}{dt} = k_{unl,+}\left([M]_{tot} - [ML_l]_1 - [ML_{unl}]\right)[L_{unl}] - k_{unl,-}[ML_{unl}] \\
&= k_{unl,+}[L_{unl}][M]_{tot} - k_{unl,+}[L_{unl}][ML_l]_1 - \left(k_{unl,+}[L_{unl}] + k_{unl,-}\right)[ML_{unl}]
\end{aligned}$$

i.e.,

$$k_{unl,+}[L_{unl}][ML_l]_1 + \left(\frac{d}{dt} + k_{unl,+}[L_{unl}] + k_{unl,-}\right)[ML_{unl}] = k_{unl,+}[L_{unl}][M]_{tot} \quad \text{(S3.14)}$$

The equation to solve Eigen values of Equations S3.13 and S3.14 is

$$\begin{vmatrix} -\lambda + k_{l,+1}[L_l] + k_{l,-1} + k_{l,+2} & k_{l,+1}[L_l] \\ k_{unl,+}[L_{unl}] & -\lambda + k_{unl,+}[L_{unl}] + k_{unl,-} \end{vmatrix}$$
$$= \left(-\lambda + k_{l,+1}[L_l] + k_{l,-1} + k_{l,+2}\right)\left(-\lambda + k_{unl,+}[L_{unl}] + k_{unl,-}\right) - k_{l,+1}[L_l]k_{unl,+}[L_{unl}]$$
$$= \lambda^2 - \left(k_{l,+1}[L_l] + k_{l,-1} + k_{l,+2} + k_{unl,+}[L_{unl}] + k_{unl,-}\right)$$
$$+ \left(k_{l,-1} + k_{l,+2}\right)k_{unl,+}[L_{unl}] + \left(k_{l,+1}[L_l] + k_{l,-1} + k_{l,+2}\right)k_{unl,-} = 0$$

The solutions of the equation are the two observed rate constants of the period,

$$\lambda_{1,2} = \frac{1}{2}\Big(k_{l,+1}[L_l] + k_{l,-1} + k_{l,+2} + k_{unl,+}[L_{unl}] + k_{unl,-}$$
$$\pm\sqrt{\left(k_{l,+1}[L_l] + k_{l,-1} + k_{l,+2} + k_{unl,+}[L_{unl}] + k_{unl,-}\right)^2 - 4\left(k_{l,-1} + k_{l,+2}\right)k_{unl,+}[L_{unl}] - 4\left(k_{l,+1}[L_l] + k_{l,-1} + k_{l,+2}\right)k_{unl,-}}\Big)$$

(S3.15)

To further characterize the features of the two observed rate constants, further approximation is needed. The faster observed rate constant of the two can be re-written as

$$\lambda_1 = \frac{1}{2}\Big(k_{l,+1}[L_l] + k_{l,-1} + k_{l,+2} + k_{unl,+}[L_{unl}] + k_{unl,-}$$
$$+\sqrt{\left(k_{l,+1}[L_l] + k_{l,-1} + k_{l,+2} + k_{unl,+}[L_{unl}] + k_{unl,-}\right)^2 - 4\left(k_{l,-1} + k_{l,+2}\right)k_{unl,+}[L_{unl}] - 4\left(k_{l,+1}[L_l] + k_{l,-1} + k_{l,+2}\right)k_{unl,-}}\Big)$$
$$= \frac{1}{2}\Big(k_{l,+1}[L_l] + k_{l,-1} + k_{l,+2} + k_{unl,+}[L_{unl}] + k_{unl,-}$$
$$+\sqrt{\left(k_{l,+1}[L_l] + k_{l,-1} + k_{l,+2} + k_{unl,+}[L_{unl}] - k_{unl,-}\right)^2 + 4k_{unl,+}[L_{unl}]\left(k_{unl,-} - k_{l,-1} - k_{l,+2}\right)}\Big)$$

(S3.16)

or

$$= \frac{1}{2}\Big(k_{l,+1}[L_l] + k_{l,-1} + k_{l,+2} + k_{unl,+}[L_{unl}] + k_{unl,-}$$
$$+\sqrt{\left(k_{l,+1}[L_l] - k_{l,-1} - k_{l,+2} + k_{unl,+}[L_{unl}] + k_{unl,-}\right)^2 + 4k_{l,+1}[L_l]\left(k_{l,-1} + k_{l,+2} - k_{unl,-}\right)}\Big)$$

(S3.16')

It means the value of λ_1 is always between $k_{l,+1}[L_l] + k_{l,-1} + k_{l,+2} + k_{unl,+}[L_{unl}]$ and $k_{l,+1}[L_l] + k_{unl,+}[L_{unl}] + k_{unl,-}$ for all titrating [L_{unl}] unlabeled ligand concentration, i.e.,

$$k_{l,+1}[L_l] + k_{l,-1} + k_{l,+2} + k_{unl,+}[L_{unl}] \geq \lambda_1 > k_{l,+1}[L_l] + k_{unl,+}[L_{unl}] + k_{unl,-}, \quad \text{if } k_{l,-1} + k_{l,+2} \geq k_{unl,-}$$
$$k_{l,+1}[L_l] + k_{l,-1} + k_{l,+2} + k_{unl,+}[L_{unl}] \leq \lambda_1 < k_{l,+1}[L_l] + k_{unl,+}[L_{unl}] + k_{unl,-}, \quad \text{if } k_{l,-1} + k_{l,+2} < k_{unl,-}$$

(S3.17)

At [L_{unl}] = 0, it should $\lambda_1 = k_{l,+1}[L_l] + k_{l,-1} + k_{l,+2}$, therefore, we choose

$$\lambda_1 \sim k_{l,+1}[L_l] + k_{l,-1} + k_{l,+2} + k_{unl,+}[L_{unl}] \qquad \text{(S3.18)}$$

to be approximately the faster observed rate constant for any unlabeled ligand concentration for consistency with the case when $[L_{unl}] = 0$. It is a linear function of $[L_{unl}]$ with *y*-intercept of $k_{l,+1}[L_l] + k_{l,-1} + k_{l,+2}$ and slope of $k_{unl,+}$. With this approximation, the slower observed rate constant becomes:

$$\lambda_2 = \frac{\lambda_1\lambda_2}{\lambda_1} = \frac{\left(k_{l,-1} + k_{l,+2}\right)k_{unl,+}[L_{unl}] + \left(k_{l,+1}[L_l] + k_{l,-1} + k_{l,+2}\right)k_{unl,-}}{\lambda_1}$$

$$\sim \frac{\left(k_{l,-1} + k_{l,+2}\right)k_{unl,+}[L_{unl}] + \left(k_{l,+1}[L_l] + k_{l,-1} + k_{l,+2}\right)k_{unl,-}}{k_{l,+1}[L_l] + k_{l,-1} + k_{l,+2} + k_{unl,+}[L_{unl}]}$$

$$= \frac{\left(k_{l,-1} + k_{l,+2}\right)k_{unl,+}[L_{unl}] + \left(k_{l,+1}[L_l] + k_{l,-1} + k_{l,+2} + k_{unl,+}[L_{unl}] - k_{unl,+}[L_{unl}]\right)k_{unl,-}}{k_{l,+1}[L_l] + k_{l,-1} + k_{l,+2} + k_{unl,+}[L_{unl}]}$$

$$= k_{unl,-} + \frac{k_{l,-1} + k_{l,+2} - k_{unl,-}}{\frac{k_{l,+1}[L_l] + k_{l,-1} + k_{l,+2}}{k_{unl,+}} + [L_{unl}]}[L_{unl}] \qquad \text{(S3.19)}$$

Therefore, λ_2 is approximately a hyperbola with initial and final values of $k_{unl,-}$ and $k_{l,-1}+k_{l,+2}$ and it reaches a half of maximum at $[L_{unl}] = \frac{k_{l,+1}[L_l] + k_{l,-1} + k_{l,+2}}{k_{unl,+}}$.

In time region after unlabeled ligand binding and the first step of the ligand binding reach equilibrium, has only one differential equation left

$$\frac{d[ML_l]_2}{dt} = k_{l,+2}[ML_l]_1 - k_{l,-2}[ML_l]_2 \qquad \text{(S3.20)}$$

According to equilibrium among ligand unbound macromolecule, those with unlabeled ligand bound and the first species of labeled ligand bound, we have

$$[ML_l]_1 = \frac{[M][L_l]}{K_{l,1}}$$
$$[ML_{unl}] = \frac{[M][L_{unl}]}{K_{unl}} \quad \text{(S3.21)}$$

and

$$\begin{aligned}[M]_{tot} &= [M] + [ML_l]_1 + [ML_l]_2 + [ML_{unl}] \\ &= \frac{K_{l,1}[ML_l]_1}{[L_l]}\left(1 + \frac{[L_{unl}]}{K_{unl}}\right) + [ML_l]_1 + [ML_l]_2 \\ &= \left(\frac{K_{l,1}}{[L_l]}\left(1 + \frac{[L_{unl}]}{K_{unl}}\right) + 1\right)[ML_l]_1 + [ML_l]_2 \end{aligned} \quad \text{(S3.22)}$$

Substitute Equation S3.22 into Equation S3.20

$$\frac{d[ML_l]_2}{dt} = k_{l,+2}\frac{[M]_{tot} - [ML_l]_2}{\frac{K_{l,1}}{[L_l]}\left(1 + \frac{[L_{unl}]}{K_{unl}}\right) + 1} - k_{l,-2}[ML_l]_2$$

$$= \frac{k_{l,+2}[M]_{tot}}{\frac{K_{l,1}}{[L_l]}\left(1 + \frac{[L_{unl}]}{K_{unl}}\right) + 1} - \left(\frac{k_{l,+2}}{\frac{K_{l,1}}{[L_l]}\left(1 + \frac{[L_{unl}]}{K_{unl}}\right) + 1} + k_{l,-2}\right)[ML_l]_2$$

(S3.23)

The above first order linear equation has the following solution

$$[ML_l]_2 = A_3 e^{-\lambda_3 t} + \frac{\dfrac{k_{l,+2}[M]_{tot}}{\dfrac{K_{l,1}}{[L_l]}\left(1+\dfrac{[L_{unl}]}{K_{unl}}\right)+1}}{\dfrac{k_{l,+2}}{\dfrac{K_{l,1}}{[L_l]}\left(1+\dfrac{[L_{unl}]}{K_{unl}}\right)+1}+k_{l,-2}}$$

$$= A_3 e^{-\lambda_3 t} + \frac{k_{l,+2}[M]_{tot}}{k_{l,+2}+k_{l,-2}\left(\dfrac{K_{l,1}}{[L_l]}\left(1+\dfrac{[L_{unl}]}{K_{unl}}\right)+1\right)}$$

with rate constant

$$\lambda_3 = \frac{k_{l,+2}}{\dfrac{K_{l,1}}{[L_l]}\left(1+\dfrac{[L_{unl}]}{K_{unl}}\right)+1}+k_{l,-2}$$

$$= \frac{\dfrac{K_{unl}[L_l]}{K_{l,1}}k_{l,+2}}{K_{unl}\left(1+\dfrac{[L_l]}{K_{l,1}}\right)+[L_{unl}]}+k_{l,-2}$$

$$= \frac{\dfrac{k_{l,+2}[L_l]}{\left(K_{l,1}+[L_l]\right)}\left(K_{unl}\left(1+\dfrac{[L_l]}{K_{l,1}}\right)+[L_{unl}]-[L_{unl}]\right)}{K_{unl}\left(1+\dfrac{[L_l]}{K_{l,1}}\right)+[L_{unl}]}+k_{l,-2}$$

$$= \frac{k_{l,+2}[L_l]}{\left(K_{l,1}+[L_l]\right)}+k_{l,-2}-\frac{\dfrac{k_{l,+2}[L_l]}{K_{l,1}+[L_l]}[L_{unl}]}{K_{unl}\left(1+\dfrac{[L_l]}{K_{l,1}}\right)+[L_{unl}]} \qquad \text{(S3.24)}$$

The third observed rate constant is a downward hyperbola of [L_{unl}] with initial and final values of $\frac{k_{l,+2}[L_l]}{(K_{l,1}+[L_l])}+k_{l,-2}$ and $k_{l,-2}$, and it reaches a half of maximum when $[L_{unl}]=K_{unl}\left(1+\frac{[L_l]}{K_{l,1}}\right)$. *gaa*

In this case, that unlabeled ligand binding is comparable to the first step of labeled ligand the binding, the time course follows 3 exponentials and the fastest observed rate constant scales with unlabeled ligand concentration, while the two slower observed phases are hyperbolic functions.

Time courses in Figure 3.5A were fit to a sum of two or three exponential functions (continuous lines) and the observed rate constants were globally fit (Figure 3.5B, solid lines) to Equation (A) below (from Equations S3.18, S3.19 and S3.24):

$$\begin{aligned}\lambda_1 &\sim k_{l,+1}[L_l]+k_{l,-1}+k_{l,+2}+k_{unl,+}[L_{unl}]\\ \lambda_2 &= k_{unl,-}+\frac{k_{l,-1}+k_{l,+2}-k_{unl,-}}{\frac{k_{l,+1}[L_l]+k_{l,-1}+k_{l,+2}}{k_{unl,+}}+[L_{unl}]}[L_{unl}]\\ \lambda_3 &= \frac{k_{l,+2}}{\frac{K_{l,1}}{[L_l]}\left(1+\frac{[L_{unl}]}{K_{unl}}\right)+1}+k_{l,-2}\end{aligned} \qquad \text{(A)}$$

Where L_l is mantADP, L_{unl} is ATP, $K_{l,1}$ is the equilibrium constant for the first mantADP binding step, K_{unl} is the equilibrium constant for ATP binding, and $k_{unl,-}$, $k_{unl,+}$, $k_{l,+1}$, $k_{l,-1}$, $k_{l,+2}$, $k_{l,-2}$ correspond to k_{-ATP}, k_{+ATP}, k_{45}, k_{54}, k_{56}, and k_{65} in Scheme 3.2. The best fit estimates for k_{+ATP} and k_{-ATP} from Equation (A) are 0.6 ± 0.1 μM^{-1}

s^{-1} and 3.3 ± 1.1 s^{-1} (Table 3.1), respectively, consistent with MATLAB fittings. We note that modeling the ATP kinetic competition data with Scheme 3.2 is valid as little hydrolysis occurs within the time scales of the mantADP binding time courses (see **Results**).

3. Unlabeled ligand binding is comparable to the slow step of labeled ligand binding and both are much slower than the first step binding of labeled ligand, In this case, $k_{unl,+}[L_{unl}] \sim k_{l,+2} << k_{l,-1}$, the labeled ligand first binding step reaches equilibrium before labeled ligand second step binding and unlabeled ligand binding taking place. The equations for this case are

$$\frac{d[ML_l]_2}{dt} = k_{l,+2}[ML_l]_1 - k_{l,-2}[ML_l]_2 \tag{S3.25}$$

$$\frac{d[ML_{unl}]}{dt} = k_{unl,+}[M][L_{unl}] - k_{unl,-}[ML_{unl}] \tag{S3.26}$$

$$[ML_l]_1 = \frac{[M][L_l]}{K_{l,1}} \tag{S3.27}$$

$$\begin{aligned}[M]_{tot} &= [M] + [ML_l]_1 + [ML_l]_2 + [ML_{unl}] \\ &= \left(1 + \frac{[L_l]}{K_{l,1}}\right)[M] + [ML_l]_2 + [ML_{unl}] \\ &= \left(\frac{K_{l,1}}{[L_l]} + 1\right)[ML_l]_1 + [ML_l]_2 + [ML_{unl}]\end{aligned} \tag{S3.28}$$

Equation S3.25 and S3.26 can be re-written as

$$\frac{d[ML_l]_2}{dt} = k_{l,+2}\frac{[M]_{tot} - [ML_l]_2 - [ML_{unl}]}{1 + \frac{K_{l,1}}{[L_l]}} - k_{l,-2}[ML_l]_2$$

$$= \frac{k_{l,+2}[M]_{tot}}{1+\frac{K_{l,1}}{[L_l]}} - \left(\frac{k_{l,+2}}{1+\frac{K_{l,1}}{[L_l]}} + k_{l,-2} \right) [ML_l]_2 - k_{l,+2} \frac{[ML_{unl}]}{1+\frac{K_{l,1}}{[L_l]}} \quad \text{(S3.29)}$$

$$\frac{d[ML_{unl}]}{dt} = k_{unl,+}[L_{unl}] \frac{[M]_{tot} - [ML_l]_2 - [ML_{unl}]}{1+\frac{[L_l]}{K_{l,1}}} - k_{unl,-}[ML_{unl}]$$

$$= \frac{k_{unl,+}[L_{unl}][M]_{tot}}{1+\frac{[L_l]}{K_{l,1}}} - \frac{k_{unl,+}[L_{unl}][ML_l]_2}{1+\frac{[L_l]}{K_{l,1}}} - \left(\frac{k_{unl,+}[L_{unl}]}{1+\frac{[L_l]}{K_{l,1}}} + k_{unl,-} \right) [ML_{unl}] \quad \text{(S3.30)}$$

In this case, the time course follows 2 exponentials and according to Equations S3.29 and S3.30, the equation for the Eigen values of differential equations S3.29 and S3.30 is

$$\begin{vmatrix} -\lambda + \frac{k_{l,+2}}{1+\frac{K_{l,1}}{[L_l]}} + k_{l,-2} & \frac{k_{l,+2}}{1+\frac{K_{l,1}}{[L_l]}} \\ \frac{k_{unl,+}[L_{unl}]}{1+\frac{[L_l]}{K_{l,1}}} & -\lambda + \frac{k_{unl,+}[L_{unl}]}{1+\frac{[L_l]}{K_{l,1}}} + k_{unl,-} \end{vmatrix}$$

$$= \left(-\lambda + \frac{k_{l,+2}}{1+\frac{K_{l,1}}{[L_l]}} + k_{l,-2} \right) \left(-\lambda + \frac{k_{unl,+}[L_{unl}]}{1+\frac{[L_l]}{K_{l,1}}} + k_{unl,-} \right) - \frac{k_{l,+2}}{1+\frac{K_{l,1}}{[L_l]}} \frac{k_{unl,+}[L_{unl}]}{1+\frac{[L_l]}{K_{l,1}}}$$

$$= \lambda^2 - \left(\frac{k_{l,+2}}{1+\frac{K_{l,1}}{[L_l]}} + k_{l,-2} + \frac{k_{unl,+}[L_{unl}]}{1+\frac{[L_l]}{K_{l,1}}} + k_{unl,-} \right) \lambda + k_{l,-2} \frac{k_{unl,+}[L_{unl}]}{1+\frac{[L_l]}{K_{l,1}}} + \left(\frac{k_{l,+2}}{1+\frac{K_{l,1}}{[L_l]}} + k_{l,-2} \right) k_{unl,-} = 0$$

The solutions are

$$\lambda_{\pm} = \frac{1}{2} \left(\frac{k_{l,+2}}{1+\frac{K_{l,1}}{[L_l]}} + k_{l,-2} + \frac{k_{unl,+}[L_{unl}]}{1+\frac{[L_l]}{K_{l,1}}} + k_{unl,-} \right.$$
$$\left. \pm \sqrt{\left(\frac{k_{l,+2}}{1+\frac{K_{l,1}}{[L_l]}} + k_{l,-2} + \frac{k_{unl,+}[L_{unl}]}{1+\frac{[L_l]}{K_{l,1}}} + k_{unl,-} \right)^2 - 4k_{l,-2} \frac{k_{unl,+}[L_{unl}]}{1+\frac{[L_l]}{K_{l,1}}} - 4 \left(\frac{k_{l,+2}}{1+\frac{K_{l,1}}{[L_l]}} + k_{l,-2} \right) k_{unl,-}} \right)$$

(S3.31)

For further approximation, the fast rate constant in Equation S3.31 can be re-written as

$$\lambda_{+} = \frac{1}{2} \left(\frac{k_{l,+2}}{1+\frac{K_{l,1}}{[L_l]}} + k_{l,-2} + \frac{k_{unl,+}[L_{unl}]}{1+\frac{[L_l]}{K_{l,1}}} + k_{unl,-} \right.$$
$$\left. + \sqrt{\left(\frac{k_{l,+2}}{1+\frac{K_{l,1}}{[L_l]}} + k_{l,-2} + \frac{k_{unl,+}[L_{unl}]}{1+\frac{[L_l]}{K_{l,1}}} - k_{unl,-} \right)^2 + 4\left(k_{unl,-} - 4k_{l,-2} \right) \frac{k_{unl,+}[L_{unl}]}{1+\frac{[L_l]}{K_{l,1}}}} \right) \quad \text{(S3.32)}$$

or

$$= \frac{1}{2}\left(\frac{k_{l,+2}}{1+\frac{K_{l,1}}{[L_l]}} + k_{l,-2} + \frac{k_{unl,+}[L_{unl}]}{1+\frac{[L_l]}{K_{l,1}}} + k_{unl,-} \right.$$
$$\left. + \sqrt{\left(\frac{k_{l,+2}}{1+\frac{K_{l,1}}{[L_l]}} - k_{l,-2} + \frac{k_{unl,+}[L_{unl}]}{1+\frac{[L_l]}{K_{l,1}}} + k_{unl,-} \right)^2 + 4\frac{k_{l,+2}}{1+\frac{K_{l,1}}{[L_l]}}\left(k_{l,-2} - k_{unl,-}\right)} \right) \quad \text{(S3.32')}$$

Apparently, the fast observed rate constant in this case is between

$$\frac{k_{l,+2}}{1+\frac{K_{l,1}}{[L_l]}} + k_{l,-2} + \frac{k_{unl,+}[L_{unl}]}{1+\frac{[L_l]}{K_{l,1}}} \quad \text{and} \quad \frac{k_{l,+2}}{1+\frac{K_{l,1}}{[L_l]}} + \frac{k_{unl,+}[L_{unl}]}{1+\frac{[L_l]}{K_{l,1}}} + k_{unl,-}$$

, i.e.,

$$\frac{k_{l,+2}}{1+\frac{K_{l,1}}{[L_l]}} + k_{l,-2} + \frac{k_{unl,+}[L_{unl}]}{1+\frac{[L_l]}{K_{l,1}}} \geq \lambda_+ > \frac{k_{l,+2}}{1+\frac{K_{l,1}}{[L_l]}} + \frac{k_{unl,+}[L_{unl}]}{1+\frac{[L_l]}{K_{l,1}}} + k_{unl,-}, \quad \text{if } k_{l,-2} \geq k_{unl,-}$$
$$\frac{k_{l,+2}}{1+\frac{K_{l,1}}{[L_l]}} + k_{l,-2} + \frac{k_{unl,+}[L_{unl}]}{1+\frac{[L_l]}{K_{l,1}}} \leq \lambda_+ < \frac{k_{l,+2}}{1+\frac{K_{l,1}}{[L_l]}} + \frac{k_{unl,+}[L_{unl}]}{1+\frac{[L_l]}{K_{l,1}}} + k_{unl,-}, \quad \text{if } k_{l,-2} < k_{unl,-}$$

(S3.33)

$$\lambda_+ = \frac{k_{l,+2}}{1+\frac{K_{l,1}}{[L_l]}} + k_{l,-2}, \quad \text{when } [L_{unl}] = 0$$

To be consistent with , we choose the approximated form of the fast rate constant to be

$$\lambda_+ \sim \frac{k_{l,+2}}{1+\frac{K_{l,1}}{[L_l]}} + k_{l,-2} + \frac{k_{unl,+}[L_{unl}]}{1+\frac{[L_l]}{K_{l,1}}} \quad \text{(S3.34)}$$

at any unlabeled ligand concentration. It is a linear function of unlabeled ligand concentration with *y*-intercept of $\frac{k_{l,+2}}{1+\frac{K_{l,1}}{[L_l]}}+k_{l,-2}$ and slope of $\frac{k_{unl,+}}{1+\frac{[L_l]}{K_{l,1}}}$. Under this fast phase approximation, the slow phase is approximated to

$$\lambda_- = \frac{\lambda_-\lambda_+}{\lambda_+} \sim \frac{k_{l,-2}\frac{k_{unl,+}[L_{unl}]}{1+\frac{[L_l]}{K_{l,1}}}+\left(\frac{k_{l,+2}}{1+\frac{K_{l,1}}{[L_l]}}+k_{l,-2}\right)k_{unl,-}}{\frac{k_{l,+2}}{1+\frac{K_{l,1}}{[L_l]}}+k_{l,-2}+\frac{k_{unl,+}[L_{unl}]}{1+\frac{[L_l]}{K_{l,1}}}}$$

$$= \frac{k_{l,-2}\frac{k_{unl,+}[L_{unl}]}{1+\frac{[L_l]}{K_{l,1}}}+\left(\frac{k_{l,+2}}{1+\frac{K_{l,1}}{[L_l]}}+k_{l,-2}+\frac{k_{unl,+}[L_{unl}]}{1+\frac{[L_l]}{K_{l,1}}}-\frac{k_{unl,+}[L_{unl}]}{1+\frac{[L_l]}{K_{l,1}}}\right)k_{unl,-}}{\frac{k_{l,+2}}{1+\frac{K_{l,1}}{[L_l]}}+k_{l,-2}+\frac{k_{unl,+}[L_{unl}]}{1+\frac{[L_l]}{K_{l,1}}}}$$

$$= k_{unl,-} + \frac{k_{l,-2}\frac{k_{unl,+}[L_{unl}]}{1+\frac{[L_l]}{K_{l,1}}}-\frac{k_{unl,+}[L_{unl}]}{1+\frac{[L_l]}{K_{l,1}}}k_{unl,-}}{\frac{k_{l,+2}}{1+\frac{K_{l,1}}{[L_l]}}+k_{l,-2}+\frac{k_{unl,+}[L_{unl}]}{1+\frac{[L_l]}{K_{l,1}}}}$$

$$= k_{unl,-} + \frac{\left(k_{l,-2}-k_{unl,-}\right)[L_{unl}]}{\frac{K_{l,1}+[L_l]}{K_{l,1}k_{unl,+}}\left(\frac{k_{l,+2}[L_l]}{[L_l]+K_{l,1}}+k_{l,-2}\right)+[L_{unl}]} \qquad \text{(S3.35)}$$

The approximated slow phase is a hyperbola with initial and final values of $k_{unl,-}$ and $k_{l,-2}$, and it reaches a half of maximum at $[L_{unl}] = \frac{K_{l,1} + [L_l]}{K_{l,1} k_{unl,+}} \left(\frac{k_{l,+2}[L_l]}{[L_l] + K_{l,1}} + k_{l,-2} \right)$.

In the case both unlabeled ligand binding and the second step of labeled ligand binding is much slower than the equilibrium of the labeled ligand first step binding, the time course follows 2 exponentials. The fast phase rate constant scales linearly with unlabeled ligand concentration, whereas the slow phase concentration is a hyperbola of unlabeled ligand concentration.

SECTION S3

The effects of Gle1 on ADP binding were measured through kinetic competition by incubating 1 μM Dbp5 with 10 μM Gle1 for at least 2 hours at room temperature and subsequently mixing with 20 μM mantADP with various concentrations of ADP. Time courses of mantADP binding in the presence of ADP are best fit by a sum of two exponential functions (Figure S3.3A), indicating that one of the three binding steps equilibrates much faster than the other two (Scheme 3.2). Given that the rate constants for mantADP binding are independently known, Gle1-Dbp5 binding ADP is likely a rapid equilibration. Under these conditions, the fast and slow phase observed rate constants should display an [ADP]-dependent decrease (**Supplemental Information**, section **S2-1**). However, the noise associated with fitting the fast phase is significant. Therefore, we utilize only the [ADP]-dependance of the slow phase to estimate the ADP affinity (Figure S3.3B) with Equation S3.5 above (see **Supplemental**

Information section **S2-1**), yielding an affinity (K_{d94}) of 240 ± 15 μM for Gle1-Dbp5 binding ADP.

SECTION S4

Inclusion of up to 10 mM free phosphate does not significantly alter steady-state ATP hydrolysis by Dbp5 under saturating ATP and Gle1 conditions. This indicates that the apparent binding affinity of free phosphate for Gle1-Dbp5 complex during steady state ATP hydrolysis $K_{Pi,\,SS} \geq 10$ mM, because the equilibrium binding affinity between Gle1-Dbp5 and free phosphate ($K_{Pi,eq}$) is always greater than $K_{Pi,\,SS}$ (25), $K_{Pi,eq} > K_{Pi,\,SS} \geq 10$ mM. Therefore, phosphate rebinding does not need to be considered as no more than 80 μM (<< 10 mM) free phosphate is present in solution during the time scale of the quench-flow experiment.

SECTION S5

The maximum solution ionic strength (*I*, calculated from molality, so is unitless) change in our study < 2-fold over the [ATP] range examined, ranging from *I* = 0.14 (in assay buffer without other components added) to *I* = 0.21 with 15 mM Mg-ATP (50% change; Figure 3.1) or *I* = 0.23 with 15 mM Mg-ATP and 10 mM phosphate in the buffer solution (64.3% change; see below). At the high ATP used (~15 mM), this change has notable effect on the activity coefficient of ATP and reduces the effect ATP concentration < 23%. For example, the effective concentration of 15 mM ATP in the assay buffer with 10 mM phosphate is 11.6

mM. Consequently, there is no effect on the observed steady-state ATPase behaviors, which is the only experiment where such high [ATP] is used. This is supported by the fact that the ATPase activity in the presence of saturating [Gle1] is comparable in 0.1 mM Mg-ATP (~ k_{cat} = 0.15, saturated; Figure 3.7; I ~ 0.14 assay buffer ionic strength; see below) and 15 mM Mg-ATP (~ k_{cat} = 0.16; Figure 3.1; I = 0.21; see below). In addition, the Dbp5 ATPase, both in the presence (this work) and absence (previous work from our group (25)) of Gle1 was not affected by inclusion of 10 mM phosphate. Nevertheless, we provide calculations of our solution ionic strength here to inform readers.

1. *Ionic strength of assay buffer*: The ionic strength of the assay buffer is mainly from 1 of each K^+ and Cl^+ in KCl (100 mM), 1 Mg^{2+} and 2 Cl^+ in $MgCl_2$ (2 mM), and 1.5 charge from HEPES (30 mM). The ionic strength is I ~ $0.5([KCl]\times(1^2+1^2)+[MgCl_2]\times(2^2+2\times 1)+[HEPES]\times 1^2 = 0.14$

2. *Concentration of ions in our 100 mM ATP stock solution*: To make ATP stock solution at pH 7.0, we dissolve disodium ATP powder (Sigma-Aldrich, cat# A7699) in ddH_2O and immediately bring the pH up to 7.0 with KOH. In neutral pH solution, a ATP loses 3 protons and the affinity of the 4th proton is log(K) = 6.51 (119). Therefore, in pH 7.0, the ratio of ATP with the 4th proton off and on is

$$\log\left(\frac{\left[\mathrm{ATP}^{4-}\right]}{\left[\mathrm{HATP}^{3-}\right]}\right) = pH - pKa = 7 - 6.51 = 0.49$$

i.e.,

$$\frac{\left[\mathrm{ATP}^{4-}\right]}{\left[\mathrm{HATP}^{3-}\right]} = 10^{0.49} = 3.09$$

.

For 100 mM ATP stock solution in pH 7.0, 100/4.09 ~ 24.4 mM of it is $HATP^{3-}$ and 75.6 mM of it is ATP^{4-}. Consequently, $3[HATP^{3-}]+4[ATP^{4-}] = 3\times24.4+4\times75.6 = 375.6$ mM proton H^+ is dissociated from disodium ATP into solution in pH 7.0 and it needs the same molar equivalent KOH to neutralize the released H^+. In conclusion, in 100 mM ATP stock solution, there is 375.6 mM of K^+ ion in the solution from KOH added apart from $2\times100 = 200$ mM Na^{2+} from disodium ATP complex.

3. *Ionic strength of 15 mM MgATP in the assay buffer*: 15 mM MgATP solution was made by adding 15 mM ATP from 100 mM K^+ATP pH 7 stock and 15 mM $MgCl_2$. When adding 15 mM ATP from stock solution, $375.6\times15/100 \sim 56$ mM K^+ and $200\times15/100 = 30$ mM Na^+ are also carried into the solution from K^+ATP stock. Then the ion concentration in 15 mM ATP buffer solution includes:

K^+: 100 + 56 =156 mM

Na^+: 30 mM

Monovalent metal ion: 156+30 = 186 mM, adjusted to 176.4 mM free (see below)

Cl^-: 100 + 2×2 + 2×15 = 134 mM

Mg^{2+}: 2+15 = 17 mM, adjusted to 2 mM free (see below)

$HEPES^{1.5-}$: 30 mM

$MgATP^{2-}$: 15-9.6 = 5.4 mM (see below)

$KMgATP^-$: 9.6 mM (see below).

However, not all the ions above are free. K^+ and Na^+ have the same charge and their affinities for ATP are similar ~ 100 mM (119). Therefore, we treat K^+ and Na^+ the same in their conjugating to ATP and in calculation of ionic strength, i.e., the total monovalent metal concentration is 156 of K^+ + 30 of Na^+ = 186 mM in which

$$\left[\mathrm{K^+\ ATP}\right]=\frac{1}{2}\left(\left[\mathrm{ATP}\right]_{tot}+\left[\mathrm{K^+}\right]_{tot}+K_{K^+}-\sqrt{\left(\left[\mathrm{ATP}\right]_{tot}+\left[\mathrm{K^+}\right]_{tot}+K_{K^+}\right)^2-4\left[\mathrm{ATP}\right]_{tot}\left[\mathrm{K}\right]_{tot}}\right)$$

9.6 mM is conjugated with ATP and 176.4 mM is free ($[K^+]_{tot}$ is treated as total of both K^+ and Na^+).

In the presence of ~100 mM KCl or NaCl, the affinity of Mg^{2+} for ATP is reduced to ~0.21 mM (119), but is still tight. Thus, in the presence of 17 mM Mg^{2+} and 15 mM ATP, almost all the ATP has a Mg^{2+} complexed.

In summary, in our experimental condition and buffer, 2 of 4 negative charges in ATP are neutralized by Mg^{2+} conjugation to become $MgATP^{2-}$. 1 of 2 negative

charges in the majority of $MgATP^{2-}$ (9.6 mM) is further neutralized by a K^+ or Na^+ binding, becoming $KMgATP^-$ and the rest of $MgATP^{2-}$ is most possibly staying as $MgATP^{2-}$ since pK_a of $MgATP^{2-}$ is 4.55 (119). Finally, in all consideration, the ionic strength in 15 mM MgATP buffer is:

$$I = \frac{1}{2}\left(0.1764\times 1^2 + 0.134\times 1^2 + 0.002\times 2^2 + 0.03\times 1.5^2 + 0.0096\times 1^2 + 0.0054\times 2^2\right) = 0.21$$

.

15 mM MgATP adds an additional 0.21-0.14 = 0.07 to the assay buffer strength and it is ~ 0.07/0.14=50% change in ionic strength from assay buffer alone. According to Debye-Hückel equation (120), the population weighted average activity coefficient for MgATP is:

$$\log \gamma_{MgATP} = -0.509\sqrt{I}\,\overline{z_{MgATP}{}^2}$$
$$= -0.509\times\sqrt{0.21}\times 2.08 = -0.48$$

where the population averaged charge square is:

$$\overline{z_{MgATP}{}^2} = \frac{[KMgATP^-]\times(-1)^2 + [MgATP^{2-}]\times(-2)^2}{[KMgATP^-] + [MgATP^{2-}]}$$
$$= \frac{9.6\times(-1)^2 + 5.4\times(-2)^2}{15} = 2.08$$

Therefore, the MgATP activity coefficient in 15 mM MgATP buffer is γ_{MgATP} = 0.33 and it is slightly change compared to γ_{MgATP} = 0.40 if the MgATP is in buffer without ATP (I = 0.14; $\overline{z_{MgATP}{}^2} = 2.08$).

4. *Ionic strength of 10 mM phosphate (PO_4) in assay buffer*: The highest phosphate (PO_4) concentration used in this study is 10 mM, which was made by the assay buffer pH 7.5 supplemented with 10 mM phosphate taken from 1 M phosphate stock solution with H_2O pH 7.5. The phosphate stock solution was made by dissolving different amounts of monobasic (KH_2PO_4, acid) and dibasic (K_2HPO_4, base) potassium phosphate powder, respectively, into H_2O to final 1 M phosphate and pH 7.5. There are 3 dissociable protons in a phosphate and their pK_a values are 2.15, 6.82, and 12.38 (121). Therefore, in the final pH 7.5, the 1st proton should be all dissociated, the 2nd one partially dissociated and the 3rd one should stay bound with phosphate. In the 1 M phosphate stock solution pH 7.5, using the Henderson-Hasselbalch (HH) equation:

$$pH = pK_a + \log([Base] / [Acid])$$

with pK_a = 6.82, the ratio of base to acid is:

$$[Base] / [Acid] = 10^{7.5-6.82} = 4.79.$$

Since

$$[Base] + [Acid] = 1\ M$$

$$[Acid] = 1/(1+4.79) = 0.17\ M \text{ and } [Base] = 1- 0.17 = 0.83\ M$$

are the final base and acid concentration in the phosphate stock solution. Since the proton contribution from solution pH change (10^{-7} to $10^{-7.5}$) is negligible, the calculated final base and acid concentration is the concentration of dibasic and monobasic potassium phosphate dissolved (121). Consequently, K^+ concentration in the phosphate stock from both mono- and dibasic potassium phosphate is:

$$[K^+] = 0.83 \times 2 + 0.17 \times 1 = 1.83 \text{ M}$$

and $1830 \times 0.01 = 18.3$ mM was carried over with 10 mM phosphate when using phosphate stock to make buffer. The ions in 10 mM phosphate assay buffer solution are:

K^+: 100 + 18.3=118.3 mM, adjusted to 118.3-2.8 = 115.5 mM (see below)

Cl^-: 100 + 4 = 104 mM

Mg^{2+}: 2 mM

$HEPES^{1.5-}$: 30 mM.

HPO_4^-: 1.7 mM

PO_4^{2-}: 8.3 mM, adjusted to 8.3–2.8 = 5.5 mM by K^+ binding (see below)

KPO_4^-: 2.8 mM

The affinity of K^+ for PO_4^{2-} is weak, $\log K = 0.64$ or $K_d \sim 230$ mM (119). The concentration of K^+ bound at the 2nd phosphate proton position of PO_4^{2-} (8.3 mM) is:

$$\left[\mathrm{KPO_4^-}\right]=\frac{1}{2}\left(\left[\mathrm{PO_4^{2-}}\right]_{tot}+\left[\mathrm{K^+}\right]_{tot}+K_{K^+}-\sqrt{\left(\left[\mathrm{PO_4^{2-}}\right]_{tot}+\left[\mathrm{K^+}\right]_{tot}+K_{K^+}\right)^2-4\left[\mathrm{PO_4^{2-}}\right]_{tot}\left[\mathrm{K^+}\right]_{tot}}\right)$$

$$=\frac{1}{2}\left(8.3+118.3+230-\sqrt{\left(8.3+118.3+230\right)^2-4\times8.3\times118.3}\right)\sim 2.8\ \mathrm{mM}$$

Finally, the ionic strength is:

I = 0.5×(0.1155+0.102+0.002×2^2+0.03×1.5^2+0.0045+0.0055×2^2) ~ -0.16

It is 0.02/0.14=4.3% change from assay buffer ionic strength.

5. *Ionic strength of 15 mM MgATP with 10 mM phosphate (PO_4) in assay buffer*: similar to the case above, 15 mM MgATP in buffer adds ~0.07 to the assay buffer ionic strength, 15 mM MgATP would add ~0.07 to 10 mM phosphate buffer, such that the final ionic strength is I ~ 0.16+0.07 = 0.23 and it is 64.3% change compared to the ionic strength of buffer alone. The MgATP activity coefficient in 15 mM MgATP with 10 mM phosphate is γ_{MgATP} = 0.31 and reduced 0.09 (22.5%) from activity coefficient in assay buffer (0.40). At this activity coefficient vs. that in the assay buffer alone, the effect concentration of 15 mM MgATP reduces to:

$[MgATP]_{eff}$ = 0.31×15/0.4 = 11.6 mM.

SECTION S6

Below are the formulas used to calculate unmeasured values in Scheme 3.3 using detailed balance (Table 3.1). Uncertainties were calculated with conventional error propagation methods (122).

$$K_{d107} = \frac{K_{d74}K_{d41}}{K_{d101}} = \frac{5.5 \times \dot{0}.8}{3000} = 1.5 \pm 0.8\ nM$$

$$K_{d118} = \frac{K_{d87}K_{d107}}{K_{d1110}} = \frac{1.7 \times 0.0015}{0.004} = 0.6 \pm 0.2\ \mu M$$

$$K_{d129} = \frac{K_{d94}K_{d41}}{K_{d121}} = \frac{240 \times 0.8}{360} = 0.5 \pm 0.2\ \mu M$$

FIGURES

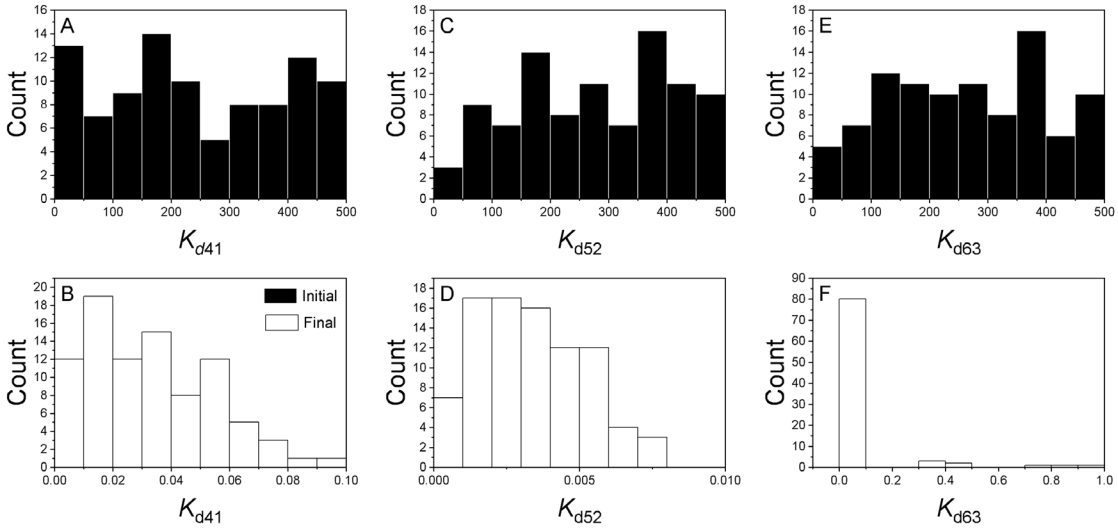

Figure S3.1. Distribution of initial (A, C, E) and final (B, D, F) K_{d41}, K_{d52}, and K_{d63} (Scheme 3.1) from global fits in Figure 3.2B, 3.3A, and 3.4A (dashed lines) using numerical integration techniques in a custom MATLAB program. $InsP_6$ is included in all experiments at an equimolar concentration with Gle1.

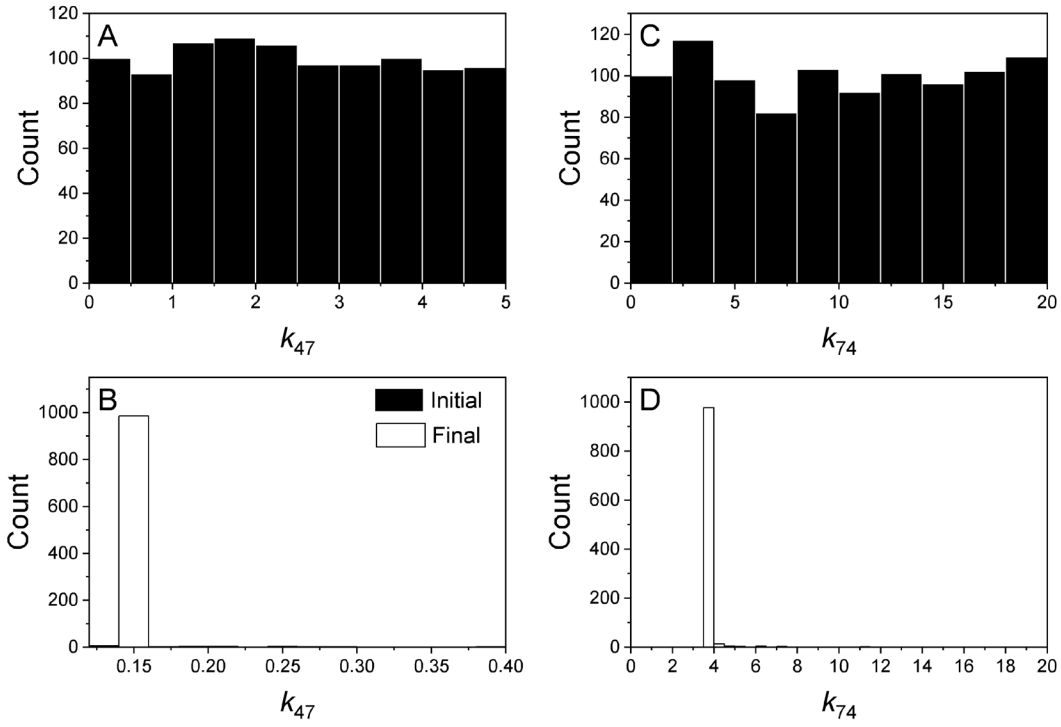

Figure S3.2. Distribution of final (B, D) and initial (A, C) ATP association (k_{47}) and dissociation (k_{74}) rate constants (Scheme 3.2) from fits to a kinetic simulation of Scheme 3.2 in Figure 3.5 using numerical integration techniques in a custom MATLAB program. Rate constants for Gle1-Dbp5 binding mantADP were fixed to values determined from fits in Figure 3.4. $InsP_6$ is included in all experiments at an equimolar concentration with Gle1.

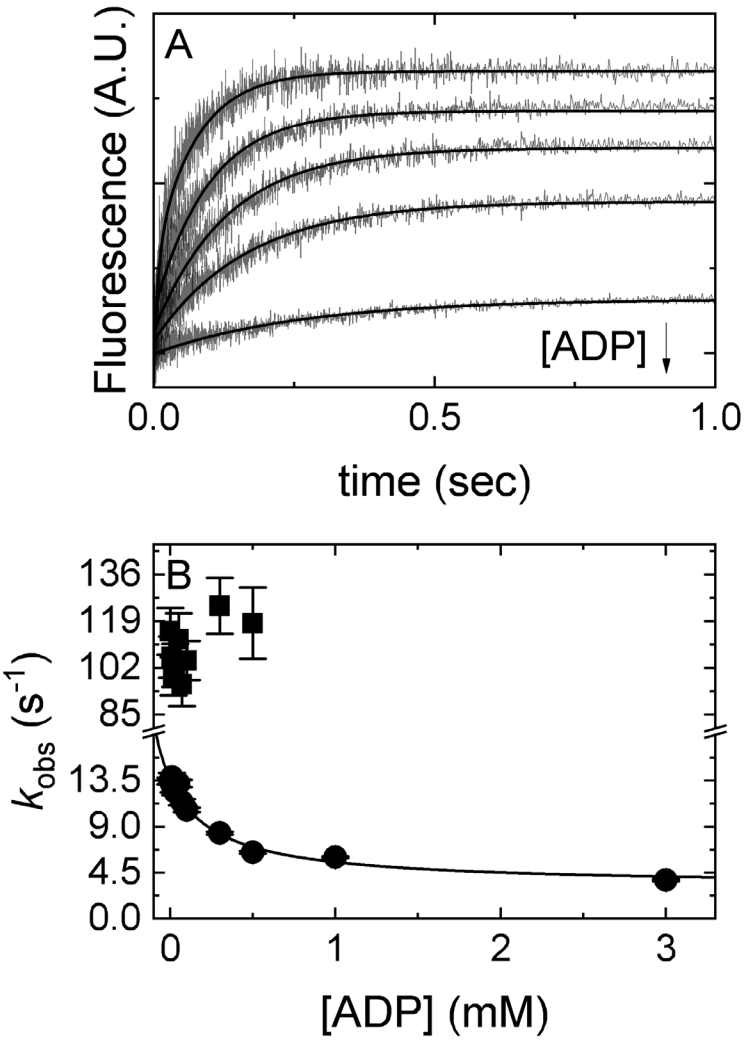

Figure S3.3. ADP rapidly equilibrates with Gle1-Dbp5 complex. (A). Time courses of FRET signal changes in pre-equilibrated solution of 2 μM Dbp5 (1 μM after mixing) with 20 μM Gle1 (10 μM after mixing) upon rapid mixing with an equal volume of 40 μM mantADP (20 μM after mixing) with various concentrations of ADP (from 0 to 3 mM after mixing). Continuous lines through the data are the best fits to double or single exponential functions (solid lines). (B) [ADP]-dependence of the observed rate constants from exponential fits in A

(solid lines) for mantADP binding pre-formed Gle1-Dbp5 complex. The continuous line through the data is the best fit to Eq. S3.5 (Supplemental Information, section 2-1). Uncertainty bars represent standard error in the fits and are contained within the data points. The best fit yields an affinity for Gle1-Dbp5 binding ADP (K_{d94}) of 240 ± 15 μM. $InsP_6$ is included in all experiments at an equimolar concentration with Gle1.

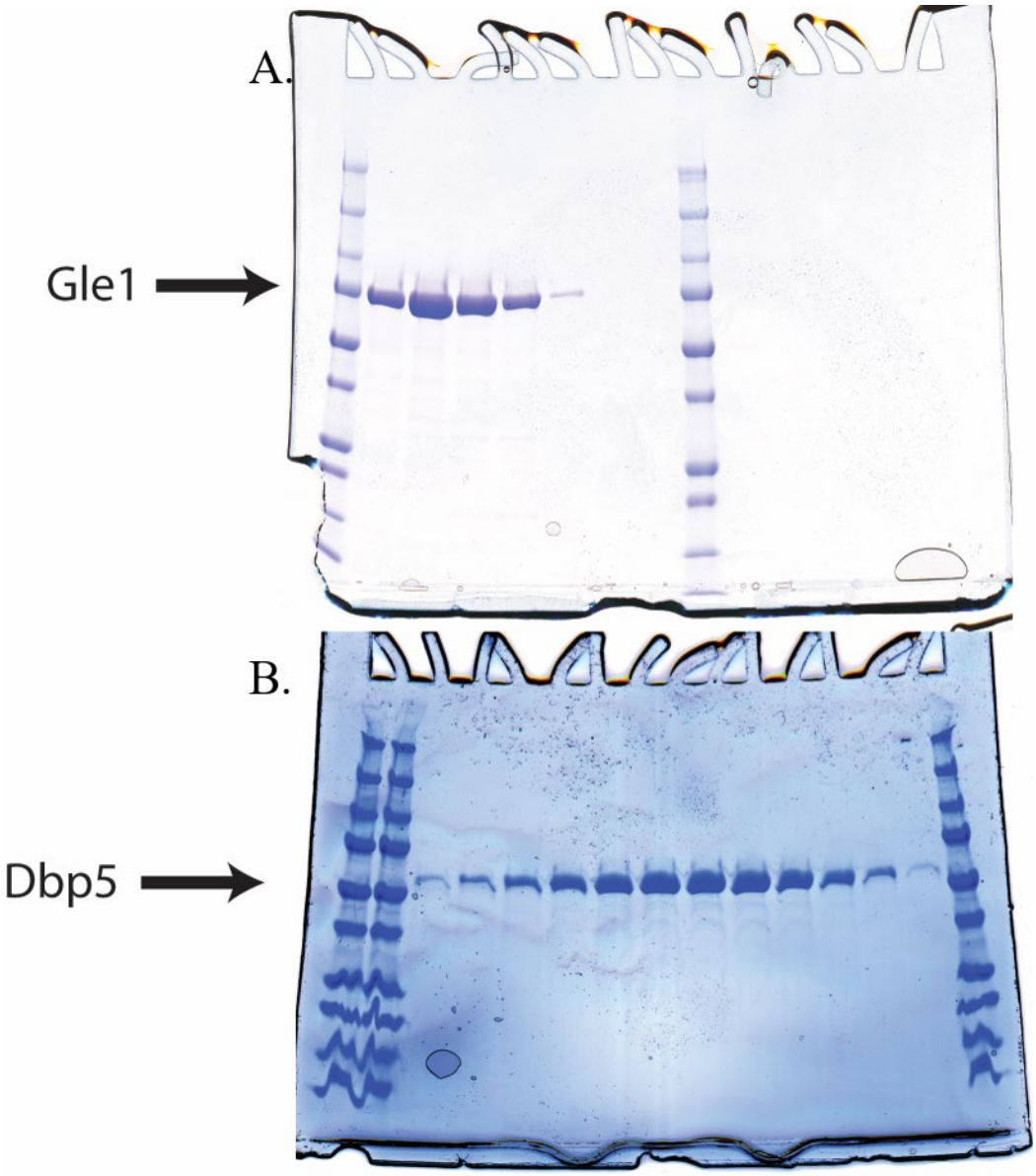

Figure S3.4. Representative SDS-PAGE gel of purified Dbp5 and Gle1. (A). SDS-PAGE gel of purified Gle1-MBP fractions following final FPLC separation. (B). SDS-PAGE gel of purified Dbp5 fractions following final FPLC separation. $InsP_6$ is included in all experiments at an equimolar concentration with Gle1.

Chapter 4: Unpublished Results and Future Directions

The overall interaction time between RNA and Dbp5 during a single ATP hydrolysis cycle is at least 0.4 seconds (25), much longer than the 50-200 millisecond export times observed *in vivo* (36). Slow RNA binding to Dbp5-ATP accounts for approximately half of this delay time (25). By accelerating RNA binding, Gle1 may be able to shorten the Dbp5-RNA interaction time to a scale that matches the mRNA export durations observed *in vivo*.

To measure RNA binding to Dbp5-ATP and Gle1-Dbp5-ATP, we took advantage of our knowledge regarding the kinetics of native and Gle1 stimulated Dbp5 ATPase in a series of dual mixing experiments. We first mixed either Dbp5 or preformed Gle1-Dbp5 complex with ATP, allowed the solution to age long enough (0.1 second) for ATP to bind (but prior to any significant hydrolysis), then mixed with fluoresceine labeled, 12-mer, ploy-U RNA (Figure 4.1). When Dbp5 binds fluorescein labeled RNA, substantial quenching of the fluorescent signal is observed (Figure 4.1 A, B). Time courses of Dbp5-ATP (Figure 4.1B) and Gle1-Dbp5-ATP (Figure 4.1A) binding RNA fit well to single exponential functions, yielding observed RNA binding rate constants. Fitting the [Dbp5-ATP] or [Gle1-Dbp5-ATP]-dependence of observed RNA binding rate constants to a linear function yields the fundamental association rate constant of Dbp5-ATP (0.1 ± 0.02 $\mu M^{-1}\ s^{-1}$) or Gle1-Dbp5-ATP (8.5 ± 0.4 $\mu M^{-1}\ s^{-1}$) binding RNA from the slope and the fundamental dissociation rate constant of RNA unbinding from RNA-Dbp5-ATP (1.2 ± 0.3 s^{-1}) or RNA-Gle1-Dbp5-ATP (5.7 ± 0.2 s^{-1}) from the y-intercept (Figure 4.1 D), respectively. This yields an affinity of Dbp5-ATP and

Gle1-Dbp5-ATP for 12-mer, poly-U RNA of 12 ± 3.8 and 1.5 ± 0.1 μM, respectively. Direct fitting of fluorescence quenching amplitudes (Figure 4.1 C) from exponential fits in Figure 4.1 A, B to a simple rectangular hyperbola yield an affinity of Dbp5-ATP and Gle1-Dbp5-ATP for 12-mer, poly-U RNA of 23 ± 15 and 0.4 ± 0.1 μM, respectively. Thusly, Gle1 accelerates RNA binding and unbinding to Dbp5-ATP ~ 85 and 5-fold, respectively. The net result of Gle1 is to increase the affinity of Dbp5-ATP for RNA ~ 60-fold.

Mex67-Mtr2 has long been thought of as a remodeling substrate for Dbp5 (46). However, this has never been tested biochemically. Dbp5 is proposed to remove Mex67-Mtr2 from mRNPs following export. Although Dbp5 does not copurify with Mex67-Mtr2, it may transiently bind Mex67-Mtr2 directly to elicit RNA dissociation. Alternatively, Dbp5 may bind near Mex67-Mtr2 along the RNA lattice and change the local RNA conformation to promote Mex67-Mtr2 release. Regardless of the exact mechanism, for this to occur Dbp5 must function as a Mex67-Mtr2 “exchange factor” to accelerate the fundamental rate constant governing Mex67-Mtr2 dissociation from RNA. An important avenue for future studies will be to measure Mex67-Mtr2 dissociation from RNA in the absence and presence of Dbp5 (±ATP) and other regulatory factors (Nup159, Gle1, IP6). Furthermore, it will be important to understand which step(s) along the Dbp5 ATPase cycle are coupled to Mex67-Mtr2 removal and whether or not Gle1 and other regulatory nucleoporins (Nup159, Nup42) are required for this activity.

FIGURES

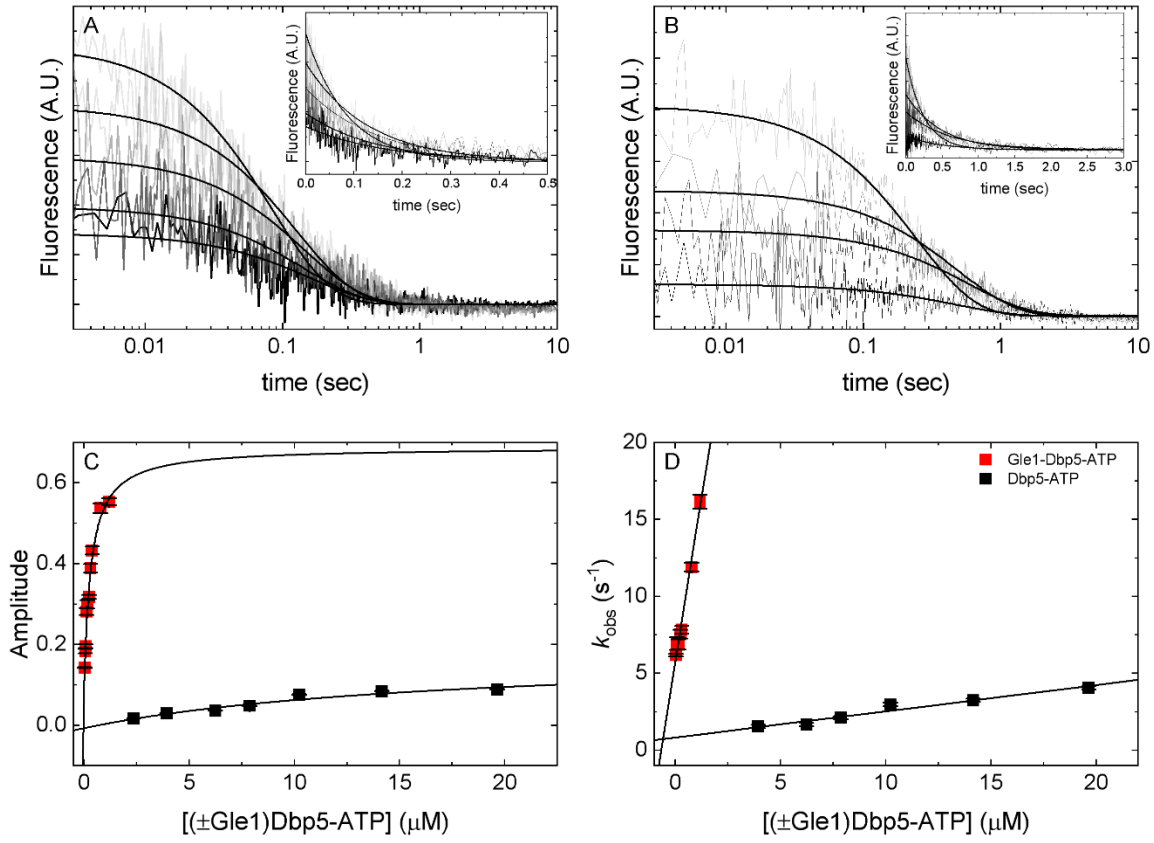

Figure 4.1. 12mer poly-U RNA binding to Dbp5-ATP and Gle1-Dbp5-ATP. (A). Time courses of fluorescence quenching of fluorescein labeled RNA after mixing a pre-aged (0.1 second age time) solution of Gle1-Dbp5 (0.05, 0.1, 0.2, 0.3, 0.4, 1, 1.5 μM after final mix) and ATP (100 μM after final mix) with fluorescein labeled 12-mer poly-U RNA (5 nM after final mix). The final concentrations of Gle1-Dbp5-ATP calculated from the affinity of Gle1 for Dbp5 and Gle1-Dbp5 for ATP (27) after 0.1 second aging are 0.04, 0.08, 0.15, 0.24, 0.31, 0.78, 1.2 μM. Continuous lines through the data represent the best fits to single exponential functions. The inset is a linear-scale depiction of the same time courses in A. (B). Time courses of fluorescence quenching of fluorescein

labeled RNA after mixing a pre-aged (0.1 second age time) solution of Dbp5 (3, 5, 8, 10, 13, and 18 μM after final mix) and ATP (8 mM after final mix) with fluorescein labeled 12-mer poly-U RNA (100 nM after final mix). The final concentrations of Dbp5-ATP calculated from the affinity of Dbp5 and ATP (25) after 0.1 second aging are 2.4, 4, 6.3, 7.9, 10.3, 14.2, and 18.9 μM. Continuous lines through the data represent the best fits to single exponential functions. The inset is a linear-scale depiction of the same time courses in B. (C). [Dbp5-ATP] (black squares) or [Gle1-Dbp5-ATP]-dependance (red squares) of the amplitudes for RNA binding from exponential fits in A and B. The continuous line through the data represents the best fit to a simple rectangular hyperbola yielding the affinity of Dbp5-ATP and Gle1-Dbp5-ATP for RNA of 23 ± 15 and 0.4 ± 0.1 μM, respectively. (D). [Dbp5-ATP] or [Gle1-Dbp5-ATP]-dependance of the observed rate constants from exponential fits in A and B. The continuous line through the data represents the best fit to a linear function yielding the fundamental association (0.1 ± 0.02 μM^{-1} s^{-1}) and dissociation (1.2 ± 0.3 s^{-1}) rate constants for Dbp5-ATP binding RNA from the slope and y-intercept, respectively. The fundamental association and dissociation rate constants of Gle1-Dbp5-ATP binding RNA are 8.5 ± 0.4 μM^{-1} s^{-1} and 5.7 ± 0.2 s^{-1}, respectively. These rate constants yield an affinity of Dbp5-ATP and Gle1-Dbp5-ATP of 12 ± 3.8 and 1.5 ± 0.1 μM, respectively.

Chapter 5: Summary and Conclusions

Dbp5 has been at the investigative forefront of mRNA nuclear export since its identification in 1998 (6). However, the exact role of Dbp5 in mRNA export and its regulatory mechanism remains largely unknown. A multitude of conflicting models for Dbp5 mediated mRNA export (Figure 1.3) and regulation by the nucleoporins Nup159 and Gle1 (Figure 1.5) have been proposed, although a consensus has yet to be reached. Further complicating the issue is the fact that Dbp5 has been implicated in myriad cellular processes including mRNA export, transcription, and translation (6,15,38). Thus, testing the kinetic predictions made by the major Dbp5 regulatory models is critical to understanding mRNA export as a whole.

Published models of Dbp5 mediated mRNA export and regulation make inherently kinetic arguments regarding the influence of Gle1 and Nup159 on the rate constants dictating Dbp5 ATPase and RNA binding (19,23,24). For example, Noble and colleagues (i.e. Wente & Cole model in Figure 1.5) (24) propose that Nup159 functions as a NEF to accelerate ADP dissociation from Dbp5, while Montpetit et al. (i.e. Weis & Burger model in Figure 1.5) suggest that a combination of Nup159 and Gle1 is required for NEF activity (23) (Figure 1.5). In order to test these assertions, we measured the dissociation rate constant of mantADP unbinding from Dbp5-ADP, Nup159-Dbp5-ADP, Gle1-Dbp5-ADP, and Gle1-Nup159-Dbp5-ADP (Chapter 2). Many NEFs promote nucleotide dissociation by removing the magnesium cation (Mg^{2+}) associated with bound

nucleotides. By measuring the [Mg^{2+}]-dependance of ADP dissociation, we were not only able to test for putative NEF activity but also the mechanism. We found that neither Nup159, Gle1, nor a combination of the two accelerated ADP dissociation (Chapter 2). Nup159 was actually found to weaken the affinity of Gle1 for ADP bound Dbp5 by ~ 18-fold. Therefore, Nup159 may function as a "Gle1 exchange factor" to remove Gle1 from Dbp5 following ATP hydrolysis (26), although mRNA export defects resulting from interruption of the Nup159-Dbp5 interaction can be completely rescued by Dbp5 overexpression (14). Therefore, Nup159 may function as part of a larger complex independent of Dbp5 mediated mRNA export.

Noble et al. further advocate that Gle1 acts to "load" Dbp5 with ATP (24) (i.e. Wente & Cole model in Figure 1.5). Ultimately, this would require that Gle1 enhance the affinity of Dbp5 for ATP by either slowing ATP dissociation, accelerating binding, or a combination of the two. In Chapter 3 we investigate this claim while characterizing the Gle1 stimulated ATPase cycle of Dbp5 (27). We find that Gle1 promotes ATP binding > 150-fold mostly by slowing ATP dissociation. Moreover, Gle1 accelerates steady-state Dbp5 ATPase by promoting rate limiting P_i release ~ 20-fold, although P_i release remains rate limiting (27).

The native ATPase cycle of Dbp5 is limited by slow ATP hydrolysis and even slower P_i release (25). Although P_i release remains partially rate limiting during RNA stimulated ATPase, RNA binding to Dbp5-ATP (or a slow isomerization following binding) introduces a new, partially rate limiting step (25).

Gle1 has been shown to accelerate the steady-state ATPase of Dbp5 in the presence of saturating RNA (20,23). Consequently, Gle1 must accelerate RNA binding to Dbp5-ATP (which we have shown in Chapter 4), P_i release from RNA-Dbp5-ADP-P_i, or both.

From our previous publications (25-27), the data presented here, and the current literature we can introduce a probable Dbp5 regulatory mechanism (Figure 5.1). Although we have shown that Nup159 weakens the affinity of Gle1 for ADP bound Dbp5, this functionality is likely not required for mRNA export *in vivo* as overexpression of Dbp5 can overcome mRNA export defects resulting from deletion of the Dbp5 binding domain on Nup159 (14). Likewise, overexpression of Nup159 induces mRNA export defects that can be rescued by concomitant Dbp5 overexpression. Together, these results suggest that Nup159 does not play a direct role in regulating Dbp5 ATPase/RNA binding, but rather maintains a local concentration of Dbp5 around the nuclear rim. The human homolog of Nup159 (Nup214) binds *apo*DDX19 much more tightly than any other nucleotide state (22). Therefore, Nup159 may maintain a dynamic pool of functional Dbp5 at the NPC.

Although Dbp5 alone binds ATP in rapid equilibrium (25) ($H + T \rightleftharpoons HT$ in Figure 5.1), the affinity (~ 4 mM) is less than the concentration of cellular ATP (~ 1 – 2 mM from (123)). Gle1 tightens the affinity of Dbp5 for ATP by > 150-fold, binds *apo*Dbp5 with a relatively tight affinity (27), and accelerates ATP resynthesis to poise Dbp5 for RNA binding by promoting the high RNA affinity ATP state (27). Therefore, Gle1 likely promotes the high RNA affinity Dbp5-ATP

state and accelerates RNA binding to Dbp5-ATP (Figure 4.1) at the cytoplasmic face of the NPC.

Gle1 accelerates RNA stimulated Dbp5 steady-state ATPase (20,23), which is partially limited by P_i release (25). Therefore, Gle1 likely accelerates the release of inorganic phosphate from Dbp5-RNA-ADP-P_i ($HRDP_i$ in Figure 5.1). As a result, it is probable that Gle1 remains bound to the Dbp5-RNA-nucleotide complex until after phosphate has dissociated. All DPBs studies to date demonstrate weak RNA affinities while bound to ADP (42). Consequently, RNA seemingly dissociates following P_i release from $HRGDP_i$ in Figure 5.1. However, Gle1 has a relatively high affinity (~ 0.5 μM) for Dbp5-ADP (27) in the absence of RNA and likely remains bound to Dbp5 throughout mRNA remodeling, although it is possible that Nup159 accelerates Gle1 dissociation from Dbp5-ADP at this point. This predominant pathway is outlined in Figure 5.1.

FIGURES

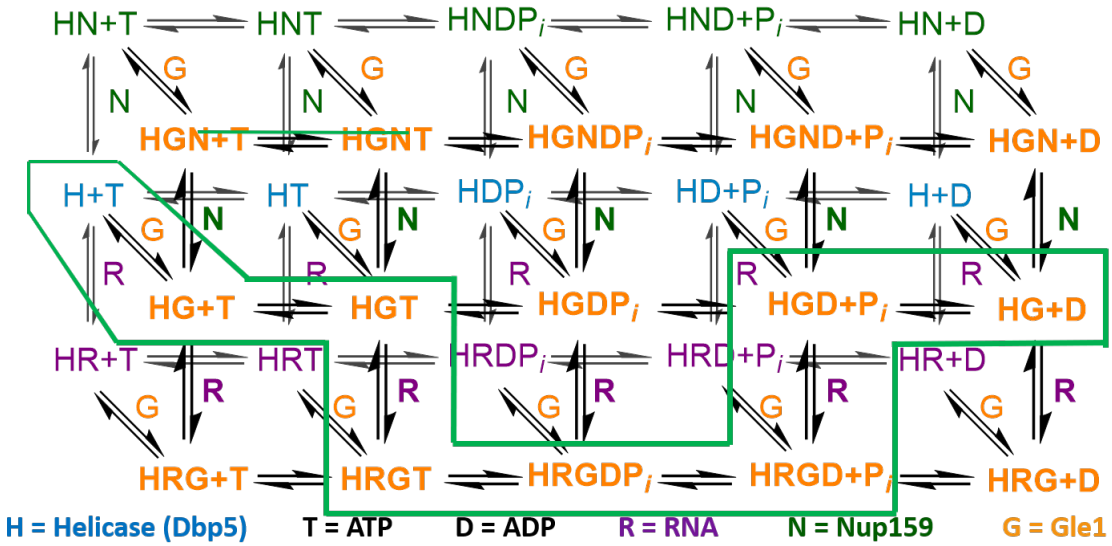

Figure 5.1. Proposed mRNA export and regulatory mechanism of Dbp5

REFERENCES

1. Taanman, J.W. (1999) The mitochondrial genome: structure, transcription, translation and replication. *Biochimica et biophysica acta*, **1410**, 103-123.
2. Takemura, R., Inoue, Y. and Izawa, S. (2004) Stress response in yeast mRNA export factor: reversible changes in Rat8p localization are caused by ethanol stress but not heat shock. *Journal of cell science*, **117**, 4189-4197.
3. Rollenhagen, C., Hodge, C.A. and Cole, C.N. (2004) The nuclear pore complex and the DEAD box protein Rat8p/Dbp5p have nonessential features which appear to facilitate mRNA export following heat shock. *Molecular and cellular biology*, **24**, 4869-4879.
4. Torres, M., Becquet, D., Franc, J.L. and Francois-Bellan, A.M. (2018) Circadian processes in the RNA life cycle. *Wiley interdisciplinary reviews. RNA*, **9**, e1467.
5. Schmitt, C., von Kobbe, C., Bachi, A., Pante, N., Rodrigues, J.P., Boscheron, C., Rigaut, G., Wilm, M., Seraphin, B., Carmo-Fonseca, M. *et al.* (1999) Dbp5, a DEAD-box protein required for mRNA export, is recruited to the cytoplasmic fibrils of nuclear pore complex via a conserved interaction with CAN/Nup159p. *EMBO J*, **18**, 4332-4347.
6. Snay-Hodge, C.A., Colot, H.V., Goldstein, A.L. and Cole, C.N. (1998) Dbp5p/Rat8p is a yeast nuclear pore-associated DEAD-box protein essential for RNA export. *EMBO J*, **17**, 2663-2676.
7. Tseng, S.S., Weaver, P.L., Liu, Y., Hitomi, M., Tartakoff, A.M. and Chang, T.H. (1998) Dbp5p, a cytosolic RNA helicase, is required for poly(A)+ RNA export. *EMBO J*, **17**, 2651-2662.
8. Venters, B.J. and Pugh, B.F. (2009) How eukaryotic genes are transcribed. *Critical reviews in biochemistry and molecular biology*, **44**, 117-141.
9. Papasaikas, P. and Valcarcel, J. (2016) The Spliceosome: The Ultimate RNA Chaperone and Sculptor. *Trends Biochem Sci*, **41**, 33-45.
10. Stewart, M. (2010) Nuclear export of mRNA. *Trends Biochem Sci*, **35**, 609-617.
11. Hocine, S., Singer, R.H. and Grunwald, D. (2010) RNA processing and export. *Cold Spring Harbor perspectives in biology*, **2**, a000752.
12. Kong, J. and Lasko, P. (2012) Translational control in cellular and developmental processes. *Nature reviews. Genetics*, **13**, 383-394.
13. Zhao, J., Jin, S.B., Bjorkroth, B., Wieslander, L. and Daneholt, B. (2002) The mRNA export factor Dbp5 is associated with Balbiani ring mRNP from gene to cytoplasm. *EMBO J*, **21**, 1177-1187.
14. Hodge, C.A., Colot, H.V., Stafford, P. and Cole, C.N. (1999) Rat8p/Dbp5p is a shuttling transport factor that interacts with Rat7p/Nup159p and Gle1p and suppresses the mRNA export defect of xpo1-1 cells. *EMBO J*, **18**, 5778-5788.
15. Estruch, F. and Cole, C.N. (2003) An early function during transcription for the yeast mRNA export factor Dbp5p/Rat8p suggested by its genetic and physical interactions with transcription factor IIH components. *Mol Biol Cell*, **14**, 1664-1676.
16. Strahm, Y., Fahrenkrog, B., Zenklusen, D., Rychner, E., Kantor, J., Rosbach, M. and Stutz, F. (1999) The RNA export factor Gle1p is located on the cytoplasmic fibrils of the NPC and physically interacts with the FG-nucleoporin Rip1p, the DEAD-box protein Rat8p/Dbp5p and a new protein Ymr 255p. *EMBO J*, **18**, 5761-5777.
17. Weirich, C.S., Erzberger, J.P., Berger, J.M. and Weis, K. (2004) The N-terminal domain of Nup159 forms a beta-propeller that functions in mRNA export by tethering the helicase Dbp5 to the nuclear pore. *Mol Cell*, **16**, 749-760.

18. Alcazar-Roman, A.R., Tran, E.J., Guo, S. and Wente, S.R. (2006) Inositol hexakisphosphate and Gle1 activate the DEAD-box protein Dbp5 for nuclear mRNA export. *Nat Cell Biol*, **8**, 711-716.
19. Tieg, B. and Krebber, H. (2013) Dbp5 - from nuclear export to translation. *Biochimica et biophysica acta*, **1829**, 791-798.
20. Weirich, C.S., Erzberger, J.P., Flick, J.S., Berger, J.M., Thorner, J. and Weis, K. (2006) Activation of the DExD/H-box protein Dbp5 by the nuclear-pore protein Gle1 and its coactivator InsP6 is required for mRNA export. *Nat Cell Biol*, **8**, 668-676.
21. Dossani, Z.Y., Weirich, C.S., Erzberger, J.P., Berger, J.M. and Weis, K. (2009) Structure of the C-terminus of the mRNA export factor Dbp5 reveals the interaction surface for the ATPase activator Gle1. *Proceedings of the National Academy of Sciences of the United States of America*, **106**, 16251-16256.
22. von Moeller, H., Basquin, C. and Conti, E. (2009) The mRNA export protein DBP5 binds RNA and the cytoplasmic nucleoporin NUP214 in a mutually exclusive manner. *Nat Struct Mol Biol*, **16**, 247-254.
23. Montpetit, B., Thomsen, N.D., Helmke, K.J., Seeliger, M.A., Berger, J.M. and Weis, K. (2011) A conserved mechanism of DEAD-box ATPase activation by nucleoporins and InsP6 in mRNA export. *Nature*, **472**, 238-242.
24. Noble, K.N., Tran, E.J., Alcazar-Roman, A.R., Hodge, C.A., Cole, C.N. and Wente, S.R. (2011) The Dbp5 cycle at the nuclear pore complex during mRNA export II: nucleotide cycling and mRNP remodeling by Dbp5 are controlled by Nup159 and Gle1. *Genes & development*, **25**, 1065-1077.
25. Wong, E.V., Cao, W., Voros, J., Merchant, M., Modis, Y., Hackney, D.D., Montpetit, B. and De La Cruz, E.M. (2016) P(I) Release Limits the Intrinsic and RNA-Stimulated ATPase Cycles of DEAD-Box Protein 5 (Dbp5). *J Mol Biol*, **428**, 492-508.
26. Wong, E.V., Gray, S., Cao, W., Montpetit, R., Montpetit, B. and De La Cruz, E.M. (2018) Nup159 Weakens Gle1 Binding to Dbp5 But Does Not Accelerate ADP Release. *J Mol Biol*, **430**, 2080-2095.
27. Gray, S., Cao, W., Montpetit, B. and De La Cruz, E.M. (2022) The nucleoporin Gle1 activates DEAD-box protein 5 (Dbp5) by promoting ATP binding and accelerating rate limiting phosphate release. *Nucleic acids research*.
28. Capelson, M. and Hetzer, M.W. (2009) The role of nuclear pores in gene regulation, development and disease. *EMBO Rep*, **10**, 697-705.
29. Simon, D.N. and Rout, M.P. (2014) Cancer and the nuclear pore complex. *Advances in experimental medicine and biology*, **773**, 285-307.
30. Cohen, S., Etingov, I. and Pante, N. (2012) Effect of viral infection on the nuclear envelope and nuclear pore complex. *International review of cell and molecular biology*, **299**, 117-159.
31. Yarbrough, M.L., Mata, M.A., Sakthivel, R. and Fontoura, B.M. (2014) Viral subversion of nucleocytoplasmic trafficking. *Traffic*, **15**, 127-140.
32. Adams, R.L., Mason, A.C., Glass, L., Aditi and Wente, S.R. (2017) Nup42 and IP6 coordinate Gle1 stimulation of Dbp5/DDX19B for mRNA export in yeast and human cells. *Traffic*, **18**, 776-790.
33. Watkins, J.L., Murphy, R., Emtage, J.L. and Wente, S.R. (1998) The human homologue of Saccharomyces cerevisiae Gle1p is required for poly(A)+ RNA export. *Proceedings of the National Academy of Sciences of the United States of America*, **95**, 6779-6784.
34. Linder, P. and Jankowsky, E. (2011) From unwinding to clamping — the DEAD box RNA helicase family. *Nat Rev Mol Cell Biol*, **12**, 505-516.

35. Lin, D.H. and Hoelz, A. (2019) The Structure of the Nuclear Pore Complex (An Update). *Annual review of biochemistry*, **88**, 725-783.
36. Siebrasse, J.P., Kaminski, T. and Kubitscheck, U. (2012) Nuclear export of single native mRNA molecules observed by light sheet fluorescence microscopy. *Proceedings of the National Academy of Sciences of the United States of America*, **109**, 9426-9431.
37. Stewart, M. (2019) Polyadenylation and nuclear export of mRNAs. *Journal of Biological Chemistry*, **294**, 2977-2987.
38. Gross, T., Siepmann, A., Sturm, D., Windgassen, M., Scarcelli, J.J., Seedorf, M., Cole, C.N. and Krebber, H. (2007) The DEAD-box RNA helicase Dbp5 functions in translation termination. *Science*, **315**, 646-649.
39. Stewart, M. (2007) Ratcheting mRNA out of the nucleus. *Mol Cell*, **25**, 327-330.
40. Lari, A., Arul Nambi Rajan, A., Sandhu, R., Reiter, T., Montpetit, R., Young, B.P., Loewen, C.J. and Montpetit, B. (2019) A nuclear role for the DEAD-box protein Dbp5 in tRNA export. *Elife*, **8**.
41. Putnam, A.A. and Jankowsky, E. (2013) DEAD-box helicases as integrators of RNA, nucleotide and protein binding. *Biochimica et biophysica acta*, **1829**, 884-893.
42. Henn, A., Bradley, M.J. and De La Cruz, E.M. (2012) ATP utilization and RNA conformational rearrangement by DEAD-box proteins. *Annu Rev Biophys*, **41**, 247-267.
43. Cao, W., Coman, M.M., Ding, S., Henn, A., Middleton, E.R., Bradley, M.J., Rhoades, E., Hackney, D.D., Pyle, A.M. and De La Cruz, E.M. (2011) Mechanism of Mss116 ATPase reveals functional diversity of DEAD-Box proteins. *J Mol Biol*, **409**, 399-414.
44. Henn, A., Cao, W., Hackney, D.D. and De La Cruz, E.M. (2008) The ATPase cycle mechanism of the DEAD-box rRNA helicase, DbpA. *J Mol Biol*, **377**, 193-205.
45. Jackson, R.J., Hellen, C.U. and Pestova, T.V. (2010) The mechanism of eukaryotic translation initiation and principles of its regulation. *Nat Rev Mol Cell Biol*, **11**, 113-127.
46. Lund, M.K. and Guthrie, C. (2005) The DEAD-box protein Dbp5p is required to dissociate Mex67p from exported mRNPs at the nuclear rim. *Mol Cell*, **20**, 645-651.
47. Tran, E.J., Zhou, Y., Corbett, A.H. and Wente, S.R. (2007) The DEAD-box protein Dbp5 controls mRNA export by triggering specific RNA:protein remodeling events. *Mol Cell*, **28**, 850-859.
48. Smith, C., Lari, A., Derrer, C.P., Ouwehand, A., Rossouw, A., Huisman, M., Dange, T., Hopman, M., Joseph, A., Zenklusen, D. *et al.* (2015) In vivo single-particle imaging of nuclear mRNA export in budding yeast demonstrates an essential role for Mex67p. *The Journal of cell biology*, **211**, 1121-1130.
49. Strawn, L.A., Shen, T. and Wente, S.R. (2001) The GLFG regions of Nup116p and Nup100p serve as binding sites for both Kap95p and Mex67p at the nuclear pore complex. *The Journal of biological chemistry*, **276**, 6445-6452.
50. Segref, A., Sharma, K., Doye, V., Hellwig, A., Huber, J., Luhrmann, R. and Hurt, E. (1997) Mex67p, a novel factor for nuclear mRNA export, binds to both poly(A)+ RNA and nuclear pores. *EMBO J*, **16**, 3256-3271.
51. Katahira, J., Strasser, K., Podtelejnikov, A., Mann, M., Jung, J.U. and Hurt, E. (1999) The Mex67p-mediated nuclear mRNA export pathway is conserved from yeast to human. *EMBO J*, **18**, 2593-2609.
52. Kaminski, T., Siebrasse, J.P. and Kubitscheck, U. (2013) A single molecule view on Dbp5 and mRNA at the nuclear pore. *Nucleus (Austin, Tex.)*, **4**, 8-13.
53. Collins, R., Karlberg, T., Lehtio, L., Schutz, P., van den Berg, S., Dahlgren, L.G., Hammarstrom, M., Weigelt, J. and Schuler, H. (2009) The DEXD/H-box RNA helicase

DDX19 is regulated by an {alpha}-helical switch. *The Journal of biological chemistry*, **284**, 10296-10300.
54. Lin, D.H., Correia, A.R., Cai, S.W., Huber, F.M., Jette, C.A. and Hoelz, A. (2018) Structural and functional analysis of mRNA export regulation by the nuclear pore complex. *Nat Commun*, **9**, 2319.
55. Cordin, O., Banroques, J., Tanner, N.K. and Linder, P. (2006) The DEAD-box protein family of RNA helicases. *Gene*, **367**, 17-37.
56. Bowers, H.A., Maroney, P.A., Fairman, M.E., Kastner, B., Luhrmann, R., Nilsen, T.W. and Jankowsky, E. (2006) Discriminatory RNP remodeling by the DEAD-box protein DED1. *RNA*, **12**, 903-912.
57. Cordin, O., Tanner, N.K., Doere, M., Linder, P. and Banroques, J. (2004) The newly discovered Q motif of DEAD-box RNA helicases regulates RNA-binding and helicase activity. *EMBO J*, **23**, 2478-2487.
58. Iost, I., Dreyfus, M. and Linder, P. (1999) Ded1p, a DEAD-box Protein Required for Translation Initiation inSaccharomyces cerevisiae, Is an RNA Helicase. *Journal of Biological Chemistry*, **274**, 17677-17683.
59. Hilbert, M., Kebbel, F., Gubaev, A., Klostermeier, D. (2017) eIF4G stimulates the activity of the DEAD box protein eIF4A by a conformational guidance mechanism. *Nucleic Acids Res.*, **39**, 2260-2270.
60. Mathys, H., Basquin, J., Ozgur, S., Czarnocki-Cieciura, M., Bonneau, F., Aartse, A., Dziembowski, A., Nowotny, M., Conti, E. and Filipowicz, W. (2014) Structural and Biochemical Insights to the Role of the CCR4-NOT Complex and DDX6 ATPase in MicroRNA Repression. *Mol. Cell*.
61. Nielsen, K.H., Chamieh, H., Andersen, C.B.F., Fredslund, F., Hamborg, K., Le Hir, H. and Andersen, G.R. (2009) Mechanism of ATP turnover inhibition in the EJC. *RNA (New York, N.Y.)*, **15**, 67-75.
62. Hodge, C.A., Tran, E.J., Noble, K.N., Alcazar-Roman, A.R., Ben-Yishay, R., Scarcelli, J.J., Folkmann, A.W., Shav-Tal, Y., Wente, S.R. and Cole, C.N. (2011) The Dbp5 cycle at the nuclear pore complex during mRNA export I: dbp5 mutants with defects in RNA binding and ATP hydrolysis define key steps for Nup159 and Gle1. *Genes & development*, **25**, 1052-1064.
63. Kendirgi, F., Barry, D.M., Griffis, E.R., Powers, M.A. and Wente, S.R. (2003) An essential role for hGle1 nucleocytoplasmic shuttling in mRNA export. *The Journal of cell biology*, **160**, 1029-1040.
64. Alcazar-Roman, A.R., Bolger, T.A. and Wente, S.R. (2010) Control of mRNA export and translation termination by inositol hexakisphosphate requires specific interaction with Gle1. *The Journal of biological chemistry*, **285**, 16683-16692.
65. Folkmann, A.W., Noble, K.N., Cole, C.N. and Wente, S.R. (2011) Dbp5, Gle1-IP6 and Nup159: a working model for mRNP export. *Nucleus (Austin, Tex.)*, **2**, 540-548.
66. Neumann, B., Wu, H., Hackmann, A. and Krebber, H. (2016) Nuclear Export of Pre-Ribosomal Subunits Requires Dbp5, but Not as an RNA-Helicase as for mRNA Export. *PLoS One*, **11**, e0149571.
67. Lenzen, C., Cool, R.H., Prinz, H., Kuhlmann, J. and Wittinghofer, A. (1998) Kinetic analysis by fluorescence of the interaction between Ras and the catalytic domain of the guanine nucleotide exchange factor Cdc25Mm. *Biochemistry*, **37**, 7420-7430.
68. Pan, J.Y. and Wessling-Resnick, M. (1998) GEF-mediated GDP/GTP exchange by monomeric GTPases: a regulatory role for Mg2+? *Bioessays*, **20**, 516-521.

69. Worthylake, D.K., Rossman, K.L. and Sondek, J. (2000) Crystal structure of Rac1 in complex with the guanine nucleotide exchange region of Tiam1. *Nature*, **408**, 682-688.
70. Zhang, B., Zhang, Y., Wang, Z. and Zheng, Y. (2000) The role of Mg2+ cofactor in the guanine nucleotide exchange and GTP hydrolysis reactions of Rho family GTP-binding proteins. *The Journal of biological chemistry*, **275**, 25299-25307.
71. Goldberg, J. (1998) Structural Basis for Activation of ARF GTPase. *Cell*, **95**, 237-248.
72. Boriack-Sjodin, P.A., Margarit, S.M., Bar-Sagi, D. and Kuriyan, J. (1998) The structural basis of the activation of Ras by Sos. *Nature*, **394**, 337-343.
73. Vinson, V.K., De La Cruz, E.M., Higgs, H.N. and Pollard, T.D. (1998) Interactions of Acanthamoeba profilin with actin and nucleotides bound to actin. *Biochemistry*, **37**, 10871-10880.
74. Shang, Z., Zhou, K., Xu, C., Csencsits, R., Cochran, J.C. and Sindelar, C.V. (2014) High-resolution structures of kinesin on microtubules provide a basis for nucleotide-gated force-generation. *Elife*, **3**, e04686.
75. Cheng, J.Q., Jiang, W. and Hackney, D.D. (1998) Interaction of mant-adenosine nucleotides and magnesium with kinesin. *Biochemistry*, **37**, 5288-5295.
76. Hannemann, D.E., Cao, W., Olivares, A.O., Robblee, J.P. and De La Cruz, E.M. (2005) Magnesium, ADP, and actin binding linkage of myosin V: evidence for multiple myosin V-ADP and actomyosin V-ADP states. *Biochemistry*, **44**, 8826-8840.
77. Rosenfeld, S.S., Houdusse, A. and Sweeney, H.L. (2005) Magnesium regulates ADP dissociation from myosin V. *The Journal of biological chemistry*, **280**, 6072-6079.
78. Chin, H.F., Cai, Y., Menon, S., Ferro-Novick, S., Reinisch, K.M. and De La Cruz, E.M. (2009) Kinetic analysis of the guanine nucleotide exchange activity of TRAPP, a multimeric Ypt1p exchange factor. *J Mol Biol*, **389**, 275-288.
79. Talavera, M.A. and De La Cruz, E.M. (2005) Equilibrium and kinetic analysis of nucleotide binding to the DEAD-box RNA helicase DbpA. *Biochemistry*, **44**, 959-970.
80. Corbett, J.F. (1972) Pseudo first-order kinetics. *J. Chem. Educ.*, **49**, 663.
81. Pollard, T.D. and De La Cruz, E.M. (2013) Take advantage of time in your experiments: a guide to simple, informative kinetics assays. *Mol Biol Cell*, **24**, 1103-1110.
82. De La Cruz, E.M. and Ostap, E.M. (2009) Kinetic and equilibrium analysis of the myosin ATPase. *Methods in enzymology*, **455**, 157-192.
83. Fan, J.S., Cheng, Z., Zhang, J., Noble, C., Zhou, Z., Song, H. and Yang, D. (2009) Solution and crystal structures of mRNA exporter Dbp5p and its interaction with nucleotides. *J Mol Biol*, **388**, 1-10.
84. Tieg, B. and Krebber, H. (2013) Dbp5 - From nuclear export to translation. *Biochim. Biophys. Acta*, **1829**, 791-798.
85. Ledoux, S. and Guthrie, C. (2011) Regulation of the Dbp5 ATPase cycle in mRNP remodeling at the nuclear pore: a lively new paradigm for DEAD-box proteins. *Genes & development*, **25**, 1109-1114.
86. Linder, P. (2008) mRNA export: RNP remodeling by DEAD-box proteins. *Current biology : CB*, **18**, R297-299.
87. Cole, C.N. and Scarcelli, J.J. (2006) Transport of messenger RNA from the nucleus to the cytoplasm. *Curr Opin Cell Biol*, **18**, 299-306.
88. Andreini, C., Bertini, I., Cavallaro, G., Holliday, G.L. and Thornton, J.M. (2008) Metal ions in biological catalysis: from enzyme databases to general principles. *JBIC Journal of Biological Inorganic Chemistry*, **13**, 1205-1218.

89. Kabcenell, A.K., Goud, B., Northup, J.K. and Novick, P.J. (1990) Binding and hydrolysis of guanine nucleotides by Sec4p, a yeast protein involved in the regulation of vesicular traffic. *J. Biol. Chem.*, **265**, 9366-9372.
90. Feuerstein, J., Goody, R.S. and Wittinghofer, A. (1987) Preparation and characterization of nucleotide-free and metal ion-free p21 "apoprotein". *The Journal of biological chemistry*, **262**, 8455-8458.
91. Goitre, L., Trapani, E., Trabalzini, L. and Retta, S.F. (2014) The Ras superfamily of small GTPases: the unlocked secrets. *Methods Mol. Biol.*, **1120**, 1-18.
92. Liu, F., Putnam, A.A. and Jankowsky, E. (2014) DEAD-box helicases form nucleotide-dependent, long-lived complexes with RNA. *Biochemistry*, **53**, 423-433.
93. Putnam, A.A. and Jankowsky, E. (2013) AMP sensing by DEAD-box RNA helicases. *J Mol Biol*, **425**, 3839-3845.
94. Pecoraro, V.L., Hermes, J.D. and Cleland, W.W. (1984) Stability constants of Mg2+ and Cd2+ complexes of adenine nucleotides and thionucleotides and rate constants for formation and dissociation of MgATP and MgADP. *Biochemistry*, **23**, 5262-5271.
95. Martell, A.E. and Smith, R.H. (1976) *Critical Stability Constants*. Plenum Press, New York.
96. Goldberg, J. (1998) Structural basis for activation of ARF GTPase: mechanisms of guanine nucleotide exchange and GTP-myristoyl switching. *Cell*, **95**, 237-248.
97. Moore, K.J.M. and Lohman, T.M. (1994) Kinetic mechanism of adenine nucleotide binding to and hydrolysis by the Escherichia coli Rep monomer. 1. Use of fluorescent nucleotide analogs. *Biochemistry*, **33**, 14550-14564.
98. Simon, I., Zerial, M. and Goody, R.S. (1996) Kinetics of interaction of Rab5 and Rab7 with nucleotides and magnesium ions. *The Journal of biological chemistry*, **271**, 20470-20478.
99. Smith, C., Lari, A., Derrer, C.P., Ouwehand, A., Rossouw, A., Huisman, M., Dange, T., Hopman, M., Joseph, A., Zenklusen, D. *et al.* (2015) In vivo single-particle imaging of nuclear mRNA export in budding yeast demonstrates an essential role for Mex67p. *The Journal of Cell Biology*, **211**, 1121-1130.
100. Grunwald, D. and Singer, R.H. (2010) In vivo imaging of labelled endogenous [bgr]-actin mRNA during nucleocytoplasmic transport. *Nature*, **467**, 604-607.
101. Mor, A., Suliman, S., Ben-Yishay, R., Yunger, S., Brody, Y. and Shav-Tal, Y. (2010) Dynamics of single mRNP nucleocytoplasmic transport and export through the nuclear pore in living cells. *Nat Cell Biol*, **12**, 543-552.
102. Moore, K.J. and Lohman, T.M. (1994) Kinetic mechanism of adenine nucleotide binding to and hydrolysis by the Escherichia coli Rep monomer. 1. Use of fluorescent nucleotide analogues. *Biochemistry*, **33**, 14550-14564.
103. Napetschnig, J., Kassube, S.A., Debler, E.W., Wong, R.W., Blobel, G. and Hoelz, A. (2009) Structural and functional analysis of the interaction between the nucleoporin Nup214 and the DEAD-box helicase Ddx19. *Proceedings of the National Academy of Sciences of the United States of America*, **106**, 3089-3094.
104. Napetschnig, J., Blobel, G. and Hoelz, A. (2007) Crystal structure of the N-terminal domain of the human protooncogene Nup214/CAN. *Proceedings of the National Academy of Sciences of the United States of America*, **104**, 1783-1788.
105. Xie, Y. and Ren, Y. (2019) Mechanisms of nuclear mRNA export: A structural perspective. *Traffic*, **20**, 829-840.
106. Schindelin, J., Arganda-Carreras, I., Frise, E., Kaynig, V., Longair, M., Pietzsch, T., Preibisch, S., Rueden, C., Saalfeld, S., Schmid, B. *et al.* (2012) Fiji: an open-source platform for biological-image analysis. *Nature methods*, **9**, 676-682.

107. Brune, M., Hunter, J.L., Corrie, J.E. and Webb, M.R. (1994) Direct, real-time measurement of rapid inorganic phosphate release using a novel fluorescent probe and its application to actomyosin subfragment 1 ATPase. *Biochemistry*, **33**, 8262-8271.
108. Moore, K.J. and Lohman, T.M. (1994) Kinetic mechanism of adenine nucleotide binding to and hydrolysis by the Escherichia coli Rep monomer. 2. Application of a kinetic competition approach. *Biochemistry*, **33**, 14565-14578.
109. Bradley, M.J. and De La Cruz, E.M. (2012) In Eckhard, J. (ed.), *Methods in enzymology*. Academic Press, Vol. Volume 511, pp. 29-63.
110. Henn, A. and De La Cruz, E.M. (2005) Vertebrate myosin VIIb is a high duty ratio motor adapted for generating and maintaining tension. *The Journal of biological chemistry*, **280**, 39665-39676.
111. Henn, A., Cao, W., Licciardello, N., Heitkamp, S.E., Hackney, D.D. and De La Cruz, E.M. (2010) Pathway of ATP utilization and duplex rRNA unwinding by the DEAD-box helicase, DbpA. *Proceedings of the National Academy of Sciences of the United States of America*, **107**, 4046-4050.
112. De La Cruz, E.M., Wells, A.L., Sweeney, H.L. and Ostap, E.M. (2000) Actin and Light Chain Isoform Dependence of Myosin V Kinetics†. *Biochemistry*, **39**, 14196-14202.
113. De La Cruz, E.M., Ostap, E.M. and Sweeney, H.L. (2001) Kinetic mechanism and regulation of myosin VI. *The Journal of biological chemistry*, **276**, 32373-32381.
114. De La Cruz, E.M. and Pollard, T.D. (1995) Nucleotide-Free Actin: Stabilization by Sucrose and Nucleotide Binding Kinetics. *Biochemistry*, **34**, 5452-5461.
115. Arul Nambi Rajan, A. and Montpetit, B. (2020) Emerging molecular functions and novel roles for the DEAD-box protein Dbp5/DDX19 in gene expression. *Cellular and molecular life sciences : CMLS*.
116. De La Cruz, E.M., Sweeney, H.L. and Ostap, E.M. (2000) ADP inhibition of myosin V ATPase activity. *Biophys J*, **79**, 1524-1529.
117. Theobald, U., Mailinger, W., Baltes, M., Rizzi, M. and Reuss, M. (1997) In vivo analysis of metabolic dynamics in Saccharomyces cerevisiae : I. Experimental observations. *Biotechnol Bioeng*, **55**, 305-316.
118. Lagunas, R. and Gancedo, C. (1983) Role of phosphate in the regulation of the Pasteur effect in Saccharomyces cerevisiae. *European journal of biochemistry*, **137**, 479-483.
119. Wood, E.J. (1987) Data for biochemical research (third edition) by R M C Dawson, D C Elliott, W H Elliott and K M Jones, pp 580. Oxford Science Publications, OUP, Oxford, 1986. £35/$59. ISBN 0-19-855358-7. *Biochemical Education*, **15**, 97-97.
120. Tinoco, I. (2014) *Physical chemistry : principles and applications in biological sciences*. Pearson, Boston [etc.].
121. Sambrook, J. (2001) *Molecular cloning : a laboratory manual*. Third edition. Cold Spring Harbor, N.Y. : Cold Spring Harbor Laboratory Press, [2001] ©2001.
122. Bevington, P.R. and Robinson, D.K. (2003) *Data reduction and error analysis for the physical sciences*.
123. Albe, K.R., Butler, M.H. and Wright, B.E. (1990) Cellular concentrations of enzymes and their substrates. *Journal of theoretical biology*, **143**, 163-195.